ENZO ALBERTO CANDREVA

# A UNITARY APPROACH TO INFORMATION AND ESTIMATION THEORY IN DIGITAL COMMUNICATION SYSTEMS

Ph.D. Programme in Electronics, Computer Science and
Telecommunications - XXII Cycle
Department of Electronics, Computer Science and Systems - DEIS
Alma Mater Studiorum - Università di Bologna

# A UNITARY APPROACH TO INFORMATION AND ESTIMATION THEORY IN DIGITAL COMMUNICATION SYSTEMS

ENZO ALBERTO CANDREVA

Ph.D. Programme in Electronics, Computer Science and Telecommunications - XXII Cycle
Coordinator: Prof. Paola Mello
Supervisor: Prof. Giovanni E. Corazza

SSD: ING-INF/03

Department of Electronics, Computer Science and Systems - DEIS
Alma Mater Studiorum - Università di Bologna

March 2010

Enzo Alberto Candreva: *A Unitary Approach to Information and Estimation Theory in Digital Communication Systems,* Department of Electronics, Computer Science and Systems - DEIS, Alma Mater Studiorum - Università di Bologna © March 2010

# ABSTRACT

This thesis presents the outcomes of a Ph.D. course in telecommunications engineering. It is focused on the optimization of the physical layer of digital communication systems and it provides innovations for both multi- and single-carrier systems. For the former type we have first addressed the problem of the capacity in presence of several nuisances. Moreover, we have extended the concept of Single Frequency Network to the satellite scenario, and then we have introduced a novel concept in subcarrier data mapping, resulting in a very low Peak-to-Average-Power Ratio (PAPR) of the Orthogonal Frequency Division Multiplexing (OFDM) signal.

For single carrier systems we have proposed a method to optimize constellation design in presence of a strong distortion, such as the non linear distortion provided by satellites' on board high power amplifier, then we developed a method to calculate the bit/symbol error rate related to a given constellation, achieving an improved accuracy with respect to the traditional Union Bound with no additional complexity. Finally we have designed a low complexity Signal-to-Noise Ratio (SNR) estimator, which saves one-half of multiplication with respect to the Maximum Likelihood (ML) estimator, and it has similar estimation accuracy.

# SOMMARIO

Questa tesi presenta i risultati ottenuti durante un dottorato di ricerca in ingegneria delle telecomunicazioni. Oggetto di studio è stato il livello fisico dei sistemi di trasmissione numerica, e sono state proposte innovazioni per i sistemi multi-portante e a portante singola. Nel primo caso è stata valutata la capacità di un sistema affetto da varie non idealità. In seguito l'idea di Single Frequency Network è stata estesa dall'ambito terrestre a quello satellitare, ed infine è stata presentata una nuova tecnica per effettuare il mapping da bit a simboli, che ha permesso di raggiungere fattori di cresta particolarmente bassi per il segnale OFDM (Orthogonal Frequency Division Multiplexing).

Per i sistemi a portante singola, è stato proposto un metodo per ottimizzare il progetto delle costellazioni in presenza di una forte distorsione, quale ad esempio la distorsione non lineare dovuta agli amplificatori di potenza a bordo dei satelliti. In seguito è stato sviluppato un metodo per calcolare la probabilità d'errore per bit e per simbolo riferita ad una data costellazione. Tale metodo ha la stessa complessità dello Union Bound ma risulta essere più accurato. Infine si è progettato uno stimatore di rapporto segnale-rumore, che permette il risparmio di metà delle moltiplicazioni rispetto al tradizionale stimatore a massima verosimiglianza, ma che mantiene prestazioni di stima comparabili.

# ORIGINAL CONTRIBUTIONS

This thesis presents original contributions in different fields. For the Orthogonal Frequency Division Multiplexing (OFDM) signal, the author has extended capacity evaluation in correlated fading to the case of discrete subcarrier constellations and channel estimation errors. This analysis provided a rule to optimize the number of pilot subcarriers, whose outcomes are presented in the following. Regarding Single Frequency Satellite Networks (SFSNs), the author contributed to the problem statement and to the numerical computations involved, while for Quasi-Constant Envelope OFDM, the author contributed in devising Peak-to-Average-Power Ratio (PAPR) reduction methods for the new data mappings. The methods hereby presented can be seen as a broadening of already known methods, but they required a new parameter optimization.

For the case of single-carrier system and signal, the author extended a method used for the Additive White Gaussian Noise (AWGN) to non-linear channel, obtaining the optimal constellation, in the sense of the minimum symbol error rate. These optimized constellations are shown to be resemblant of those applied in digital satellite communications, thus the contribution of the author was a theoretical justification of a concept known from an intuitive point of view. Moreover, the author developed a new bound on the error probability of the detection of signals corrupted by AWGN. This bound is tighter than the Union Bound, having the same complexity, and never exceeds the value of 1, returning thus a meaningful estimate of a probability. Finally, the author invented a reduced complexity Signal-to-Noise Ratio (SNR) estimator, which can save one half of the multiplications while retaining a satisfactory accuracy. A paper presenting this SNR estimator has been awarded a *Best Student Paper Award*.

# PUBLICATIONS

Some proofs and figures have appeared previously in the following publications:

1. E.A. Candreva, G.E. Corazza, and A. Vanelli-Coralli, *On the Optimization of Signal Constellations for Satellite Channels*, Proceedings of International Workshop on Satellite and Space Communications 2007 (IWSSC2007), September 12-14, 2007, Salzburg, Austria, pp.299-303;
2. E.A. Candreva, G.E. Corazza, and A. Vanelli-Coralli, *On the Constrained Capacity of OFDM in Rayleigh Fading Channels*, Proceedings of International Symposium on Spread Spectrum Techniques and Applications 2008 (ISSSTA 2008), Bologna, Italy, August 2008;

3. E.A. Candreva, G.E. Corazza, and A. Vanelli-Coralli *A Reduced Complexity SNR Estimator*, Proceedings of the 29th AIAA International Communications Satellite Systems Conference, ICSSC 2009, Edinburgh, UK, June 2009 (received the BEST STUDENT PAPER AWARD);
4. G.E. Corazza, C. Palestini, E.A. Candreva, and A. Vanelli-Coralli *The Single Frequency Satellite Network Concept: Multiple Beams for Unified Coverage*, GLOBECOM 2009, Hawaii, USA, December 2009;
5. E.A. Candreva, G.E. Corazza and A. Vanelli-Coralli *A Tighter Upper Bound on the Error Probability of Signals in White Gaussian Noise*, to be submitted to ASMS 2010;
6. F. Bastia, C. Bersani, E.A. Candreva, S.Cioni, G.E. Corazza, M. Neri, C. Palestini, M. Papaleo, S. Rosati, and A Vanelli-Coralli, *LTE Air Interface over Broadband Satellite Networks*, EURASIP Journal on Wireless Communications and Networking, Vol. 2009;
7. E.A. Candreva, G.E. Corazza, and A. Vanelli Coralli *A Reduced Complexity Data-Aided SNR Estimator* to be submitted to IEEE Communication Letters;
8. S. Rosati, E.A. Candreva, G.E. Corazza and A.Vanelli-Coralli *OFDM Schemes with Quasi-Constant Envelope*, to be submitted to IEEE Transactions on Communications;
9. E.A. Candreva, G.E. Corazza and A. Vanelli-Coralli, *Pilot Design and Optimum Information Transfer in OFDM Systems*, to be sumbitted to IEEE Transactions on Communications.

*Si è così profondi, ormai, che non si vede più niente.*
*A forza di andare in profondità, si è sprofondati.*
*Soltanto l'intelligenza, l'intelligenza che è anche*
*"leggerezza", che sa essere "leggera" può sperare*
*di risalire alla superficialità, alla banalità.*

L. Sciascia, *Nero su Nero*, Einaudi, 1979

# ACKNOWLEDGMENTS

This document is a PhD Thesis, thus it is not the best place for all possible kinds of sentimental acknowledgments. However, the author would like to mention that he is deeply indebted to Professor Giovanni E. Corazza and to the bright fellows and trusted friends in his research group. The author did enjoy three years of interesting discussion about a very broad range of topics, often unrelated to Telecommunications. The author has learnt a lot in these three years, and he hopes to have contributed to the achievements of Digicomm Research Group.

# CONTENTS

I INNOVATIONS IN MULTI-CARRIER SYSTEMS 1

1 OFDM CAPACITY IN PRESENCE OF IMPAIRMENTS 3
- 1.1 Introduction 3
- 1.2 System Model 3
- 1.3 Capacity of Discrete-Input Continuous-Output Channels 4
  - 1.3.1 Constrained capacity for single-carrier systems in Additive White Gaussian Noise (AWGN) 4
  - 1.3.2 Capacity in Fading Channels 6
- 1.4 Capacity of OFDM systems 6
  - 1.4.1 Theoretical Background 6
  - 1.4.2 Results 8
- 1.5 Impact of Channel Estimation Errors over OFDM Capacity 12
  - 1.5.1 Performance Degradation 12
  - 1.5.2 Pilot Field Design 13
  - 1.5.3 Numerical Results 13
- 1.6 Conclusions 15

2 SINGLE FREQUENCY SATELLITE NETWORKS 17
- 2.1 Introduction 17
- 2.2 OFDM and CDD 19
- 2.3 SFN over Satellites 20
  - 2.3.1 Multi-beam coverage for Single Frequency Satellite Network (SFSN) 20
  - 2.3.2 Spot Beam Radiation Diagram 21
  - 2.3.3 Multi-Beam Cyclic Delay Diversity (MBCDD) Approximated Transfer Function 22
  - 2.3.4 Parameter Optimization 23
- 2.4 SFSN Capacity 25
- 2.5 First Proof of Concept for SFSN 26
- 2.6 Link Budget Analysis 27
- 2.7 Numerical Evaluation 29
- 2.8 SFSN: Pros and Cons 29
- 2.9 Conclusions 30

3 QUASI-CONSTANT ENVELOPE OFDM 33
- 3.1 Introduction 33
- 3.2 Context System Model 34
  - 3.2.1 Nonlinear Distortion 34
  - 3.2.2 Orthogonal Frequency Division Multiplexing (OFDM) signal 36
- 3.3 Rotation-Invariant Subcarrier Mapping 38
  - 3.3.1 Constellation design 38
  - 3.3.2 Spherical Active Constellation Extension (ACE) 38
  - 3.3.3 Extensions 39
- 3.4 AWGN Detectors 40
- 3.5 Numerical Results 41
- 3.6 Conclusions 45

4 FURTHER DEVELOPMENTS OF THE PRESENTED WORK 47

II INNOVATIONS IN SINGLE CARRIER SYSTEMS 49
5 OPTIMIZATION OF CONSTELLATIONS OVER NON-LINEAR CHANNELS 51
  5.1 Introduction 51
  5.2 System Model 52
    5.2.1 Received Signal 52
    5.2.2 Error Probability 53
  5.3 Proposed Algorithm 54
    5.3.1 Description 54
    5.3.2 Convergence 55
    5.3.3 Discussion 56
  5.4 Results 56
  5.5 Conclusions 57
6 A TIGHTER UPPER BOUND FOR ERROR PROBABILITY OF SIGNALS IN AWGN 61
  6.1 Introduction 61
  6.2 SER Computation for 2-dimensional Signal Constellations 62
    6.2.1 Signal Model 62
    6.2.2 Bonferroni inequalities 63
    6.2.3 Proposed Upper Bound 64
    6.2.4 Numerical Results 66
  6.3 Codeword Error Rate Computation for Binary Block Codes 68
    6.3.1 Signal Model 68
    6.3.2 Proposed Bound 70
    6.3.3 Numerical Results 70
  6.4 Conclusions 70
7 A REDUCED COMPLEXITY SIGNAL TO NOISE RATIO ESTIMATOR 75
  7.1 Introduction 75
  7.2 Signal-to-Noise Ratio Estimators 75
  7.3 Analytical Model of the Reduced Complexity Estimator 77
  7.4 Non-Ideal Phase Reference 78
  7.5 Numerical Results 79
  7.6 Conclusions 80
8 FURTHER DEVELOPMENTS OF THE PRESENTED WORK 83

III APPENDIX 85
A ON THE EFFICIENCY OF PAPR REDUCTION METHODS IN SATELLITE OFDM 87
  A.1 Introduction 87
  A.2 PAPR Reduction Techniques 87
    A.2.1 Active Constellation Extension 88
    A.2.2 Tone Reservation 88
    A.2.3 Selected Mapping 89
  A.3 Performance Results 89

BIBLIOGRAPHY 93

# LIST OF FIGURES

Figure 1 Constrained Capacity as a function of Signal-to-Noise Ratio (SNR) for Quaternary Phase Shift Keying (QPSK), 8 Phase Shift Keying (PSK), 16 Quadrature Amplitude Modulation (QAM). 5

Figure 2 Constrained Capacity as a function of SNR for QPSK, 8 PSK and 16 QAM with Rayleigh fading and comparison to AWGN channel. 6

Figure 3 Instantaneous Capacity of OFDM systems employing QPSK, 8 PSK 16 QAM and its comparison with Shannon-predicted capacity. $E_s/N_0 = 0\text{dB}$. 9

Figure 4 Cumulative Density Function (CDF) of the instantaneous capacity of OFDM systems employing QPSK, 8 PSK 16 QAM and its comparison with Shannon-predicted capacity. $E_s/N_0 = 0\text{dB}$. 9

Figure 5 Instantaneous Capacity of OFDM systems employing QPSK, 8 PSK 16 QAM and its comparison with Shannon-predicted capacity. $E_s/N_0 = 3\text{dB}$. 10

Figure 6 CDF of the instantaneous capacity of OFDM systems employing QPSK, 8 PSK 16 QAMand its comparison with Shannon-predicted capacity. $E_s/N_0 = 3\text{dB}$. 10

Figure 7 Instantaneous Capacity of OFDM systems employing QPSK, 8 PSK 16 QAMand its comparison with Shannon-predicted capacity. $E_s/N_0 = 6\text{dB}$. 11

Figure 8 CDF of the instantaneous capacity of OFDM systems employing QPSK, 8 PSK 16 QAM and its comparison with Shannon-predicted capacity. $E_s/N_0 = 6\text{dB}$. 11

Figure 9 Optimization of the number of pilot subcarriers, $E_s/N_0 = 0\text{dB}$. 14

Figure 10 Optimization of the number of pilot subcarriers, $E_s/N_0 = 3\text{dB}$. 14

Figure 11 Optimization of the number of pilot subcarriers, $E_s/N_0 = 6\text{dB}$. 15

Figure 12 3dB footprint of 400 Geostationary Earth Orbit (GEO) satellite beams over a 650.000 $\text{km}^2$ coverage area. Numerical parameters as in Table 1. 18

Figure 13 Cyclic Delay Diversity (CDD) OFDM transmitter. 19

Figure 14 Broadcasting over Europe: single beam, linguistic beams, local beams. 20

Figure 15 Spot beam radiation and mask for $T = 20\text{dB}$ and $p = 2$. 22

Figure 16 Overall transfer function for three beams and $N = 1, 2, 3, 20$ paths each beam as a function carrier index. 23

Figure 17 Effective transfer function without MBCDD. Three overlapping beams. 23

Figure 18 Effective transfer function with MBCDD. Three overlapping beams. Non-optimized parameters. 24

Figure 19 Effective transfer function with MBCDD. Three overlapping beams. Optimized parameters. 24
Figure 20 Capacity comparison in the three scenarios: single beam, two overlapping beams, three overlapping beams. 25
Figure 21 Capacity obtained in an area covered with six beams. 26
Figure 22 Snapshot of the capacity obtained in an area covered with six beams. 27
Figure 23 Capacity comparison: SFSN vs. Single Beam Single Carrier. 30
Figure 24 Circularly simmetrical constellation. 39
Figure 25 Clover constellation. 40
Figure 26 Error Probability of Two Level Mapping. 42
Figure 27 Decision Regions for Clover Mapping. 42
Figure 28 Bit Error Probability for Clover Mapping. 43
Figure 29 Peak-to-Average-Power Ratio (PAPR) distribution for Two level and Clover Mappings. 43
Figure 30 Signal-to-Distortion Ratio (SDR) on Saleh High Power Amplifier (HPA) vs Input Back Off (IBO) for the proposed mappings. 44
Figure 31 SDR on Ideal Clipping (IC) HPA vs IBO for the proposed mappings. 44
Figure 32 Bit Error Rate (BER) on Saleh HPA at IBO $= 0$ dB for the proposed mappings. 45
Figure 33 BER on IC HPA at IBO $= 0$ dB for the proposed mappings. 45
Figure 34 Optimal Signal Set for $\text{IBO} = 8$ dB, $\gamma = 10$ dB. 58
Figure 35 Optimal Signal Set for $\text{IBO} = 12$ dB, $\gamma = 10$ dB. 58
Figure 36 Optimal Signal Set for $\text{IBO} = 16$ dB, $\gamma = 10$ dB. 59
Figure 37 Optimal Signal Set for $\text{IBO} = 16$ dB, $\gamma = 14$ dB. 59
Figure 38 Constellation and bit mapping for 16-Amplitude-Phase Shift Keying (APSK), as prescribed in [30]. 66
Figure 39 Symbol error Probability for 16-APSK. 67
Figure 40 Constellation and bit mapping for 32-APSK, as prescribed in [30]. 67
Figure 41 Symbol error Probability for 32-APSK. 68
Figure 42 Codeword Error Probability for the BCH (63,24) code. 71
Figure 43 Codeword Error Probability for the BCH (63,30) code. 72
Figure 44 Codeword Error Probability for the BCH (63,36) code. 72
Figure 45 Codeword Error Probability for the BCH (63,39) code. 73
Figure 46 Maximum Likelihood (ML) SNR Estimator. 76
Figure 47 Reduced Complexity SNR Estimator. 77
Figure 48 Normalized Mean Square Error (MSE) in AWGN only, $N_p = 64$. 80

Figure 49 Normalized MSE in presence of phase error, $N_p = 64$. 80
Figure 50 Normalized MSE in AWGN only, $N_p = 1024$. 81
Figure 51 Normalized MSE in presence of phase error, $N_p = 1024$. 81
Figure 52 Total Degradation for QPSK code-rate 1/5 and various PAPR reduction techniques- 91
Figure 53 Total Degradation for QPSK code-rate 1/2 and various PAPR reduction techniques- 92
Figure 54 Total Degradation for 16-QAM code-rate 2/3 and various PAPR reduction techniques- 92

# LIST OF TABLES

Table 1 Link budget for Single Beam and SFSN systems. 28
Table 2 Values of $\alpha$ and $\beta$ for the Saleh model. 36
Table 3 Spectra of the BCH codes used in simulations. 71
Table 4 Complexity comparison of two Data-Aided SNR circuits. 77

# ACRONYMS

| | |
|---|---|
| ACE | Active Constellation Extension |
| ACI | Adjacent Channel Interference |
| AGC | Automatic Gain Control |
| APSK | Amplitude-Phase Shift Keying |
| AWGN | Additive White Gaussian Noise |
| BER | Bit Error Rate |
| BPSK | Binary Phase Shift Keying |
| CCDF | Complementary Cumulative Density Function |
| CDD | Cyclic Delay Diversity |
| CDF | Cumulative Density Function |
| CER | Codeword Error Rate |
| CRB | Cramer-Rao Bound |
| DFT | Discrete Fourier Transform |
| DTH | Direct to Home |
| EHF | Extremely High Frequency |

| | |
|---|---|
| EIRP | Effective Isotropic Radiated Power |
| FFT | Fast Fourier Transform |
| GEO | Geostationary Earth Orbit |
| HDTV | High Definition Television |
| HPA | High Power Amplifier |
| IBO | Input Back Off |
| IC | Ideal Clipping |
| IDFT | Inverse Discrete Fourier Transform |
| IFFT | Inverse Fast Fourier Transform |
| ISI | Inter-Symbol Interference |
| MBCDD | Multi-Beam Cyclic Delay Diversity |
| MIMO | Multiple-Input Multiple-Output |
| MISO | Multiple-Input Single-Output |
| ML | Maximum Likelihood |
| MMSE | Minimum Mean Square Error |
| MSE | Mean Square Error |
| OBO | Output Back Off |
| OFDM | Orthogonal Frequency Division Multiplexing |
| PAPR | Peak-to-Average-Power Ratio |
| pdf | probability density function |
| PHY | Physical Layer |
| PSK | Phase Shift Keying |
| QAM | Quadrature Amplitude Modulation |
| QPSK | Quaternary Phase Shift Keying |
| QoS | Quality of Service |
| r.v. | random variable |
| SDR | Signal-to-Distortion Ratio |
| SDTV | Standard Definition Television |
| SER | Symbol Error Rate |
| SFN | Single Frequency Network |
| SFSN | Single Frequency Satellite Network |
| SLM | Selected Mapping |
| SNR | Signal-to-Noise Ratio |
| STBC | Space-Time Block Codes |
| TR | Tone Reservation |
| TWTA | Travelling Wave Tube Amplifiers |

# Part I

# INNOVATIONS IN MULTI-CARRIER SYSTEMS

# 1

# OFDM CAPACITY IN PRESENCE OF IMPAIRMENTS

## 1.1 INTRODUCTION

The importance of Orthogonal Frequency Division Multiplexing (OFDM) is rapidly growing, because of its ability to cope with frequency-selective channels with simple equalization. This powerful multiplexing technique is being adopted on almost all new generation communication standards, in the most various scenarios: wireline, digital television, mobile radio, and satellite. Although the OFDM is an established communication technique, the investigation and the analysis on this topic were essentially developed with the error rate as a target performance indicator. On the other hand, [21] presents an attempt to characterize OFDM from an information theoretic point of view, following a simplified approach in order to assess the instantaneous capacity of OFDM systems.

The aim of this chapter is to give a realistic characterization of the capacity of an OFDM system under frequency-selective Rayleigh fading, taking into account not only the correlation of fading amongst sub-channels (as in [21]), but also the discrete nature of the signal set for every sub-channel. A special form of Central Limit Theorem [13] is used in order to derive the overall system capacity. We show that the constrained capacity is Gaussian distributed, and we compute its mean and variance. With this method it is possible to have a reasonable analytical expression for the constrained capacity of OFDM, and taking into account all the other overheads in OFDM (such as guard interval, pilot insertion, etc.) a realistic measure of the throughput available to the users is readily obtained.

The rest of this chapter is structured as follows: Section 1.2 presents a brief description of OFDM systems and fading channels. Section 1.3 describes the capacity of a discrete-input continuous-output channel, and Section 1.4 applies this result to the calculation of the overall system capacity. Section 1.5 assesses the system capacity in the presence of estimation errors, and the conclusions are presented in Section 1.6

## 1.2 SYSTEM MODEL

An OFDM system [19] with $N$ sub-carriers transmits in the $n$-th discrete time interval the data symbol $x_{k,n}$ on the $k$-th sub-carrier, where $x_{n,k} \in \mathbb{C}$ belongs to a specific constellation $\{x_i\}_{i=1}^{M}$ with cardinality $M$ and $k = 0, \dots, N-1$. Each subcarrier is assumed to have a bandwidth of $\Delta f$ and the total bandwidth is $B = N\Delta f$. The duration of each discrete time interval is $T = \frac{1}{\Delta f}$, and the signal transmitted during the $n$-th time interval (composed by the superposition of the $N$ modulated sub-carriers) is called the $n$-th OFDM symbol.

The time-domain view of the $n$-th OFDM symbol is $s_n(t)$, for $(n-1)T < t \leqslant nT$ and its samples are given by

$$s_{n,i} = \frac{1}{\sqrt{N}} \sum_{k=0}^{N-1} x_{k,n} e^{j2\pi\frac{ik}{N}}, \quad i = 0, \dots, N-1 \qquad (1.1)$$

In other terms, Eq. (1.1) states that OFDM modulation is equivalent to an Inverse Discrete Fourier Transform (IDFT) of the data symbol vector.

The signal $s_n(t)$ is transmitted through a time-varying channel whose impulse response is $h(\tau, t)$ and is further degraded by a complex Gaussian noise process with power spectral density $N_0$.

The channel is assumed to be affected by a frequency-selective Rayleigh fading, and is described by the well known Jakes model [47].

In this model, $h(t, \tau)$ describes a wide-sense stationary with uncorrelated, isotropic scattering. The delay autocorrelation function is supposed to be described as

$$\frac{1}{2}\mathbb{E}\left[h(t,\tau_1)h^*(t,\tau_2)\right] = \frac{1}{\tau_d}e^{-\frac{\tau_1}{\tau_d}}\delta(\tau_1-\tau_2) \tag{1.2}$$

assuming thus an exponential delay power profile, with root mean square delay $\tau_d$ Then the k-th sub-channel gain during $n$-th block time is $H(nT, f_k) = H_{n,k}$ where $H(t, f)$ is the Fourier transform of $h(t, \tau)$ with respect to the variable $\tau$. From [47] the complex sub-channel gain can be written as $H_{n,k} = p_{n,k} + jq_{n,k}$, where $p_{n,k}$, $q_{n,k} \sim \mathcal{N}(0, \frac{1}{2})$ without any loss of generality.

The expression for the cross-correlation between the in-phase and quadrature components of the fading random variable (r.v.) for different time intervals or frequencies can be found in [47], but is necessary to give some detail about the distribution of $|H_{n,k}|^2$, which is exponential with

$$\mathbb{E}\left[|H_{n,k}|^2\right] = 1, \quad \mathrm{Var}\left[|H_{n,k}|^2\right] = 1 \tag{1.3}$$

and correlation coefficient [55]

$$\rho(|H_{n,k}|^2, |H_{n,k+\Delta k}|^2) = \frac{1}{1+(2\pi\Delta f\Delta k\tau_d)^2} \tag{1.4}$$

While the correlation coefficient in Eq. (1.4) is always different from zero, following a pragmatic approach, the sub-channel gains on two fairly spaced sub-carriers can be considered independent if the correlation coefficient is significantly smaller than 1 (i.e. its value is less than a given threshold, like one tenth, or one hundredth).

Assuming perfect synchronization both in time and frequency, and a sufficient guard interval to avoid inter-block and inter-carrier interference, the receiver samples the received signal at rate B and performs a Discrete Fourier Transform (DFT) (recalling that Eq. (1.1) can be seen as an IDFT) obtaining

$$R_{k,n} = H_{k,n}x_{k,n} + N_{k,n} \tag{1.5}$$

where $N_{k,n}$ is an Additive White Gaussian Noise (AWGN) sample, a complex Gaussian variable having both real and imaginary part with zero mean and variance $\frac{N_0}{2}$.

## 1.3 CAPACITY OF DISCRETE-INPUT CONTINUOUS-OUTPUT CHANNELS

### 1.3.1 *Constrained capacity for single-carrier systems in AWGN*

The well known Shannon formula for Gaussian channels has to be intended as a theoretical upper bound on the capacity of communications systems. Pratical digital systems do not use Gaussian codebooks, they rather are constrained to emit symbols taken from a discrete set.

Based on this premise, the capacity of a communication systems has to be constrained, releasing the assumption of continuous input to the channel and assuming equiprobable signalling

The expression for this more realistic measure of capacity (which is usually referred to *constrained capacity*) can be found in [23, 37] and, for a signal set whose cardinality is M its value is

$$I(X,Y) = \log_2 M - \frac{1}{M}\sum_{i=0}^{M-1} \mathbb{E}\left[\log_2 \frac{\sum_{j=0}^{M-1} p(y|x_j)}{p(y|x_i)}\right] \tag{1.6}$$

where averaging is performed with respect to $p(y|x_i)$, the conditional pdf of the channel output $y$ with respect to the input symbol $x_i$. If the only nuisance is AWGN, the conditional probability density functions are gaussian and the averaging operation (which is performed with respect to channel outputs) can be numerically evaluated with Gaussian quadrature formulas. Strictly speaking, Eq. (1.6) represents a mutual information, not a capacity, but imposing the constraint of equiprobable signalling and discrete signal set, no best result can be achieved, so it is not improper referring to Eq. (1.6) as a constrained capacity. At a first glance, Eq. (1.6) shows that the mutual information cannot reach an infinite value, even in the case of an infinite signal-to-noise ratio, but it is bounded by $\log_2 M$. As an example, Fig. 1 shows the behavior of the mutual information as a function of signal-to-noise ratio for Quaternary Phase Shift Keying (QPSK), 8-Phase Shift Keying (PSK) and 16-Quadrature Amplitude Modulation (QAM).

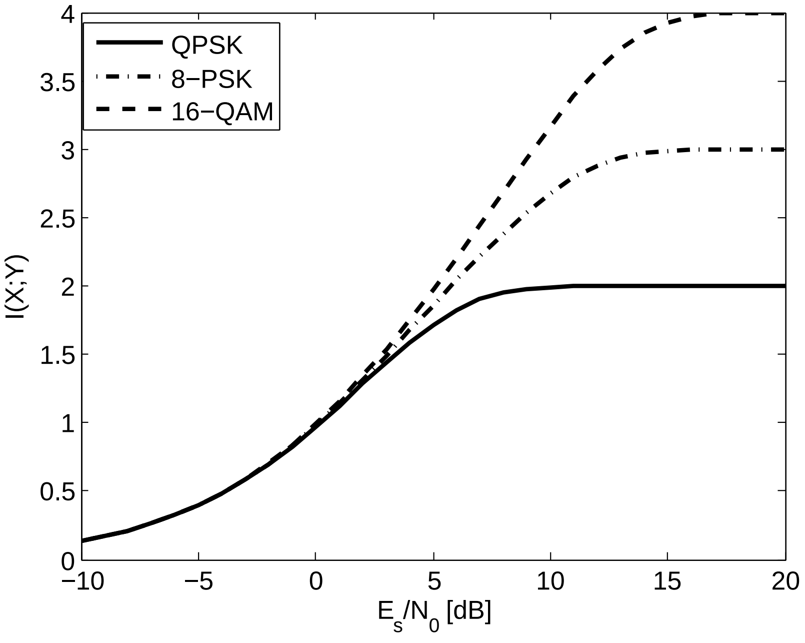

Figure 1: Constrained Capacity as a function of SNR for QPSK, 8 PSK, 16 QAM.

### 1.3.2 *Capacity in Fading Channels*

The formula in Eq. (1.6) can be extended assuming the presence of fading and perfect channel state information at the receiver, and it becomes:

$$I(X,Y|H) = \log_2 M - \frac{1}{M} \cdot \sum_{i=0}^{M-1} \mathbb{E}\left[\log_2 \frac{\sum_{j=0}^{M-1} p(y|x_j,h)}{p(y|x_i,h)}\right] \quad (1.7)$$

where $h$ is a sample of the fading r.v. $H$, and the average has to be performed with respect to both fading probability density function $p(h)$, and $p(y|x_i,h)$, the probability density of channel output conditioned to channel input and fading realization. Thus a double integral is required, and its evaluation is aided by Gaussian quadrature formulas. With the formulation of Eq. (1.7) the result is an average capacity, while the instantaneous capacity is a random variable, dependent on the realization of the fading r.v.

Fig. 2 compares the behavior of the mutual information as a function of signal-to-noise ratio in AWGN and in a Rayleigh fading environment, modeled as in Section 1.2.

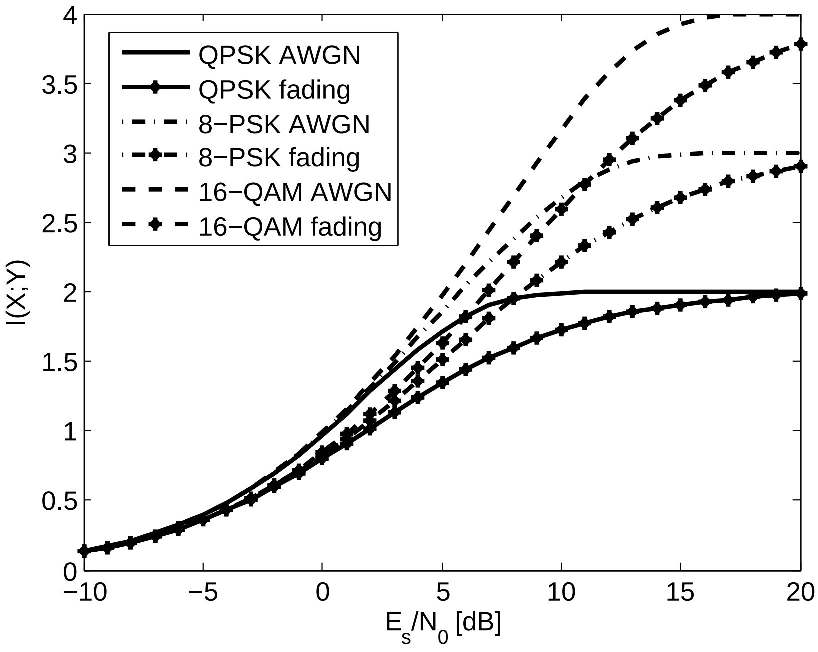

Figure 2: Constrained Capacity as a function of SNR for QPSK, 8 PSK and 16 QAM with Rayleigh fading and comparison to AWGN channel.

## 1.4 CAPACITY OF OFDM SYSTEMS

### 1.4.1 *Theoretical Background*

Given the capacity for every sub-carrier affected by fading and noise, as in Eq. (1.7), to calculate the instantaneous capacity for an OFDM system it is necessary to recall an extension of the Central Limit Theorem for correlated random variables (r.v.s). There are various papers on this topic [2, 13, 28, 29, 71] but the most effective approach is reported in [13],based on the following theorem

**Theorem 1.4.1** *Let* $\{x_j\}$ *be a sequence of random variables (r.v.s) with the following properties*

1. $\mathbb{E}\left[x_j\right] = 0$
2. $0 < \sigma_l^2 \leqslant \mathbb{E}\left[x_j^2\right] = \sigma_j^2 \leqslant \sigma_u^2 < \infty$
3. $0 < \beta_l^2 \leqslant \mathbb{E}\left[|x_j|^3\right] = \beta_j^2 \leqslant \beta_u^2 < \infty$
4. $\exists\, n < \infty : \quad \rho(x_i, x_j) = 0 \quad \mathit{if} \quad |i-j| \geqslant n$

*then it follows that*

$$M = \lim_{N \to \infty} \frac{1}{N} \sum_{i,j=1}^{N} \mathbb{E}\left[x_i x_j\right] \leqslant \infty \tag{1.8}$$

*and*

$$Y = \lim_{n \to \infty} \frac{1}{\sqrt{N}} \sum_{i=1}^{N} x_i \tag{1.9}$$

*is normally distributed with zero mean and variance* $M$.

Hypotheses 2 and 3 assures that second- and third-order moments of the r.v. $x_j$ are bounded between two positive constants, respectively $\sigma_l^2$ and $\sigma_u^2$ for the second-order moment and $\beta_l^2$ and $\beta_u^2$ for the third-order moment. Based on these hypotheses, $M$ is finite and, although it can be simply upper-bounded by $(2n+1)\sigma_j^2$, a more accurate representation is given by the evaluation of Eq. (1.8) which can be further simplified as

$$M = \sum_{j=-n}^{n} E[x_0 x_j] \tag{1.10}$$

This theorem is fundamental in evaluating the capacity of an OFDM system: the r.v. $x_i$ in theorem 1.4.1 is $C_i - \mathbb{E}\left[C_i\right]$, where $C_i$ and $\mathbb{E}\left[C_i\right]$ are the capacity of the $i$-th sub-carrier and its mean, as given by Eq. (1.7) (the verification that $C_k$ fulfills the hypotheses of Theorem 1.4.1 is trivial and may be obtained by numerical evaluation).

Based on this premise, we have:

$$\frac{1}{N} \sum_{i=1}^{N} C_i \sim \mathcal{N}\left(\mathbb{E}\left[C\right], \frac{1}{N} \sum_{j=-n}^{n} \sigma_C^2 \rho\left[j\right]\right) \tag{1.11}$$

where $\sigma_C^2$ is the variance of $C_i$ and $\rho\left[j\right]$ is the correlation coefficient between the capacity associated at two carriers separated by $j\Delta f$.

In order to have a good estimation of the variance in Eq. (1.11) we follow a pragmatic approach, that prevents the variance of suffering by numerical errors when $\rho\left[j\right]$ is very low. Thus $n$, the number of correlation coefficients to be considered is given by

$$n = \max\{j : \rho\left[j\right] \geqslant 0.01\} \tag{1.12}$$

This truncation is not significant, because of the scaling coefficient $1/N$ in the expression of variance in Eq. (1.11), and, on the other hand, reduces significantly the computation time.

A qualitative analysis of this result ensures that the Gaussian distribution will converge in probability to its mean value as the number of sub-carriers tends to infinity, as expected by the law of Large Numbers, in its weak formulation.

In other words, following an operational point of view, to evaluate the instantaneous capacity of an OFDM system, it is necessary to evaluate the mean and the variance of the capacity of a single sub-channel affected by AWGN and fading, and then the distribution of the instantaneous capacity can be obtained.

This approach in calculating the instantaneous capacity is different from the one followed in [21] and yields a mean capacity closer to actual values, since it releases the assumption of Gaussian signalling for each sub-channel.

Starting from this theoretically-predicted capacity, the actual capacity of an OFDM system can be derived, taking into account the guard interval, block duration, and the number of active carriers. Furthermore, the outage capacity of an OFDM system can be obtained, by fixing a capacity value which corresponds to a given value of the cumulative distribution of the mutual information.

### 1.4.2 *Results*

The numerical results are obtained assuming 2048 subcarriers spaced of 4464 Hz, a channel model as in Section 1.2, with $\tau_m = 19ns$. These values for the numerical parameters are chosen to be compliant with the newly adopted DVB-T2 [33]. Each subcarrier is transmitted with equal energy $E_s$, so the total transmitted energy is $NE_s$. N, the number of sub-carriers is assumed equal to 2048. The received SNR of the k-th sub-carrier is $|H_{n,k}|^2 \frac{E_s}{N_0}$.

Fig. 3 shows the capacity prediction of a system employing QPSK, 8 PSK, and 16 QAM at $\frac{E_s}{N_0} = 0\,\mathrm{dB}$ and these predictions are compared with those based on Shannon formula. Fig. 4 shows the Cumulative Density Function (CDF) of the instantaneous capacity in the same scenario.Fig. 5 and Fig. 6 show the same comparison at $\frac{E_s}{N_0} = 3\,\mathrm{dB}$, and finally, Fig. 7 and Fig. 8 show the same comparison at $\frac{E_s}{N_0} = 6\,\mathrm{dB}$.

It appears clearly from these results that the Shannon approach overestimates the instantaneous capacity of an OFDM system, while other measures, based upon constrained capacity, can be closer to the capacity of a real system. The difference between these estimates depends on signal-to-noise ratio, because the constrained capacity curves tend to "saturate" to a finite value, and on the environment, since the variance of the Gaussian distributions are a function of the memory of the channel: the higher the correlation, the higher the variance of the instantaneous capacity. By the same argument, if the carrier spacing is smaller, the sub-channels will be more correlated, thus increasing the variance.

Adaptive coding and modulation techniques with waterfilling appear to be attracting, thus, in order to exploit the variety of the instantaneous capacity rather than a conservative worst-case design.

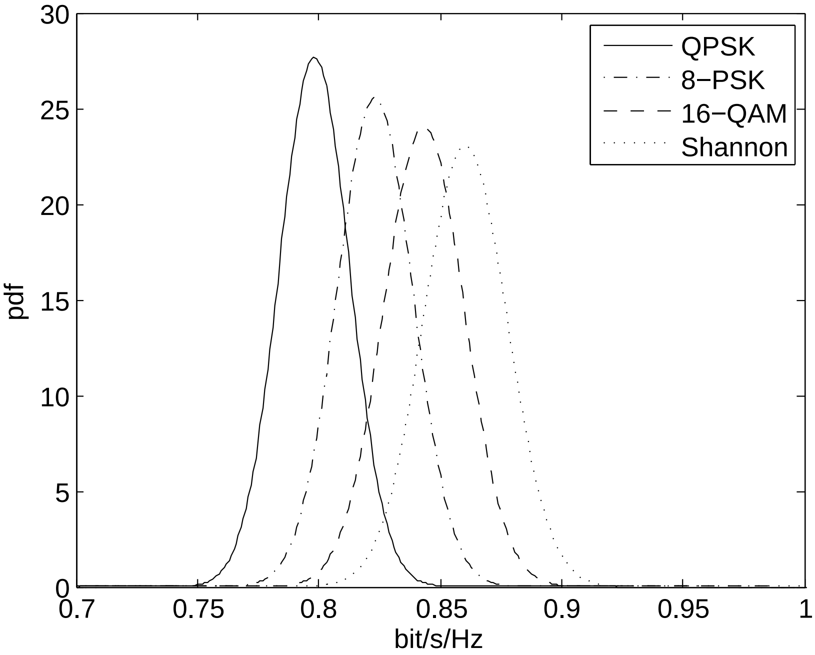

Figure 3: Instantaneous Capacity of OFDM systems employing QPSK, 8 PSK 16 QAM and its comparison with Shannon-predicted capacity. $E_s/N_0 = 0$dB.

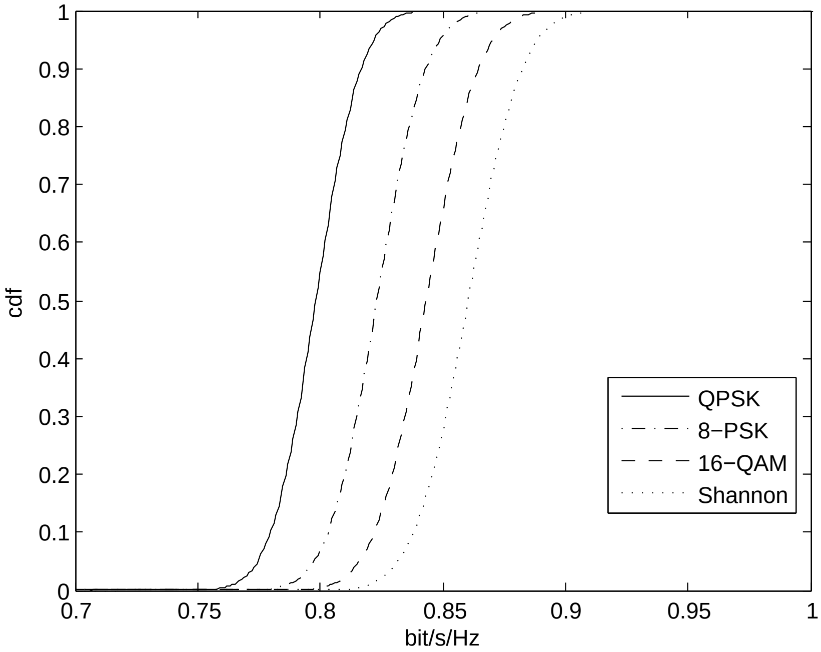

Figure 4: CDF of the instantaneous capacity of OFDM systems employing QPSK, 8 PSK 16 QAM and its comparison with Shannon-predicted capacity. $E_s/N_0 = 0$dB.

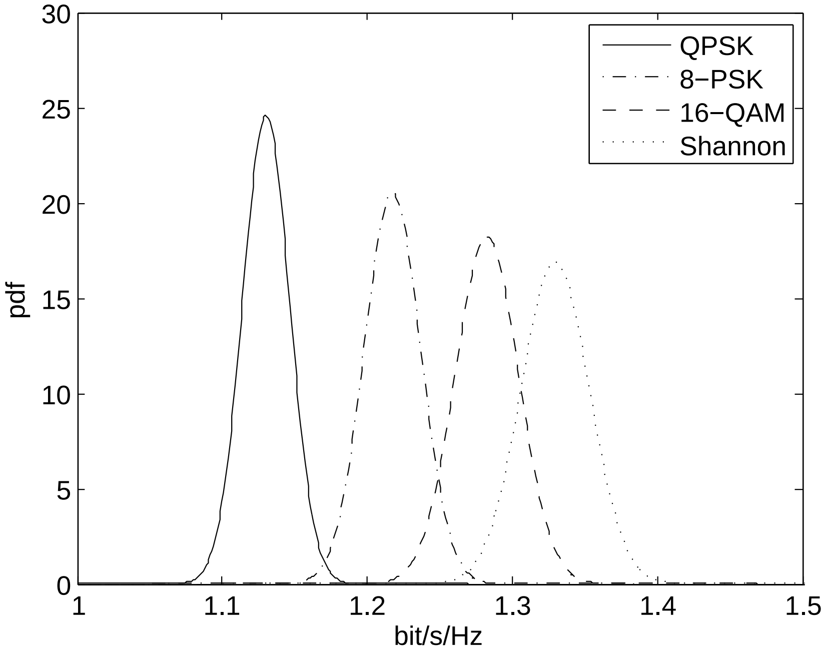

Figure 5: Instantaneous Capacity of OFDM systems employing QPSK, 8 PSK 16 QAM and its comparison with Shannon-predicted capacity. $E_s/N_0 = 3\text{dB}$.

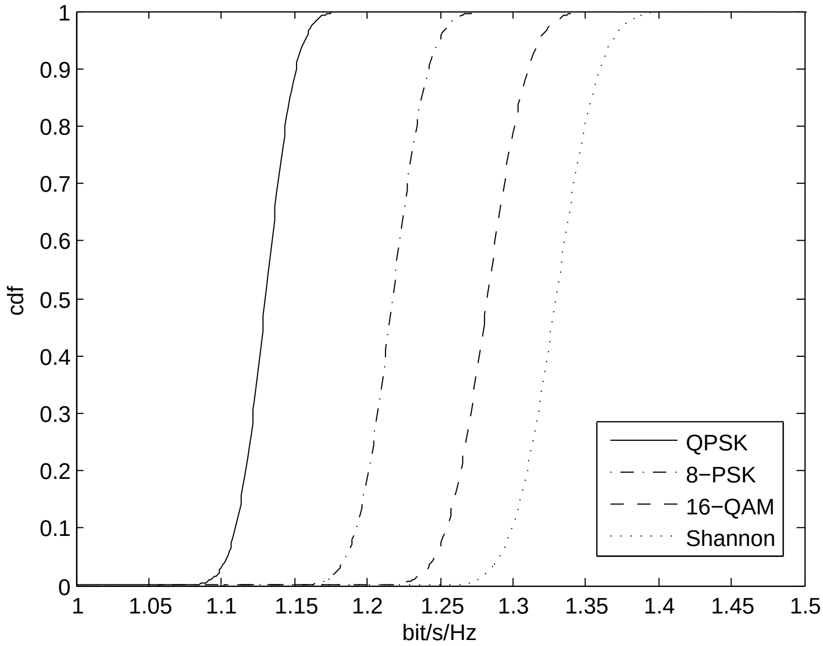

Figure 6: CDF of the instantaneous capacity of OFDM systems employing QPSK, 8 PSK 16 QAMand its comparison with Shannon-predicted capacity. $E_s/N_0 = 3\text{dB}$.

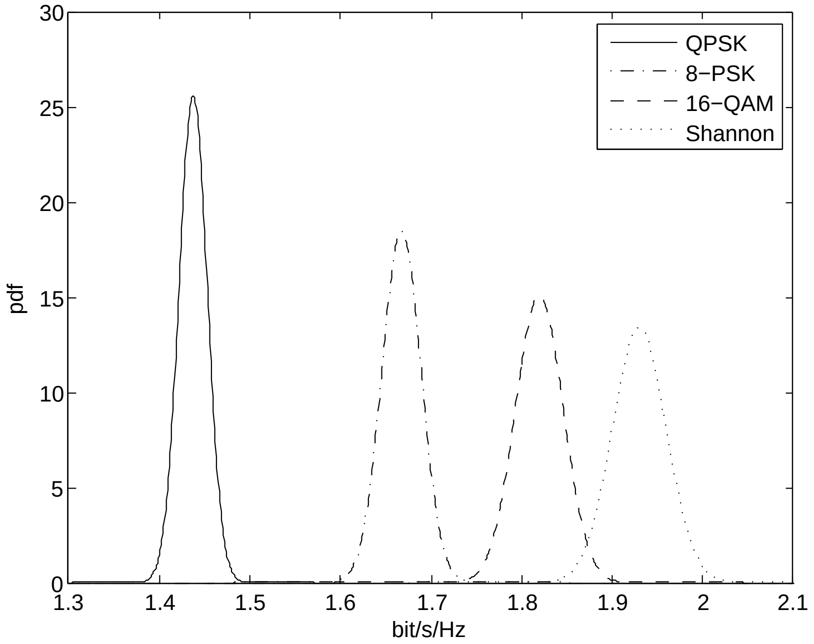

Figure 7: Instantaneous Capacity of OFDM systems employing QPSK, 8 PSK 16 QAMand its comparison with Shannon-predicted capacity. $E_s/N_0 = 6dB$.

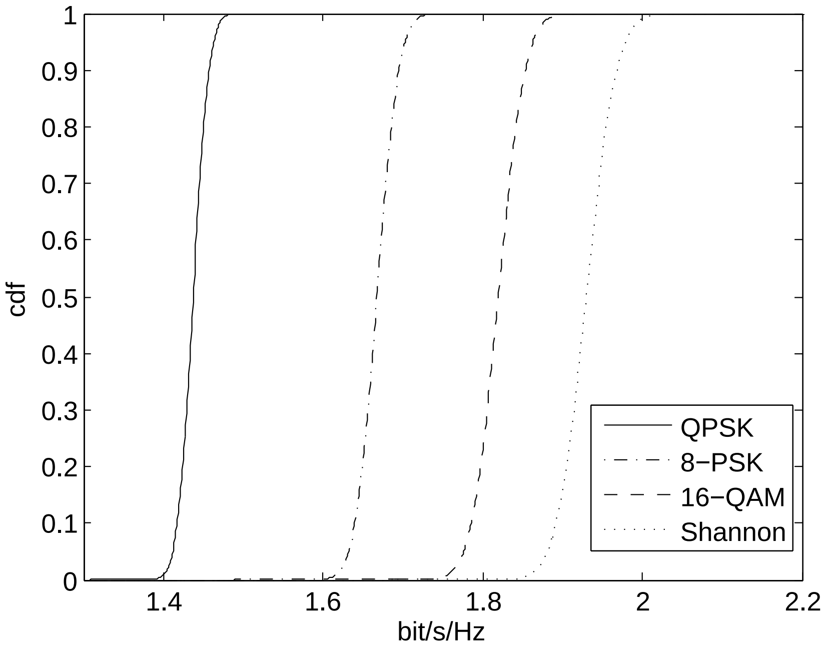

Figure 8: CDF of the instantaneous capacity of OFDM systems employing QPSK, 8 PSK 16 QAM and its comparison with Shannon-predicted capacity. $E_s/N_0 = 6dB$.

## 1.5 IMPACT OF CHANNEL ESTIMATION ERRORS OVER OFDM CAPACITY

### 1.5.1 *Performance Degradation*

Channel estimation for OFDM is now a well consolidated field, in which some very important results have been achieved, from both theoretical and implementation point of view. From the theoretical side, the optimal estimator has been derived, which is dependent on the assumptions from the channel model, while from the practical standpoint, a big number of low complexity channel estimators have been designed, to strike a balance between estimation accuracy and computational complexity. In this section we will not derive the optimal estimators, rather we will focus on the differences between two commonly used approaches, and show their performances. A starting point in designing a channel estimator is given by the Maximum Likelihood (ML) criterion, for which the channel has unknown but deterministic parameters, i. e. the number of taps, their delays and amplitudes. This criterion allows to design a "rugged" estimator, which can operate under very different possible conditions. This estimator has a simple closed form for the variance of the estimation error, given by the Cramer-Rao Bound (CRB).

A different estimator, which leads to an improved performance, is based on the Minimum Mean Square Error (MMSE) criterion. In this case the channel response is regarded as a random quantity, whose probability distribution is known at the receiver. In this case the variance of the estimation error is lower than the CRB, because the hypotesis is different, and it has to be averaged not only over the observed data, but also on the channel realizations.

For further details on the OFDM channel estimation problems, the reader is referred to the very interesting results presented in [17, 43, 58, 59, 77]. In what follows, we will present one of the main results collected in [58], i. e. the analytical expression for the variance of the estimation error for a multi-tap channel and OFDM signals. Assuming a noise variance of $N_0$, a channel with L taps having energy $\sigma_k^2$, $k = 1, \ldots, L$ and $N_p$ equispaced pilot subcarriers, we have

$$\sigma_{ML}^2 = \frac{N_0 L}{N_p} \tag{1.13}$$

and

$$\sigma_{MMSE}^2 = \lambda \cdot \sigma_{ML}^2 \tag{1.14}$$

where $\lambda < 1$ and it is given by

$$\lambda = \frac{1}{L} \sum_{k=1}^{L} \frac{1}{1 + \frac{N_0}{\sigma_k^2 N_p}} \tag{1.15}$$

It is important noticing that both $\sigma_{ML}^2$ and $\sigma_{MMSE}^2$ are independent of the subcarrier index, and they both confirm the intuitive feeling that the estimation accuracy degrades as the number of pilot tones decreases or the number of channel taps increases, for a given SNR.

The next step to evaluate the impact of an imperfect channel estimation over the reliability of the transmission is to consider the effect of the estimation error over each subcarrier. As it is shown for example in

[3, 41, 56], the effect of estimation error is twofold, since it causes both a reduction in the useful signal power and a contribution to the noise. Using the Shannon formula for the sake of simplicity, we can conclude that the capacity for a channel (here intended as the single subcarrier) affected by fading and non-ideal estimation is

$$C = \mathbb{E}_{H,\varepsilon}\left[\log_2\left(1+\frac{(H-\varepsilon)^2 E_s}{N_0+\varepsilon^2 E_s}\right)\right] \tag{1.16}$$

where $\varepsilon$ represents the estimation error.

### 1.5.2 *Pilot Field Design*

Based on the previous section, here we propose a method to optimize the pilot field design for an OFDM system. We will assume that the transmission is not continuous (i. e. it is performed in bursts) and the channel does not vary significantly over an OFDM symbol. Futhermore we will assume that the pilot subcarriers are equispaced over the symbol, with the caveat in [58, 59] that these locations are optimal if we assume no guard bands, otherwise the pilots shall be denser close to the guard bands. However, the assumption of equispaced pilots is instrumental for the analytical tractability of the problems, and still can provide a sort of "rule of thumb" for the OFDM system designer. Another important aspect in the pilot field design is the loss in throughput due to the subcarriers reserved for estimation. There is an obvious trade off between the accuracy and the loss in data rate: Eq. (1.13), (1.15) show an inverse proportionality between the number of pilots and the variance of the estimation error. On the other hand, the greater the number of pilot subcarriers, the less the available subcarriers for data transmission. Given this point of view, it is natural to ask whether the number of pilot subcarriers shall be reduced to achieve what can seem an unsatisfactory estimation performance, leaving room, in this way, to an higher data transmission capability.

### 1.5.3 *Numerical Results*

In this section we show the optimization of the mean value in Eq. (1.11), where the impact of estimation error is taken into account as in Eq. (1.16), but assuming a discrete constellation, and the throughput loss due to channel estimation is considered by the insertion of a multiplicative factor

$$\frac{N_{fft}-N_p}{N_{fft}} \tag{1.17}$$

The channel is assumed to have 9 taps, as the channel models presented in [70] to extend ITU channel models for OFDM systems. Fig. 9 shows the optimization of the number of pilot subcarriers, compared to the case of ideal channel state information, for an OFDM system employing QPSK, 8PSK, or 16QAM at $\frac{E_s}{N_0} = 0$ dB. The red lines show the case of ideal channel state information, where there is no estimation error neither throughput loss, while the black lines show the twofold impact of estimation errors on the subcarrier capacity, jointly with the throughput loss due by pilots insertion. Fig. 10 show the same optimization at $\frac{E_s}{N_0} = 3$ dB, and finally, Fig. 11 show the same optimization at $\frac{E_s}{N_0} = 6$ dB.

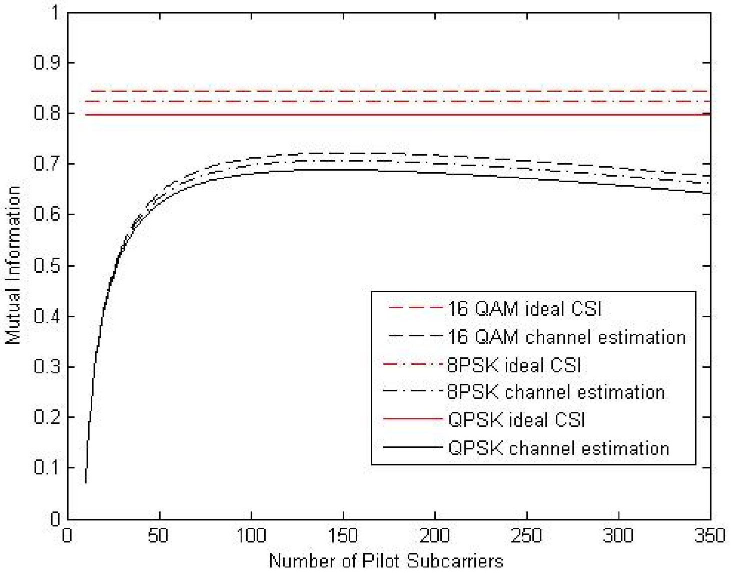

Figure 9: Optimization of the number of pilot subcarriers, $E_s/N_0 = 0\text{dB}$.

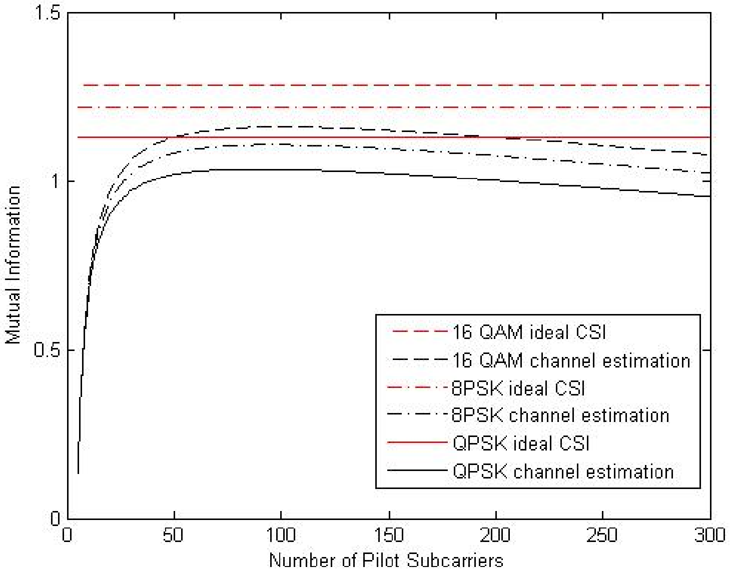

Figure 10: Optimization of the number of pilot subcarriers, $E_s/N_0 = 3\text{dB}$.

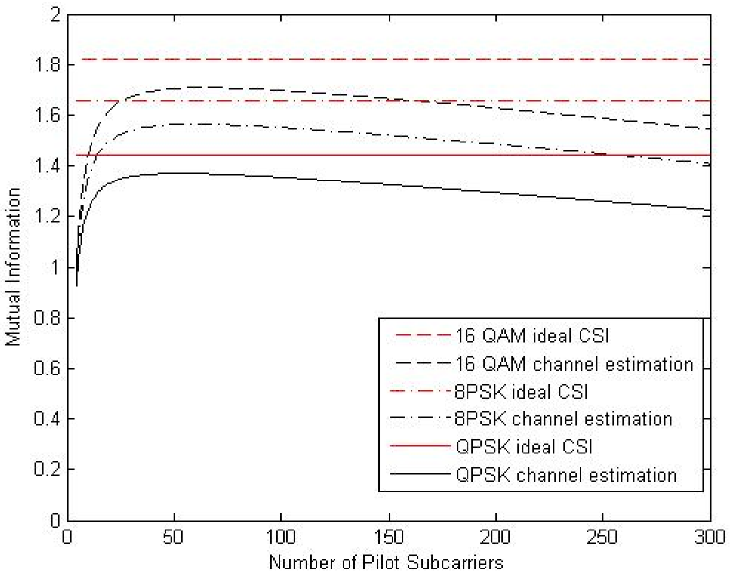

Figure 11: Optimization of the number of pilot subcarriers, $E_s/N_0 = 6\text{dB}$.

As it is shown in Fig. 9,10,11, before the optimum, the number of pilot subcarriers follows a law of diminishing returns: increasing by one the number of pilot tones leads to completely different performances whether the pilot tones number is already high or not. After the optimum number, the capacity will decrease, the higher the SNR the steeper the decrease. In addition, the optimal number of pilot tones is highly dependent on the subcarrier modulation, and this is more evident for high SNR

## 1.6 CONCLUSIONS

This chapter presented an attempt to characterize the instantaneous capacity of an OFDM system, based on constrained capacity arguments and on the application of Central Limit Theorem. The results show that the unconstrained capacity formula is inaccurate in predicting the instantaneous OFDM capacity, which depends on the modulation used and on the environment. The proposed approach based on Central Limit Theorem has an accuracy which is adequate for all practical DFT sizes. Moreover, we have analyzed the capacity of an OFDM system in the presence of channel estimation errors. We have shown its effect on the capacity and derived a method to optimize the number of subcarriers reserved for channel estimation, maximizing the information transfer. This method can be useful in OFDM system design, giving at a first glance an approximation for the capacity of the system and the number of subcarrier to be assigned to pilots.

# SINGLE FREQUENCY SATELLITE NETWORKS 2

## 2.1 INTRODUCTION

Satellite communications are experiencing very significant technical evolutions, which will be key in defining the role of satellites in future networks as a means to provide broadband access to the Internet over vast coverages. These changes have been enabled by new techniques and technologies: adaptive coding and modulation for the exploitation of EHF bands, where several GHz of bandwidth are available; on board processing for in-space routing; large reflectors for multi-beam antennas with hundreds of spot beams; exploitation of digital beam-forming network concept; as well as significant improvements in on-board power amplification. All of this goes in the direction of maximizing system capacity and flexibility, and in general its effectiveness.

On the other hand, satellite broadcasting systems are naturally still focused on the objective of ensuring good coverage over vast areas and, consequently, have hardly exploited the new techniques potential. In fact, the classic Direct to Home (DTH) TV broadcasting satellite network provides service with a single beam typically operated in $K_u$ band, where hundreds of Standard Definition Television (SDTV) or High Definition Television (HDTV) channels can be carried over the entire service area. This is a successful paradigm with seemingly little room for innovation. More recent developments are in the area of Mobile Broadcasting to hand-held terminals, which require a lower frequency band with a more benign propagation environment, such as the S band. Since spectrum availability is here much scarcer (a maximum of 30 MHz), it is necessary to use more efficiently the radio resource by exploiting frequency reuse. Considering European coverage, the satellite antenna pattern is typically organized into country-specific linguistic beams, which are grouped in clusters and assigned different frequency sub-bands, which can be reused in non-adjacent beams. Interference is caused by antenna side-lobes, which must be carefully kept under control. Unfortunately, the amount of reuse that can be achieved is small, and essentially determined by geographic configuration.

We propose here a *radical increase* in the fragmentation of the service area, both for fixed and for mobile applications, through the only exploitation of signal processing techniques over multi-beam antennas with hundreds of beams, also for broadcasting systems. Wherever content is identical in different beams (over a region, a country, or the entire service area) the same frequency band is used to realize a Single Frequency Satellite Network (SFSN), reminiscent of the Single Frequency Network (SFN) concept of terrestrial broadcasting systems, without resorting to any complexity increase in the antenna beamforming or any impact on the receiver. This architecture allows to have unprecedented flexibility in satellite broadcasting systems, as will be discussed shortly.

The reason why this idea has never been considered, or it has been rejected altogether, is that the signals carried by multiple beams in a SFSN mutually interfere in overlapping regions, inducing null-capacity zones wherever interference is destructive (see Fig. 12 for an example of overlapping beams). If no countermeasures are taken, it proves impossible to provide uniform Quality of Service (QoS) throughout the service area. The innovative idea is to use Orthogonal Frequency Division Multiplexing (OFDM) [79] jointly with a new form of Multi-Beam Cyclic Delay Diversity (MBCDD) which creates synthetic multipath through the assignment of beam specific power delay profiles. In this way, frequency selectivity is introduced which results in sufficient diversity to avoid destructive interference, guaranteeing correct signal reception in the entire coverage area. Let us dwell briefly over the advantages and disadvantages of this approach. As for the main positive aspects, we consider the possibility to: use the same antenna pattern to provide broadcasting and broadband access, for triple play services; deliver efficiently local content and reuse that part of the spectrum extensively; shape precisely and adaptively the contour of beams by grouping spots; use power control selectively over those narrow beams where atmospheric conditions are bad; use a large number of small High Power Amplifiers (HPAs) instead of a few powerful HPAs for the same total power. On the down side, the use of OFDM and MBCDD is not as power efficient as conventional single-carrier techniques, and requires the use of channel equalizers in the receivers.

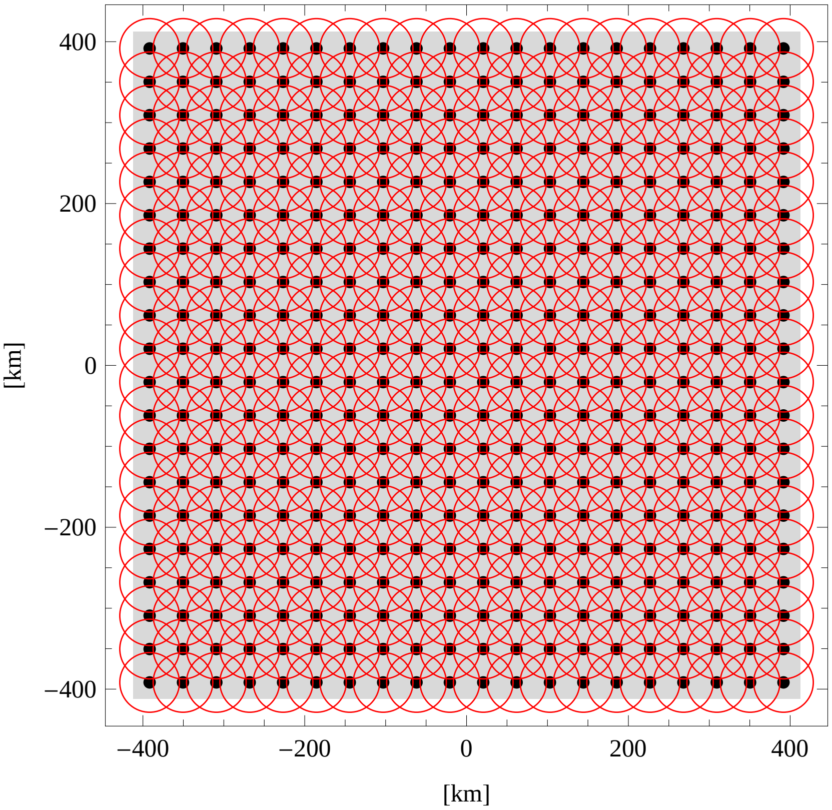

Figure 12: 3dB footprint of 400 GEO satellite beams over a 650.000 km$^2$ coverage area. Numerical parameters as in Table 1.

We believe that the advantages largely surpass the negative points. In this chapter, we describe how this idea takes practical form.

## 2.2 OFDM AND CDD

This section briefly describes the concept of Cyclic Delay Diversity (CDD) for OFDM systems. As well known, OFDM is a multicarrier transmission technique, which splits the available spectrum into several narrowband parallel channels, corresponding to multiple sub-carriers modulated at a low symbol rate. The OFDM signal can be expressed as

$$s(t) = \sum_{k=0}^{N_{FFT}-1} x_k \cdot e^{j2\pi k \frac{t}{T}}, \qquad -T_g \leqslant t < T \tag{2.1}$$

where $x_k$ are the complex-valued modulated data symbols, $N_{FFT}$ is the total number of sub-carriers, $T$ is the useful OFDM symbol time, $T_g$ is the guard interval duration. The guard interval is filled with a cyclic prefix to maintain orthogonality in multipath. Note that, in order to avoid adjacent channel interference, only $N_a < N_{FFT}$ active carriers are typically used.

Besides using the bandwidth very efficiently, OFDM guarantees high robustness against multipath delay spread, by allowing extremely simple equalization in the frequency domain. So much so that we can increase artificially the channel delay spread by inserting TX-antenna specific cyclic delays. CDD [26], [25] is a Multiple-Input Multiple-Output (MIMO) scheme which allows to enhance the frequency selectivity by inserting additional multiple paths that would not naturally occur. Figure 13 illustrates the block diagram of an OFDM transmitter applying CDD on its $N_{TX}$ antennas. As shown, the same OFDM modulated signal is transmitted over $N_{TX}$ antennas with an antenna specific cyclic shift. These shifts are indicated in the time domain by $\delta_i$, $i = 1, ..., N_{TX} - 1$, $\delta \in Z$ and correspond to a multiplication by a phase factor $\psi_i(f) = e^{-j2\pi f \frac{\delta_i}{N_{FFT}}}$. The latter, together with the normalization term used to split equally the transmission power among the antennas, can be interpreted as due to the channel, leading to an equivalent overall channel transfer function reported in Eq. (2.2) [26]:

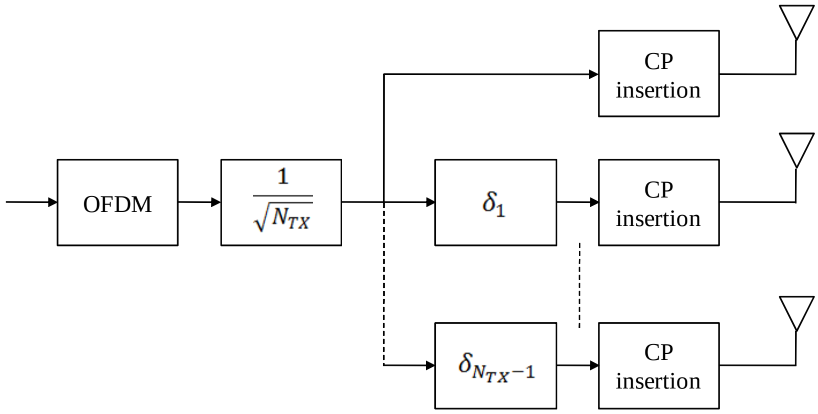

Figure 13: CDD OFDM transmitter.

$$H_{eq}(f,t) = \frac{1}{\sqrt{N_{TX}}} \sum_{i=0}^{N_{TX}-1} \psi_i(f) \cdot H_i(f,t) \tag{2.2}$$

where $H_i(f,t)$ denotes the channel transfer function from the $i$-th transmitter antenna to the receiver antenna. Eq. (2.2) applies to the Multiple-

Input Single-Output (MISO) case, and can obviously be extended to MIMO. Compared to the original propagation channel, the composite channel using CDD shows a much richer multi-path profile, i.e. an increased frequency diversity of the received signal due to the contribution of the CDD transmission scheme. This is especially useful on poor multi-path scenarios in combination with a powerful coding scheme.

Here we are interested in the potential of the CDD technique as applied to SFSNs, in association to coded OFDM. Indeed, CDD has been considered for Digital Video Broadcasting Terrestrial (DVB-T) applications [25], but it has never been thought for satellite broadcasting. This is the contribution of the present chapter.

## 2.3 SFN OVER SATELLITES

Since the general aim of a broadcast service is to deliver the same signal to a very large audience dislocated over a wide area, one of the most effective solutions is to establish a satellite network. As clearly explained in the Introduction, the main novelty consists in providing broadcasting services through a multi-spot antenna synthesizing local beams, whereby several spots may be sending identical signals, to realize a SFSN. On board multi-beam antennas can be realized through the adoption of a Cassegrain reflector (which includes a parabolic primary mirror and a hyperbolic secondary mirror) and multi-feed horns; a similar structure to those utilized in Earth station antennas. More precisely, instead of having a single focal point where the feed must be located, the multi-beam antenna has a focal surface on which various feeds can be placed. Such an antenna system has a very compact structure and an adequate flexibility. The design of the reflectors position and feeders configuration realizes the desired beam geometry, in particular the beam overlapping areas on ground and the antenna side-lobes which are the main interference sources. Let us see how a SFSN can be designed exploiting such a multi-beam antenna, through the combined use of OFDM and MBCDD, performing signal processing at the gateway and assuming a transparent satellite transponder with beamforming.

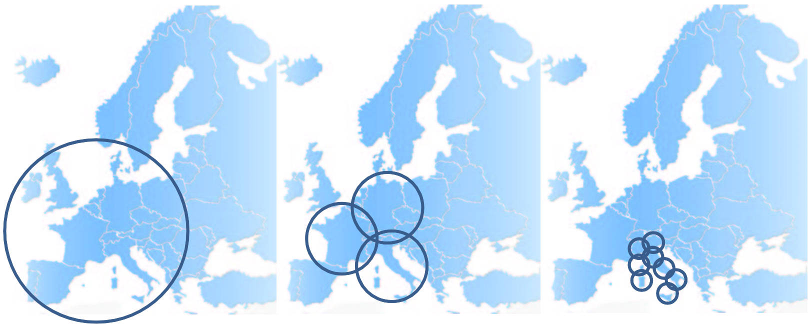

Figure 14: Broadcasting over Europe: single beam, linguistic beams, local beams.

### 2.3.1 *Multi-beam coverage for SFSN*

As mentioned before, combining signals coming from two or more overlapping beams generates null-capacity zones wherever they interfere destructively, causing deep fade events. If fading is frequency non-selective, this means that in certain points of the Earth surface no useful energy can be received. Obviously, this situation would be unacceptable for a broadcasting service since it is impossible to provide a uniform QoS throughout the coverage area. The proposed strategy, relying on the adoption of OFDM on the satellite link, is to apply MBCDD to each beam by imposing a specific delay profile that guarantees frequency selectivity over the signal bandwidth, generating a new source of diversity. This frequency selectivity is beneficial since it can be exploited through coded OFDM and leads to an overall transfer function without any null zone in the entire bandwidth.

Consider the k-th beam. Let $H^k(f, \alpha, \phi)$ be the channel transfer function corresponding to this beam as seen by a point on Earth reached through a link with amplitude gain $\alpha$ and overall phase rotation $\phi$. Clearly, $\alpha$ accounts for the path loss, while $\phi$ includes the initial phase imposed by the gateway transmitter, the phase rotation due to satellite beamforming and that due to propagation delay. Both $\alpha$ and $\phi$ are assumed to be constant over the entire signal bandwidth.

Let $H_n^k = H^k(n\Delta f, \alpha_k, \phi_k)$ be the transfer function coefficient pertaining to the n-th OFDM subcarrier, where the constants $\alpha_k$ and $\phi_k$ are implicit for notation simplicity. Assume MBCDD is applied by creating $N_k$ synthetic signal replicas at the gateway, each delayed by $\delta_{i,k}$ and scaled by an amplitude coefficient $A_{i,k}$, for $i = 1, \ldots, N_k$. Thus, the n-th transfer function coefficient can be described as:

$$H_n^k(\alpha_k, \phi_k) = \alpha_k e^{j\phi_k} \sum_{i=1}^{N_k} A_{i,k} e^{-j2\pi n \frac{\mathrm{mod}(\delta_{i,k}, N_{FFT})}{N_{FFT}}} \tag{2.3}$$

where $\mathrm{mod}(a, b)$ indicates a module b. The $2N_k + 1$ parameters characterizing the power delay profile synthesized for the generic k-th beam give great flexibility, with plenty of degrees of freedom in selecting delays and amplitudes. These parameters can be optimized in the transmitter without any consequences at the receiver. The only constraint is that non selective fading per subcarrier should be guaranteed at all locations, in order to allow simple equalization; besides, channel estimation could became too challenging if the number of paths increases excessively.

Note that the application of CDD is not realized with different antennas as in its original form, but through digital processing at the gateway. In this way the system results to be more flexible, since no limitation in the number of delays is introduced, independently of the number of antenna elements.

### 2.3.2 *Spot Beam Radiation Diagram*

In order to describe the radiation pattern of each beam, the model described in [78] and [16] has been used. The generic tapered-aperture antenna radiation pattern is reported in the following equation:

$$\begin{aligned} G(u_k) &= G_{M,k} \left( \frac{(p+1)(1-T)}{(p+1)(1-T)+T} \right)^2 \\ &\cdot \left( \frac{2J_1(u_k)}{u_k} + 2^{p+1} p! \frac{T}{1-T} \frac{J_{p+1}(u_k)}{u_k^{p+1}} \right)^2 \end{aligned} \tag{2.4}$$

where $G_{M,k}$ is the maximum gain for the k-th beam, p is a design parameter, T is the aperture edge taper, $J_p(u)$ is the Bessel function of the first kind and order p, $u_k = \frac{\pi d_a}{\lambda} \sin\theta_k$, $d_{a,k}$ is the effective antenna aperture for the k-th beam, and $\lambda$ is the wavelength. Note that in the following, the mask corresponding to $G(u_k)$ with $T = 20\text{dB}$ and $p = 2$, depicted in Fig. 15, has been used. For simplicity, a flat model of the Earth surface has been assumed, which is sufficiently accurate for beams which are not too large and not far from the sub-satellite point.

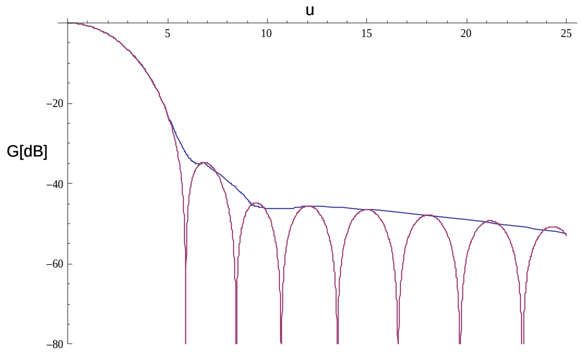

Figure 15: Spot beam radiation and mask for $T = 20\text{dB}$ and $p = 2$.

### 2.3.3 *MBCDD Approximated Transfer Function*

Now we are in the position to evaluate the overall effect of beam superposition. Let $N_B$ be the number of overlapping beams insisting on a specific location with the same transmitted power, and $H_n$ be the overall transfer function coefficient corresponding to the n-th subcarrier. Note that, at any location all $\alpha_k$ coefficients are identical for any k; therefore, only $\phi_k$ needs to be explicit. It holds

$$H_n = H_n(\phi_1, \dots, \phi_{N_B}) = \sum_{k=1}^{N_B} \sqrt{G(u_k)} H_n^k(\phi_k) \tag{2.5}$$

The collection of $N_{FFT}$ channel coefficient forms the overall transfer function over the signal bandwidth. Fig. 16 shows a snapshot of this overall transfer function obtained with three overlapping beams having $1, 2, 3,$ 20 paths at the same power level for $N_{FFT} = 2048$. Note that, as desired, frequency selectivity is obtained, which enables our SFSN architecture, at the price of the introduction of channel coding and equalization.

Since the OFDM signal experiences a frequency selective channel, we need to introduce a figure that can represent the effective performance obtained over the entire band. We elect to use the *approximated transfer function*, $\bar{H}$, defined as the average of the absolute values of the channel transfer coefficients:

$$\bar{H} = \frac{1}{N_{FFT}} \sum_{n=1}^{N_{FFT}} |H_n| \tag{2.6}$$

Note that this function is an approximation of the merit figure shown in the following, which is representative of system performance. Fig. 17 shows the effective transfer function for $N_B = 3$, a fixed value for

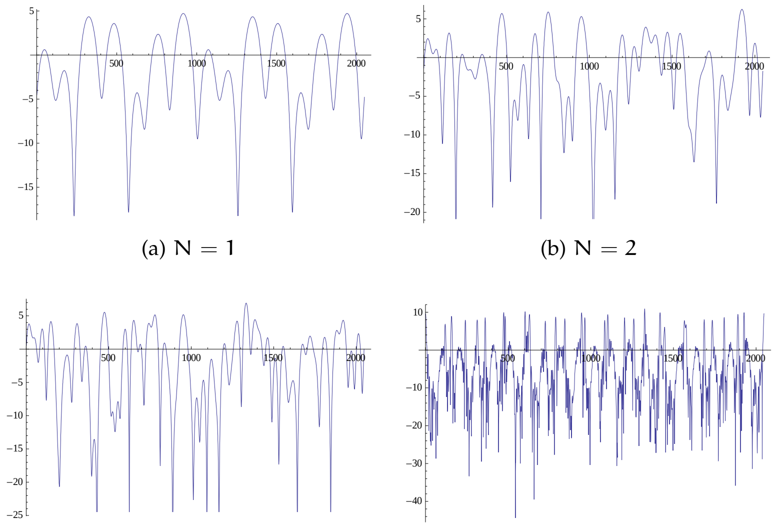

(a) $N = 1$ (b) $N = 2$

(c) $N = 3$ (d) $N = 20$

Figure 16: Overall transfer function for three beams and $N = 1, 2, 3, 20$ paths each beam as a function carrier index.

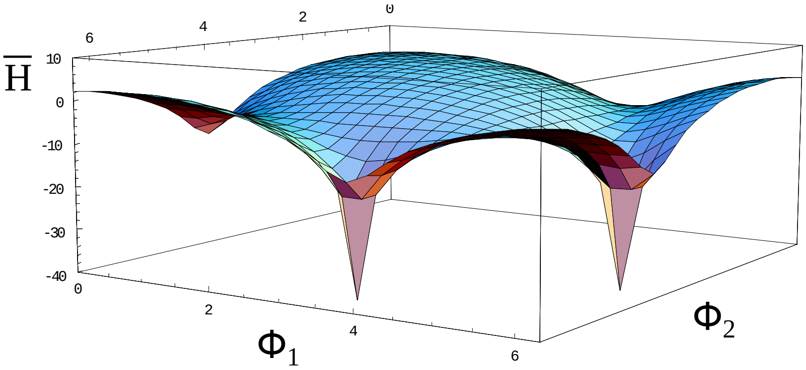

Figure 17: Effective transfer function without MBCDD. Three overlapping beams.

$\phi_3$, and variable $\phi_1$ and $\phi_2$. The overlapping beams are assumed to be at the same power level, without MBCDD. Note that for certain combinations of phases the transfer function of the channel without MBCDD presents deep fades of the effective transfer function, which correspond to a null-capacity zone. On the other hand Fig. 18 shows that these fades are resolved with the introduction of MBCDD, even without a specific optimization procedure, that will be described in the following.

### 2.3.4 *Parameter Optimization*

The optimized design of the delay profile have not only to avoid signal cancellation for any possible phase shift in the coverage area, but also to minimize the fluctuations of the effective transfer function. The worst case in terms of beam overlap is given by the three beam cluster structure. This means that three typical reception conditions have to be analyzed in order to optimize the provided QoS: one beam, two

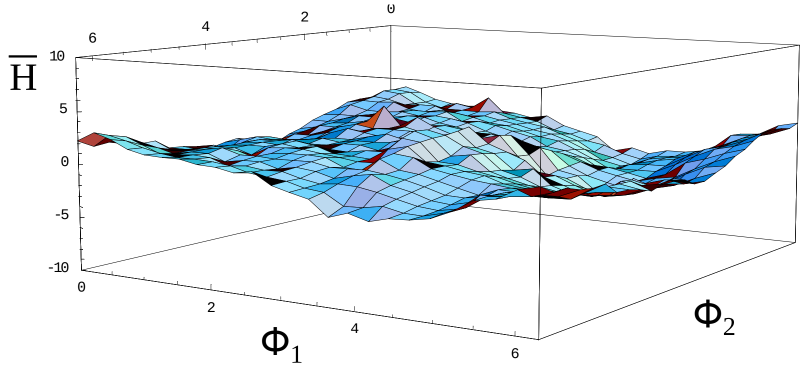

Figure 18: Effective transfer function with MBCDD. Three overlapping beams. Non-optimized parameters.

overlapping beams, and three overlapping beams. Interference coming from the other beams can be neglected. A deterministic or a statistical design can be followed in order to pursue the optimization. To reduce the number of degrees of freedom, it is possible to assume uniform amplitudes, $A_{i,k} = A \, \forall \, i, k$, and equally spaced paths, i.e. $\delta_{i,k} = i \cdot \delta_{0,k}$, under the fundamental requirement $\delta_{0,1} \neq \delta_{0,2} \neq \delta_{0,3}$. Moreover, these three parameters can be optimized through the following expression:

$$\left(\delta_{0,1}, \delta_{0,2}, \delta_{0,3}\right)_{\text{opt}} = \underset{\delta_{0,1}, \delta_{0,2}, \delta_{0,3}}{\operatorname{argmin}} \; \bar{H}_{max} - \bar{H}_{min} \tag{2.7}$$

where

$$\bar{H}_{max} = \max_{\phi_1, \phi_2, \phi_3} \left(\bar{H}\right) \qquad \bar{H}_{min} = \min_{\phi_1, \phi_2, \phi_3} \left(\bar{H}\right) \tag{2.8}$$

It can be shown that best results are obtained when the following three quantities

$$\operatorname{mod}(\delta_{0,1}, N_{FFT}), \operatorname{mod}(\delta_{0,2}, N_{FFT}), \operatorname{mod}(\delta_{0,3}, N_{FFT})$$

are incommensurable. Fig. 19 shows an optimized (flat) effective transfer function with incommensurable delays.

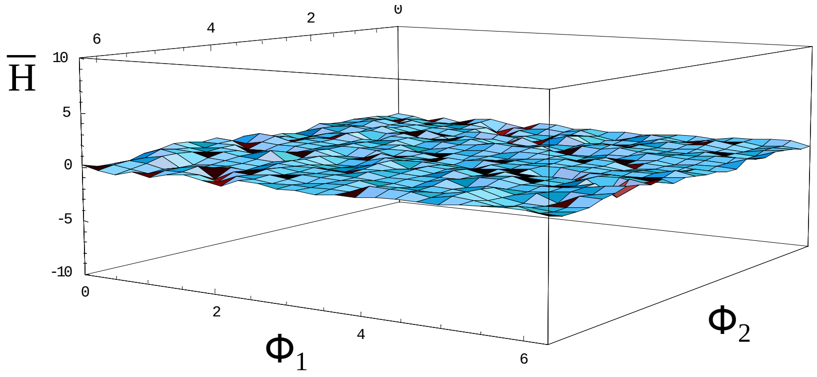

Figure 19: Effective transfer function with MBCDD. Three overlapping beams. Optimized parameters.

## 2.4 SFSN CAPACITY

In this section we introduce the SFSN capacity in information theoretic terms. Let $P/N$ be the signal-to-noise ratio over a sub-carrier that would be experienced by a receiver in the absence of self-interference generated by CDD and with an isotropic antenna. Thus, in any specific location the capacity can be obtained as [7]:

$$C = \sum_{n=1}^{N_a} \log\left(1 + \frac{F_n P}{N}\right) \tag{2.9}$$

where $F_n = |H_n|^2$ for MBCDD, while in the case of a single beam $F_n$ only accounts for the antenna gain at the specific location. This function will be used to assess the performance of a SFSN system.

Now we will use SFSN capacity shown in Eq. (2.9) to provide an initial comparison between the single and multiple beam cases. In order to ensure fairness, the capacity is estimated assuming to have the same Effective Isotropic Radiated Power (EIRP) available in the two cases. This is reasonable because with multiple beams the antenna gain increases but the beam power decreases. A fair comparison is difficult because the geometry of single-beam/multi-beam coverages are quite different. Let us make a simple assumption which favors completely the single beam case, by placing the user at the sub-satellite point for the single beam case and in the middle point of beam-overlapping regions for the multi-beam case. The capacity obtained in these conditions is shown in Fig. 20. Even in this extreme case, it can be seen that the MBCDD capacity is not far from the best case of single beam capacity, which is a good and somewhat unexpected result. The comparison would be even more favorable to MBCDD if the average capacity of the entire service area, or the worst case, would be considered. In any case, it is necessary to optimize the on-board antenna radiation diagram (beam apertures and centers) in order to maximize the flatness and fairness of the received power in the entire region.

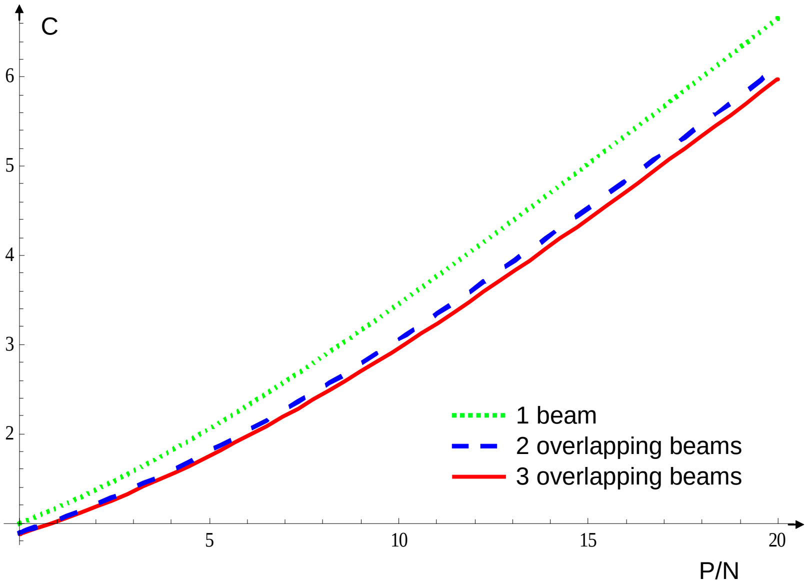

Figure 20: Capacity comparison in the three scenarios: single beam, two overlapping beams, three overlapping beams.

## 2.5 FIRST PROOF OF CONCEPT FOR SFSN

The design of the on-board antenna should be aimed at producing a uniform QoS across the entire service area. We report here a few results obtained in different beam geometry scenarios. The following assumptions have been used:

- $N_{FFT} = 2048$
- Uniform spaced delays, $\delta_i = i \cdot \delta_0$
- Number of multiple paths on each beam $N_i$ equal to 2
- Uniform amplitude delay profile $A_i = A$ within the same beam
- Same amplitude delay profile among different beams, $A_1 = A_2 = A_3$
- Incommensurable delays
- Effective antenna aperture $d_a$ equal to 1.4 m for each beam
- Fixed $\frac{P}{N}$ equal to 7dB
- Service area covered with 6 beams

The analysis has been carried out by discretizing the service area into $51 \times 51$ hexagonal cells and evaluating the capacity in their centers. Moreover, since the capacity behavior is insensitive with respect to the phases $\phi_k$, as shown in Section 2.3.4 for incommensurable delays, a set of random $\phi_k$ has been chosen for the sake of simplicity. As desired, Fig. 21 shows that a constant capacity can be achieved in the interested area, inside the projected internal circle, where the contributions of the six beams allow an extremely uniform QoS; besides, out of the service region the capacity obviously decreases since there are no

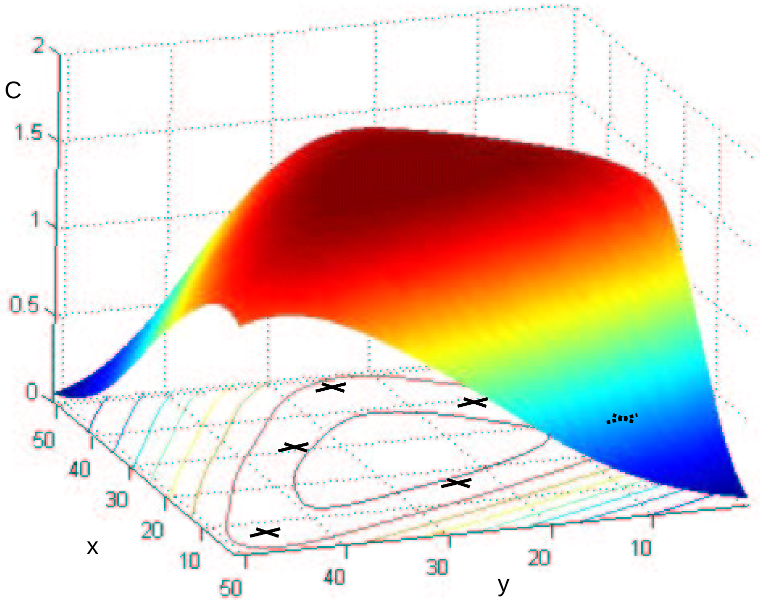

Figure 21: Capacity obtained in an area covered with six beams.

beams covering this area. This capacity shaping is clearly detailed also in Fig. 22. The proposed strategy is easily scalable to a wider service area with several beams which provide a very flat capacity all over it.

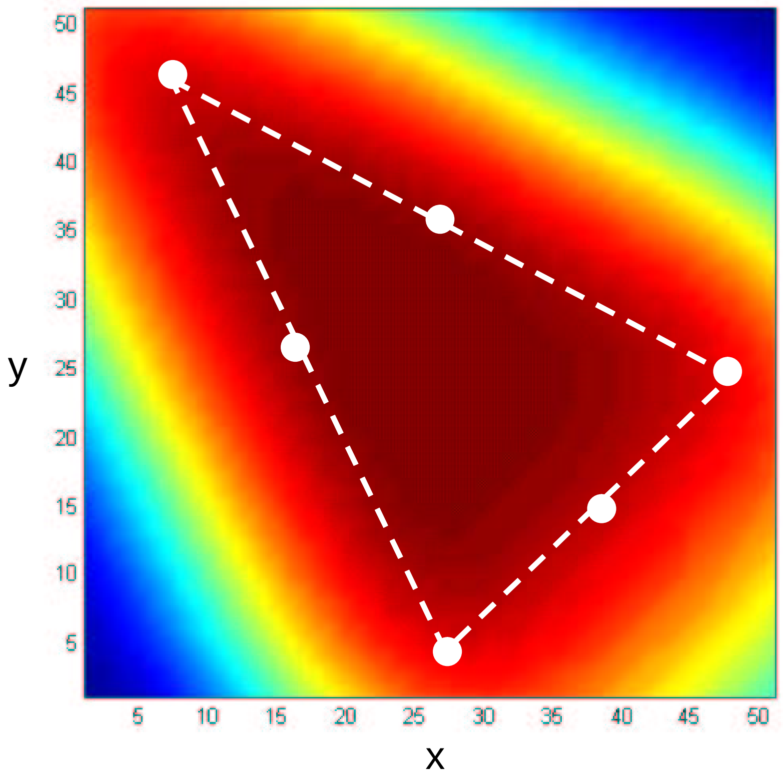

Figure 22: Snapshot of the capacity obtained in an area covered with six beams.

## 2.6 LINK BUDGET ANALYSIS

In the following a link budget analysis is shown for the SFSN concept considering, for comparison, also the single beam case with a single carrier transmission and the single beam with OFDM. Note that the analysis has been conducted for a service in $K_u$ band (carrier frequency equal to 12GHz), but the same evaluation can be carried out for other bands. Moreover, a GEO satellite is assumed.

All the systems have been dimensioned taking into account the best achievable coverage for an area of 650.000 $km^2$ with the same total transmit power. In particular, for the single beam case, the effective antenna diameter of the satellite has been set to obtain the 3dB edge loss on the border of the coverage area. On the other hand, the effective antenna diameter of each beam in the SFSN has been choose according to the considered beam geometry. In any case, in both the systems, all the parameters in Table 1 have been set in order to have the best trade-off between coverage and link budget requirements. Results in Table 1 show that different signal to noise ratios (P/N) are experienced by a receiver using the three systems. In particular, the use of OFDM both in the SFSN concept and in the single beam requires a larger Output Back Off (OBO) with respect to the single carrier approach. On the other hand, the combining of the signals coming from different beams, foreseen by the SFSN concept, can compensate the losses in the link budget. In the

Table 1: Link budget for Single Beam and SFSN systems.

| | **Single Beam** | **OFDM** | **SFSN** |
|---|---|---|---|
| Satellite $T_{sys}$ | 723K | 723K | 723K |
| Satellite Antenna Efficiency | 0.65 | 0.65 | 0.65 |
| Satellite Antenna Diameter | 1m | 1m | 16m |
| Satellite Antenna Gain | 40.11dBi | 40.11dBi | 64.20dBi |
| Satellite OBO | 1dB | 4dB | 4dB |
| Satellite Input Loss | 2dB | 2dB | 2dB |
| Satellite G/T | 11.37dB/K | 11.37dB/K | 35.45dB/K |
| Receiver $T_{sys}$ | 150K | 150K | 150K |
| Receiver Antenna Efficiency | 0.65 | 0.65 | 0.65 |
| Receiver Antenna Diameter | 0.9m | 0.9m | 0.9m |
| Receiver Antenna Gain | 39.20dB | 39.20dB | 39.20dB |
| Receiver G/T | 17.44dB/K | 17.44dB/K | 17.44dB/K |
| Clear Air Atmospheric Loss | 3dB | 3dB | 3dB |
| Frequency | 12GHz | 12GHz | 12GHz |
| Bandwidth | 500MHz | 500MHz | 500MHz |
| Path Loss | 205.10dB | 205.10dB | 205.10dB |
| Number of Beams | 1 | 1 | 400 |
| Transmit Power per Beam | 19.54dB | 19.54dB | −6.48dB |
| Total Transmit Power | 19.54dBW | 19.54dBW | 19.54dBW |
| EIRP | 53.66dB | 50.66dB | 48.72dB |
| **P/N** | 7.60dB | 4.60dB | 2.67dB |

following section, a more complete comparison of the two systems is conducted, using the signal to noise ratios obtained in this analysis.

## 2.7 NUMERICAL EVALUATION

Now we calculate the capacity obtained with the single beam scheme and with the SFSN approach. A vast service area of about 650.000 $\text{km}^2$ has been considered. Note that this value approximately corresponds to a linguistic beam coverage region. The following assumptions have been used for the SFSN system:

- Service area covered with 400 beams organized in a uniform grid $(20 \times 20)$
- $N_{FFT} = 2048$
- Uniform spaced delays, $\delta_i = i \cdot \delta_0$
- Number of multiple paths on each beam $N_i$ equal to 3
- Uniform amplitude delay profile $A_i = A$ within the same beam
- Same amplitude delay profile among different beams, $A_1 = A_2 = ... = A_i = ... = A(400)$
- Incommensurable delays

Note that the analysis has been carried out considering the outputs of Table 1, thus $\frac{P}{N}$ equal to 7.60dB in the single beam single carrier case, 4.60dB in the single beam with OFDM, and 2.67dB in the SFSN. Moreover, the service area has been discretized into $90 \times 90$ hexagonal cells and the capacity has been evaluated in their centers. Finally, since the capacity behavior is insensitive with respect to the phases $\phi_k$, as shown in Section 2.3.4 for incommensurable delays, a set of random $\phi_k$ has been chosen for the sake of simplicity. Fig. 23 shows the capacity comparison between the systems according to the link budget shown in Table 1. As expected, a quasi-constant capacity can be achieved in the interested area, where the contributions of the beams allow an uniform QoS; besides, out of the service region the capacity obviously decreases since there are no beams covering this area. On the other hand, the single beam single carrier approach outperforms SFSN in the zone closer to the center of the coverage area, but results in poorer performance in the zone around the boarder, while the single beam OFDM scheme presents the worst behavior. Note that the proposed strategy is easily scalable also to a smaller or a wider service area, just taking into account the beams position and MBCDD parameters.

## 2.8 SFSN: PROS AND CONS

Let us dwell over the advantages and disadvantages of this approach. As for the main positive aspects, we consider the possibility to: use the same antenna pattern to provide broadcasting and broadband access, for triple play services; deliver efficiently local content and reuse that part of the spectrum extensively; shape precisely and adaptively the contour of beams by grouping spots; use power control selectively over those narrow beams where atmospheric conditions are bad; use a large number of small HPAs instead of a few powerful HPAs for the same total

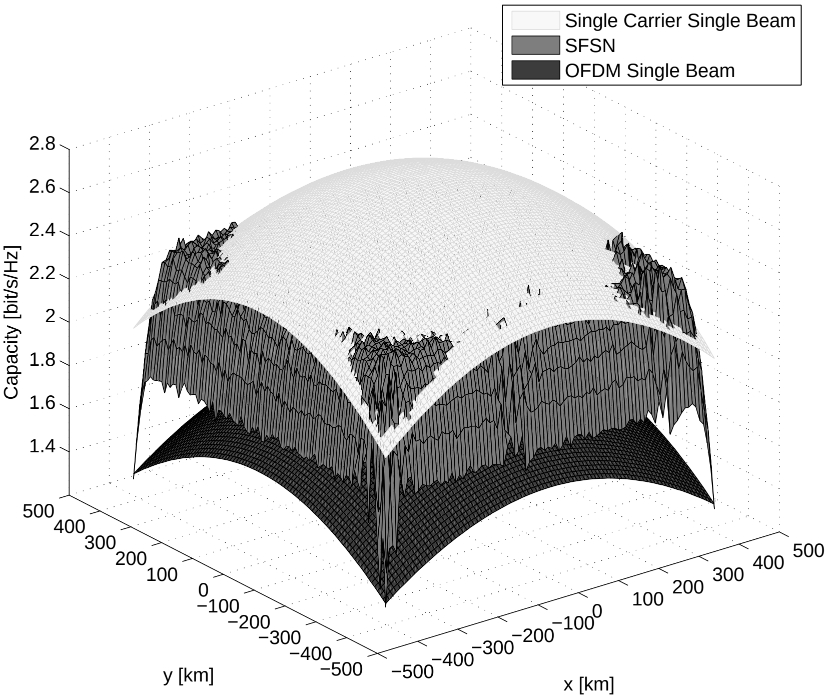

Figure 23: Capacity comparison: SFSN vs. Single Beam Single Carrier.

power, reducing thus the non-linear distortion which usually affects satellite systems. Another advantage is related to the complexity, which is confined on the gateway (for the signal processing) and on the satellite (for the increased number of feeders and HPAs) while the receiver design remains unchanged. Furthermore, the only significant issue related to the scalability is the number of beams, while the spectral efficiency is kept constant. On the down side, the use of OFDM and MBCDD is not as power efficient as conventional single-carrier techniques in the center of the beam, and requires the use of channel equalizers in the receivers. However, this is not a relevant problem, since the equalization is performed in the frequency domain and even a single carrier receivers shall provide at least an Automatic Gain Control (AGC) device in order to have channel equalization.

## 2.9 CONCLUSIONS

This chapter contains a novel approach for multi-spot broadcasting systems via satellite. Relying on the SFN concept and OFDM principles, uniform coverage and QoS can be guaranteed by applying the CDD technique on each beam to eliminate the null-capacity zones by introducing frequency selectivity. A link budget analysis is proposed in order to perform a fair comparison between SFSN and a classical single beam single carrier system. As expected, differently from the single beam, the SFSN system is able to guarantee a flat capacity over the entire service area, at the cost of a correct design of beams position and CDD parameters. However, this design is computed once for all, and involves only the gateway for signal processing and the satellite for beam shaping. No further complexity is required at the receiver. An operator adopting the concept of SFSN will enjoy unprecedented broadcasting flexibility and ease of convergence with broadband services.

# 3

# QUASI-CONSTANT ENVELOPE OFDM

## 3.1 INTRODUCTION

Orthogonal Frequency Division Multiplexing (OFDM) modulation has raised to a de-facto standard in modern wireless communication. This flexible modulation scheme can be efficiently used over frequency selective channels, with effective equalization. One of the drawbacks of OFDM systems, hovewer, is the resilience to non linear distortion, which is considerably inferior to single carrier system. This is due to the envelope fluctuation of the OFDM-modulated signal, which, by a Central Limit Theorem may be approximated by a Gaussian variable.

Several studies have been performed about the impact of non-linearities on Gaussian signals, in particular [15] and [57] gave the basis to analyze the behavior of OFDM system in presence of non linearities. Bussgang [15] stated that the output of a non linear system fed by Gaussian signal can be expressed as a scaled replica of the input and a noise uncorrelated to the input. Minkoff [57] extended this work to complex signal, highlighting the so-called *AM-PM conversion* that is the phase distortion in output signal. Based on these early studies on Gaussian signals, when OFDM started to be applied, its performance on non-linear channels were analyzed, and the large loss in performance due to the distortion can be seen in [5, 4], where the analysis is carried out for Additive White Gaussian Noise (AWGN) and fading channels, respectively. As it can be clearly seen in these reference, the loss from AWGN channels to non-linear channel is considerable, and prevented, for the first period, to apply OFDM modulation on severely degraded channels such as the Land-Mobile-Satellite channel.

Two approaches were considered against non linear distortion: *predistortion* and *Peak-to-Average-Power Ratio (PAPR) reduction*. The first one is more traditional, can be applied even to single carrier systems and consist in providing a predistorter [67], i.e. a block before the High Power Amplifier (HPA) whose aim is to invert the HPA transfer function. In other words, the cascade of predistorter and HPA should be a linear amplifier, at least in the signal dynamic range. This approach is commonly adopted, and its performances are quite interesting if the amplifier is conveniently driven far from its saturation point (an Input Back Off (IBO) of 1 to 3 dB is required for single carrier transmission, while for multicarrier the back off should increase). The second approach is more specific of OFDM system, and consists in reducing the fluctuations of the envelope of the signal. In this way, the transmitted signal should not be damaged too much by the non linear distortion. These techniques, described in [40, 48], can operate in different ways: some technique provide alternative representation of the signal, and make a side information available at the receiver. Other techniques perform operations in order to cancel the peak, using some reserved carriers or modifying the points on their initial constellations. Other techniques are related to coding schemes or to non linear processing on the signal (exponential companding and similars). The main drawback of these family of techniques is the reduction in throughput, or the complexity increase they cause. Using the pervious mentioned methods the PAPR can be kept moderately low, with a reduction of several dB with respect to the original signal. However this PAPR reduction could be not sufficient to guarantee a satisfying OFDM reception in presence of a severe non-linear channel.

Our purpose is to obtain a dramatic PAPR reduction, which yields to an OFDM signals having a quasi-constant envelope, in order to make OFDM reception feasible even in those scenarios characterized by severe non-linearities. In particular, we target to keep the PAPR around $1-2$ dB which corresponds to a reduction of almost ten dB with respect to the original signal. In order to achieve such a ambitious purpose we introduce a novel PAPR technique based on a *open* data mapping which, by exploiting some of its degree of freedom and using an optimization process can guarantee a quasi-constant envelope.

There is a straightforward trade off between the amount of flexibility that the *open* data mapping exploits to reduce the PAPR and the its robustness to gaussian noise, as well as its spectral efficiency. For this reason we also propose some different kind of open data mappings that represents different compromises between PAPR reduction and Gaussian noise robustness.

## 3.2 CONTEXT SYSTEM MODEL

### 3.2.1 *Nonlinear Distortion*

We address the distortion owing to HPA, which acts on both the envelope (AM/AM) and phase (AM/PM) of the OFDM signal. Considering a generic complex nonlinear distortion function the output signal can be expressed as:

$$s_d(t) = F[\rho(t)]e^{j\{\angle s(t)+\Phi[\rho(t)]\}} \tag{3.1}$$

Where $\rho(t)$ and $\angle s(t)$ represent respectively the envelope and the phase of $s(t)$, and $F[\cdot]$ and $\Phi[\cdot]$ represent respectively the AM/AM and AM/PM characteristics. Note that the nonlinear distortion function only depends on the envelope of the input signal.

In its original writing Bussgang Theorem states: *"For two gaussian signals, the cross-correlation function taken after one of them has undergone nonlinear amplitude distortion is identical, except for a factor of proportionality, to the cross-correlation function taken before the distortion."* The mathematical expression of this stated theorem is as follows:

$$< y(t)s_d^*(t) >= \alpha < y(t)s^*(t) > \tag{3.2}$$

where

$$<a(t)>= \lim_{T\to\infty} 1/T \int_{-T/2}^{T/2} a(t)\, dt \tag{3.3}$$

and y(t) and s(t) are gaussian random process. In the particular case of $y(t) = x(t+\tau)$:

$$< s(t+\tau)s_d^*(t) >= \alpha < s(t+\tau)s^*(t) > \quad \forall\tau \tag{3.4}$$

The Bussgang theorem gives us the proof of the separability of a non linear output as the sum of a useful attenuated input replica and an uncorrelated nonlinear distortion, thus we can write the output as:

$$s_d(t) = \alpha s(t) + d(t) \tag{3.5}$$

where

$$< s(t+\tau)d(t) >= 0 \ \forall\tau \tag{3.6}$$

and the complex attenuation coefficient $\alpha$ is given by:

$$\alpha = \frac{< s(t)s_d^*(t) >}{< s(t)s^*(t) >} \tag{3.7}$$

Assuming the ergodicity of $s(t)$, (3.7) can be expressed as:

$$\alpha = \frac{1}{\sigma^2}\left(\int_0^\infty F[\rho(t)]e^{-\jmath\Phi[\rho(t)]}\,\rho(t)\,p(\rho)\,d\rho\right)^* \tag{3.8}$$

where $\sigma^2$ represent the power of $s(t)$, $p(\rho)$ is the Rayleigh probability density function, which characterizes $\rho(t)$, the envelope of $s(t)$, and the conjugates make sense if and only if the nonlinear function has complex values.

Following the tractation in [80], it can be useful to define a scaling parameter $\beta$ such as

$$E[s_d^2] = \beta E[s^2] = |\alpha|^2 E[s^2] + E[d^2] \tag{3.9}$$

and it can be written as

$$\beta = \frac{1}{E[s^2]}\int_0^\infty |F[\rho(t)]|^2 p(\rho)d\rho \tag{3.10}$$

In this way, the power of the useful signal and the distortion noise are $|\alpha|^2$ and $(\beta - |\alpha|^2)$ respectively

The IBO is an important system parameter useful to describe the operating power of the amplifier. It is defined as the ratio between the input saturation power and the actual input average power. Similarly, the Output Back Off (OBO) is defined as the ratio between the output saturation power and the output average power. In formulas

$$\mathrm{IBO} = \frac{P_{in}^{sat}}{\mathbb{E}\left[|s|^2\right]} \tag{3.11}$$

$$\mathrm{OBO} = \frac{P_{out}^{sat}}{\mathbb{E}\left[|s_d|^2\right]} \tag{3.12}$$

Now we considerer a simple Ideal Clipping (IC) Nonlinear Distortion, also known as Soft Limiter, which is the memoryless model corresponding to the ideal case of perfect predistortion. In other words we assume that the predistortion is able to perfectly compensate the non-linearities due to the HPA up to the saturation point. In this case we have a linear transfer function before the saturation zone and an ideal clipping inside the saturation zone, thus its AM/AM and AM/PM characteristics are given respectively by:

$$F(\rho) = \begin{cases} \rho & \text{if } \rho \leqslant A \\ A & \text{if } \rho > A \end{cases} \tag{3.13}$$

$$\Phi(\rho) = 0 \tag{3.14}$$

where A is the saturation amplitude. This model has a normalized gain, which is set to 1 without loss of generality. From (3.8) the coefficient $\alpha$ is given by [27, 62]:

$$\alpha = 1 - e^{-\frac{A^2}{\sigma^2}} + \frac{\sqrt{\pi A^2/\sigma^2}}{2} \operatorname{erfc}\left(\frac{A}{\sigma}\right) \tag{3.15}$$

Similarly, for $\beta$ we have

$$\beta = 1 - e^{-\frac{A^2}{\sigma^2}} \tag{3.16}$$

Saleh model [66] is a common model for Travelling Wave Tube Amplifiers (TWTA), obtained through best-fit of sperimental data. While it may fit every TWTA, a particular choice of its parameters was widely used in analytical studies, leading to the AM/AM and AM/PM characteristics reported below

$$F(\rho) = \frac{2\rho}{1+\rho^2} \tag{3.17}$$

$$\Phi(\rho) = \frac{\pi}{6}\frac{\rho^2}{1+\rho^2} \tag{3.18}$$

This model was normalized in order to have the saturation point in $\rho = 1$. For this reason the input power is supposed to be less than 1 if the amplifier is driven in a fairly nonlinear region of its characteristic.

The calculation of the parameters $\alpha$ and $\beta$ is very difficult for this model. While a closed form expression can be difficult to evaluate, involving special functions such as the exponential integral function, while numerical integration formulas easily led to the following results

| back off [dB] | $\alpha$ | $\beta$ |
|---|---|---|
| 0 | $0.7737 + 0.2172\jmath$ | 0.7708 |
| 0.5 | $0.8233 + 0.2213\jmath$ | 0.8538 |
| 1 | $0.8738 + 0.2245\jmath$ | 0.942 |
| 2 | $0.9767 + 0.2277\jmath$ | 1.133 |
| 3 | $1.081 + 0.2266\jmath$ | 1.342 |
| 4 | $1.183 + 0.2212\jmath$ | 1.563 |
| 5 | $1.283 + 0.2118\jmath$ | 1.793 |
| 6 | $1.377 + 0.1989\jmath$ | 2.026 |

Table 2: Values of $\alpha$ and $\beta$ for the Saleh model.

The values of $\beta$ greater than one can be explained observing the expression of the AM/AM characteristic in Eq. (3.17): if the amplifier is driven in its linear region (i.e. for lower values of r), the power gain of the amplifier is 4, while if the amplifier is driven near to the saturation, the gain obviously decreases.

### 3.2.2 *OFDM signal*

We consider an OFDM signal with N total subcarriers and $N_a$, $N_a < N$, active subcarriers[1]. The $\ell$-th OFDM symbol, $\bar{s}_\ell = (s_{0,\ell}, \ldots, s_{N-1,\ell})$, is obtained as the N points Inverse Discrete Fourier Transform (IDFT) of the vector of complex symbols $\bar{x}_\ell = (x_{0,\ell}, \dots, x_{N-1,\ell})$, as

---

[1] The number of active subcarriers, $N_a$, is chosen so as to respect the spectrum mask, i.e., to introduce guard bands at the edges of the used spectrum band.

$$s_{i,\ell} = \frac{1}{\sqrt{N}} \sum_{k=0}^{N-1} x_{k,\ell} e^{\jmath 2\pi k i/N} \qquad i = 0, \dots, N-1 \tag{3.19}$$

where $x_{k,\ell} = 0$ if $k < N_B$ or $k > N - N_B$, being $N_B = \lfloor \frac{N-N_a}{2} \rfloor$ the number of subcarriers in the guardbands.

In order to avoid intersymbol interference and maintain subcarrier orthogonality even in multipath, a *cyclic prefix* of length $N_g$ samples is inserted at the beginning of each OFDM symbol. This is followed by digital to analogue conversion at sampling rate $R = 1/T$, so that the time continuous signal can be written as

$$s(t) = \frac{1}{\sqrt{T_u}} \sum_{\ell=-\infty}^{\infty} \text{rect}\left(\frac{t}{T_L} - \frac{1}{2} - \ell\right) \sum_{k=0}^{N-1} x_{k,\ell} e^{\jmath 2\pi \frac{1}{T_u} k (t - T_g)} \tag{3.20}$$

where $T_u = NT$ represents the OFDM useful symbol duration, $T_g = N_g T$ represents the duration of the guard interval associated to the cyclic prefix, therefore $T_L = T_u + T_g$ is the total OFDM symbol duration, and $f_u = 1/T_u$ is the subcarrier spacing.

If N is sufficiently large, the signal $s(t)$ expressed in (3.20) can be considered as a Gaussian complex random process as a consequence of the central limit theorem. Bussgang's theorem guarantees that the signal $s_d$ after the nonlinear distortion, can be split in two terms: a linear term that is proportional to $s(t)$ according to a constant $\alpha$, and a nonlinear distortion term, $d(t)$, that is a zero-mean (not Gaussian) process uncorrelated from $s(t)$:

$$s_d(t) = \alpha s(t) + d(t) \tag{3.21}$$

In this case it is interesting to define a merit figure, the Signal-to-Distortion Ratio (SDR), which describes the impact of signal scaling and additive distortion noise. Assuming $\mathbb{E}[|s(t)|^2] = 1$ we have:

$$\text{SDR} \doteq \frac{|\alpha|^2}{\mathbb{E}[|d(t)|^2]} \tag{3.22}$$

The OFDM signal, $s_d(t)$ is transmitted over a time-varying frequency selective fading channel, under the assumption that the channel coherence time exceeds $T_L$. The baseband equivalent channel impulse response is modeled as a tapped delay line:

$$h(t) = \sum_{j=0}^{N_m - 1} h_j(t) \delta\left(t - \tau_j(t)\right) \tag{3.23}$$

where $h_j(t)$ and $\tau_j$ are respectively the gain and delay of the j-th path, and $N_m$ represents the number of multiple propagation paths. In Rayleigh fading, at any time instant $h_j(t)$ can be modeled as a complex Gaussian random variable with zero mean and variance $\gamma_j^2/2$ per branch. The total channel energy is normalized to one, i.e. $\sum_j E[h_j^2] = \sum_j \gamma_j^2 = 1$, and the maximum delay is assumed to be smaller than the guard interval duration, i. e. $\tau_{max} = \max_j \tau_j < T_g$. The received signal can be written as

$$r(t) = h(t) * (\alpha s(t) + d(t)) + n(t) \tag{3.24}$$

where $n(t)$ represents a Complex AWGN random process, with two-sided power spectral density equal to $N_0$. Filtering and sampling the received signal every T seconds yields

$$r(uT) = \sum_j h_j(uT) \cdot \alpha s(uT - \tau_j) + d(uT - \tau_j) + n(uT) \tag{3.25}$$

Removing the guard interval and re-arranging the vector at the input of the Fast Fourier Transform (FFT), the samples belonging to the $\ell$-th OFDM symbols can be collected into a vector $\bar{r}_\ell$ with components:

$$\begin{aligned} & r_{i,\ell} = r(((\ell-1)(N+N_g)+N_g+i)T) \\ & i = |u|_{N+N_g} - N_g \qquad \ell = \lceil u/(N+N_g) \rceil \end{aligned} \tag{3.26}$$

Assuming that $h_j(t)$ remains constant over a OFDM symbol duration, at the output of the FFT, in the frequency domain, the OFDM symbol is:

$$y_{k,\ell} = \frac{1}{\sqrt{N}} \sum_{i=0}^{N-1} r_{i,\ell} \cdot e^{-\jmath 2\pi k i/N} \tag{3.27}$$

$$= H_{k,\ell}(\alpha x_{k,\ell} + D_{k,\ell}) + n_{k,\ell} \quad k = 0, \ldots, N-1 \tag{3.28}$$

where according with (3.19) Discrete Fourier Transform (DFT) normalization factor $\frac{1}{\sqrt{N}}$ has been taken into account, $n_{k,\ell}$ is the complex AWGN sample in frequency domain, and $H_{k,\ell}$ is the at the subcarrier $k$, in the $\ell$-th symbol:

$$H_{k,\ell} = \frac{1}{\sqrt{N}} \sum_{j=0}^{N-1} h_j e^{-\jmath 2\pi k \tau_j / T_u} \tag{3.29}$$

## 3.3 ROTATION-INVARIANT SUBCARRIER MAPPING

### 3.3.1 *Constellation design*

We introduce a novel concept for subcarriers data mapping where the symbols belonging to the modulation alphabet are not anchored, but they maintain some degree of freedom, for this reason we refer to it as *open* data mapping. The final positions of the transmitted complex symbols are chosen by an iterative optimization process that arranges them in order to decrease the resulting OFDM symbol PAPR.

The first open mapping scheme we propose is a very easy two-order data mapping, illustrated in figure 24, where the bit '0' is mapped in zero and the bit '1' can be mapped in any points of the belonging to the circle with radius $\sqrt{2E_b}$ and centered in zero. In formulas, the data mapping is

$$x_k = \begin{cases} 0 & \text{if } b_k = 0 \\ \sqrt{2E_b} e^{\jmath \phi_k} & \text{if } b_k = 1 \end{cases} \tag{3.30}$$

where $b_k$ is the $k$-th bit to be mapped, and the values of $\phi_k$ will be optimized according to the algorithm described in following.

### 3.3.2 *Spherical Active Constellation Extension (ACE)*

This algorithm arranges the phases $\phi_k$ in order to decrease the resulting OFDM symbol PAPR. It works alternating time and frequency domain,

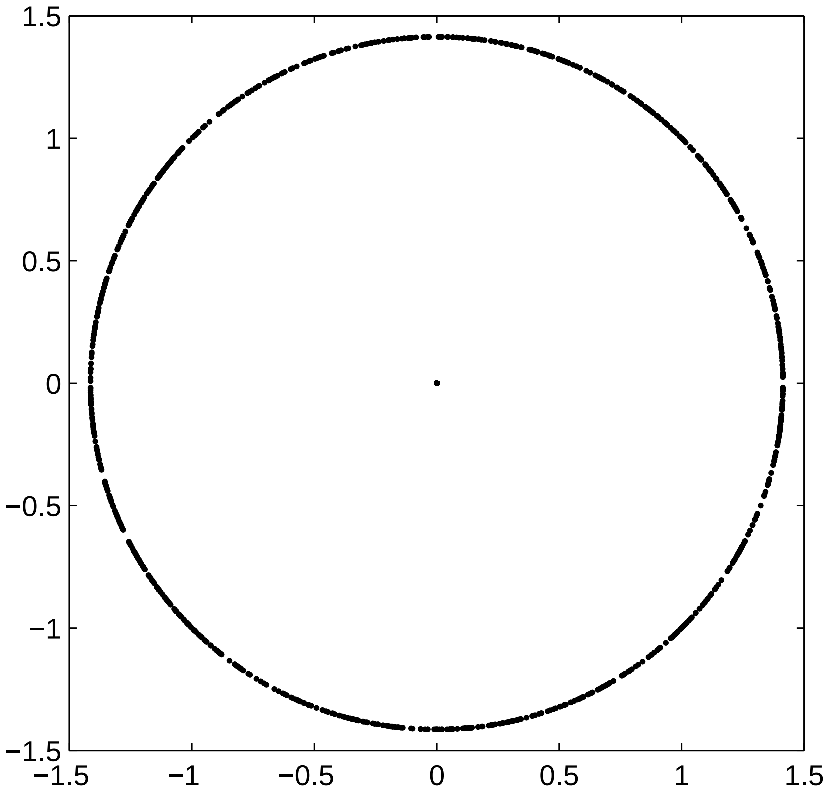

Figure 24: Circularly simmetrical constellation.

and its parameters are the number of iteration $N_{iter}$, and the threshold, $\xi$, used in clipping the signal. This iterative algorithm works alternately in time and frequency domain as follows:

- First, the time domain samples $s_i$ whose absolute value exceeds the threshold $\xi$ are clipped.
- Then, passing to frequency domain, the complex data $x_k$ are reinstated at the zero or on the circumference modifying only their absolute values. In this manner the constellation constraints are restored.
- Subsequently, in the time domain, the samples $s_i$ are clipped again, then the constellation constraints are restored. These operation are repeated $N_{iter}$ times.

This procedure converges, because it can be seen as a projection onto a convex set, and it will converge to a signal with the lowest possible PAPR. This algorithm is an original extension of the ACE method used in traditional PAPR reduction techniques [52]. The main difference is that the Spherical ACE move the complex data $x_k$ only acting on their phase. In this way the energy of each complex data $x_k$ remains constant, and the distance among the points of constellation in equal.

### 3.3.3 *Extensions*

Some further extension of this approach are possible, in order to increase the spectral efficiency or the resilience to the AWGN. For instance, a straightforward extension of the aforementioned technique requires the origin and three rings to map two information bits. Another open mapping scheme which provides spectral efficiency of 2 bit/channel and ensures an increased distance between points, is the so-called *clover* mapping, depicted in figure 25. Unfortunately in this case Gray-mapping is not applicable. In formulas, the data mapping is described

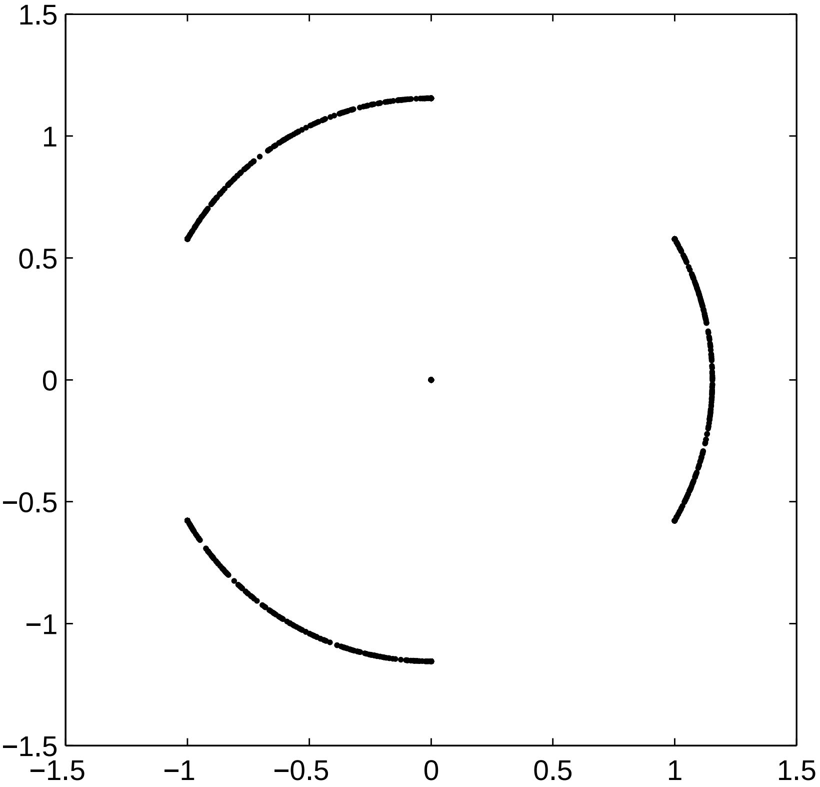

Figure 25: Clover constellation.

by Eq. (3.31)

$$x_k = \begin{cases} 0 & \text{if } \bar{b}_k = 00 \\ \sqrt{\frac{4}{3}E_s}\jmath^{\phi_k}, & \phi_k \in \left[-\frac{\pi}{6}, \frac{\pi}{6}\right] \text{if } \bar{b}_k = 01 \\ \sqrt{\frac{4}{3}E_s}\jmath^{\phi_k}, & \phi_k \in \mathcal{U}\left[\frac{\pi}{2}, \frac{5\pi}{6}\right] \text{if } \bar{b}_k = 10 \\ \sqrt{\frac{4}{3}E_s}\jmath^{\phi_k}, & \phi_k \in \mathcal{U}\left[-\frac{5\pi}{6}, \frac{\pi}{2}\right] \text{if } \bar{b}_k = 11 \end{cases} \tag{3.31}$$

## 3.4 AWGN DETECTORS

In this section, first we propose the detection scheme for our open data mappings, and secondly we analyze the performance of the proposed mapping schemes. The analytical assesment hereby presented is based on a simple AWGN channel. This is convenient for analytical simplicity and does not affect the generality of the discussion, since the effect of the HPA distortion can be modeled as a scaling of the useful signal and an additional noise source. Under these assumptions equation (3.27) becomes

$$y_{k,l} = x_{k,l} + n_{k,l} \tag{3.32}$$

where $n_{k,y} \sim \mathcal{N}(0, N_0/2)$ represents the AWGN term. For the first mapping scheme presented in Section 3.3.1 and described by equation (3.30) the envelope of the received signal can be modeled as a Rayleigh random variable if $b_k = 0$ and a Rice r.v. if $b_k = 1$. Letting $\rho_y$ be the envelope of the received signal, we have

$$p_{\rho_y}(\rho_y) = \begin{cases} \frac{2\rho_y}{N_0}{}^{-\frac{2\rho_y^2}{N_0}} & \text{if } b_k = 0 \\ \frac{2\rho_y}{N_0}{}^{-\frac{\rho_y^2+2E_b}{N_0}} I_0\left(\frac{2\rho_y\sqrt{2E_b}}{N_0}\right) & \text{if } b_k = 1 \end{cases} \tag{3.33}$$

where we have dropped the subscript $l$, for the sake of readability. The energy detector can be efficiently employed for this problem: the randomness of the phase due to spherical ACE inhibits the use of a coherent detector, and the energy detector is both robust and simple. The threshold $\xi$ on the received signal can thus be calculated by the Maximum Likelihood (ML) criterion (equal symbol a priori probability and equal cost of the errors), leading to the following non linear equation

$$p_{\rho_y|b_k=1}(\xi|b_k = 1) = p_{\rho_y|b_k=0}(\xi|b_k = 0) \tag{3.34}$$

whose solution can be found numerically. Once the value for the threshold $\xi$ is obtained, the error probability can be written as

$$\begin{aligned} P_e &= \frac{1}{2}\int_0^{\xi} p_{\rho_y|b_k=1}(\rho_k|b_k = 1)d\rho_k + \frac{1}{2}\int_{\xi}^{\infty} p_{\rho_y|b_k=0}(\rho_k|b_k = 0)d\rho_k \\ &= \frac{1}{2}e^{-\frac{2\xi}{N_0}} + \frac{1}{2}\left[1 - Q_1\left(2\sqrt{\frac{E_b}{N_0}}, \xi\sqrt{\frac{2}{N_0}}\right)\right] \end{aligned} \tag{3.35}$$

where $Q_1(a, b)$ is the Marcum-Q function [1]. In the case of a transmission impaired by a distorting HPA, the noise term must include also the effect of the HPA (the term $D_{k,l}$) in equation 3.27

The performances of the proposed detector are shown in figure 26

The Clover constellation detection problem is analytically involved, since it would require a perfect knowledge of the phase distribution after the Spherical ACE routine. This knowledge will be necessary to define the likelihood functions related to the four different symbol hypotheses. Since the phase distribution is almost impossible to determine in an analytical fashion, and it depends strongly on the clipping thresholds, we preferred to employ an sub-optimal detector, rather than to postulate a model for the phase distribution.

In our approximate model the detection is performed in two steps: in the first the central symbol is separated out of the 3 symbols lying on the external ring. In this stage an energy detector is again employed, but it has a different threshold with respect to the case of the Saturn Modulation, due to difference in both signal amplitude and probability of the outer ring. Once this first detection has been performed, in case the signal is supposed to belong to the outer ring, a phase detector is employed. Summarizing, figure 27 reports the decision regions, while figure 28 shows the performance of this sub-optimal detector on the AWGN channel

## 3.5 NUMERICAL RESULTS

The first result in Fig. 29 we present is the Complementary Cumulative Density Function (CCDF) of the PAPR distribution for the modulation

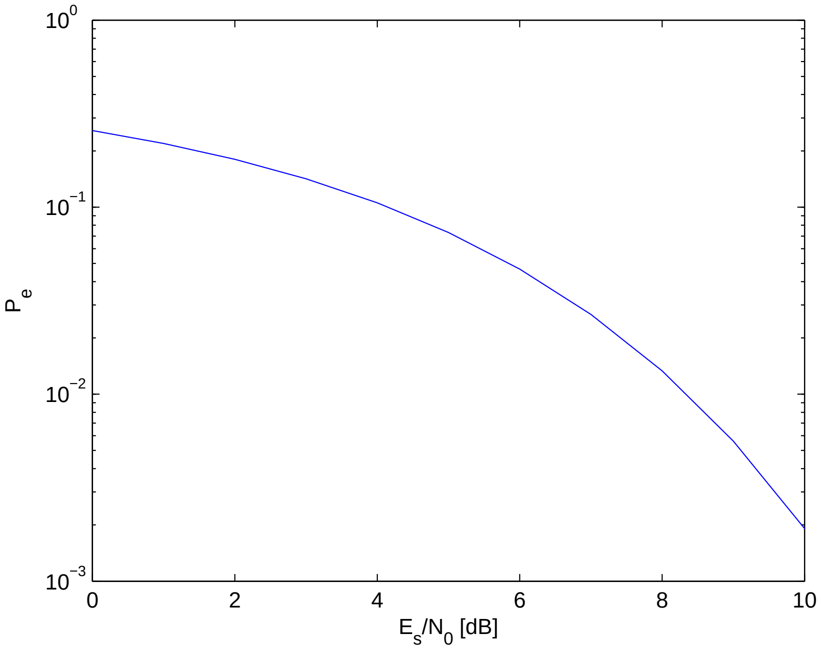

Figure 26: Error Probability of Two Level Mapping.

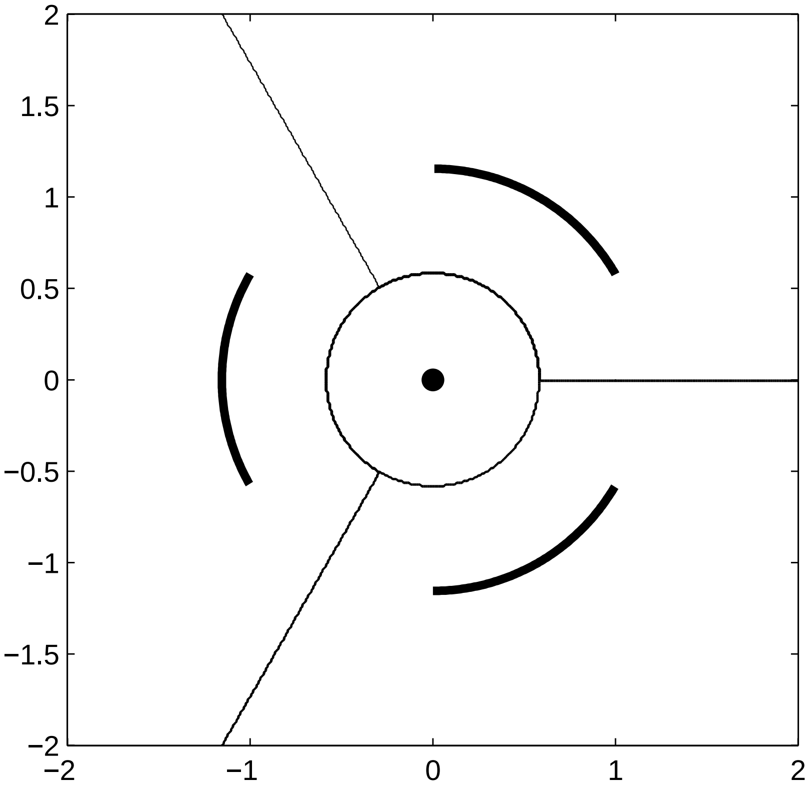

2
1.5
1
0.5
0
−0.5
−1
−1.5
−2
−2
−1
0
1
2

Figure 27: Decision Regions for Clover Mapping.

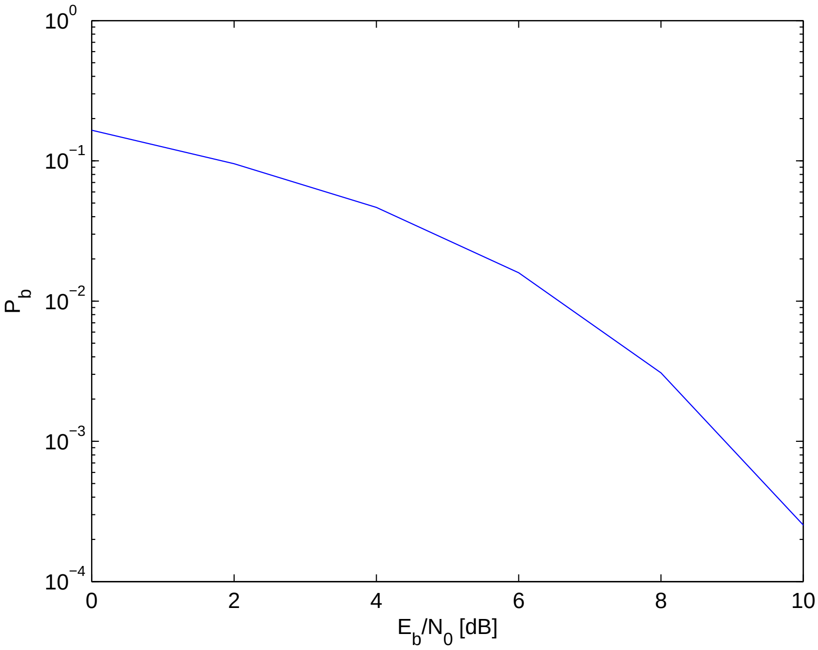

Figure 28: Bit Error Probability for Clover Mapping.

scheme introduced in the previous sections. Although the PAPR reduction offered by ACE is surely significant, our proposed mappings can achieve a quasi constant envelope, resulting in a very low PAPR.

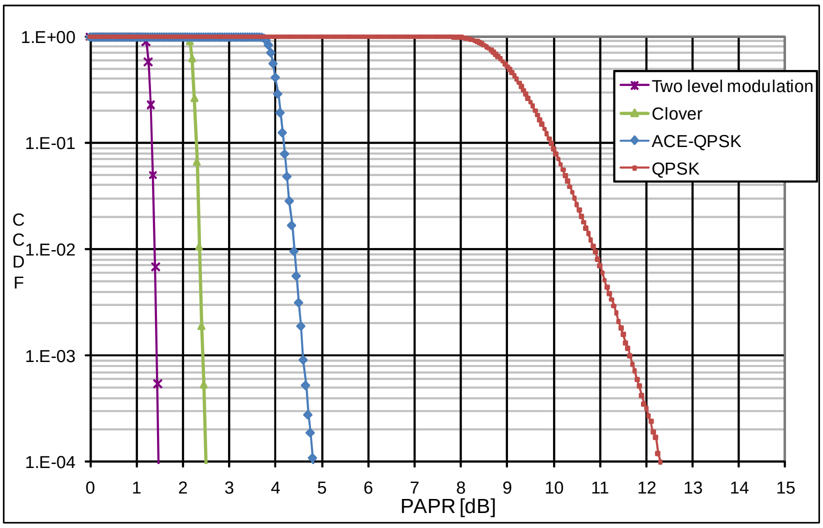

Figure 29: PAPR distribution for Two level and Clover Mappings.

The impact of such a low PAPR is highlighted by Fig. 30,31: our proposed schemes achieve the best performances in terms of SDR over a strongly non-linear channel (the IBO for both Saleh and IC HPAs is lower than 1)

Finally, Fig. 32,33 show the impact in terms of Bit Error Rate (BER) of the excellent PAPR reduction achieved by our proposals. As the figures show, the PAPR reduction does not directly translate into a BER improvement. However, our scheme allow to communicate reliably over

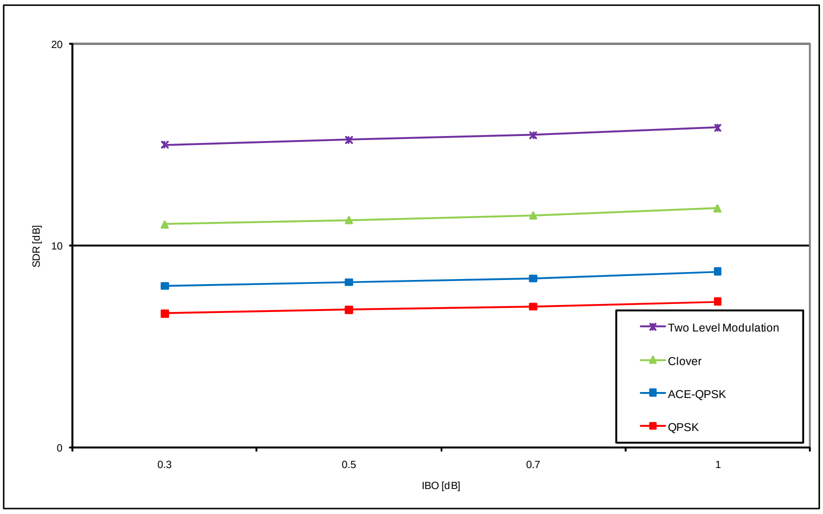

Figure 30: SDR on Saleh HPA vs IBO for the proposed mappings.

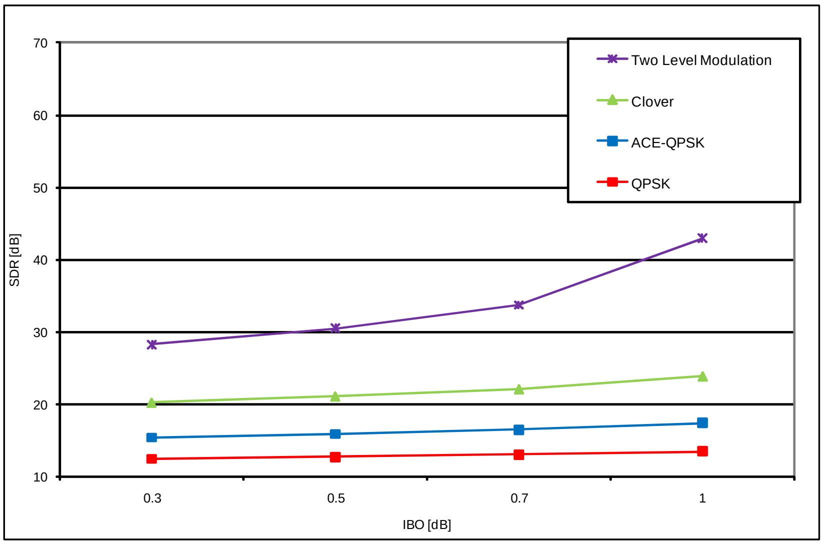

Figure 31: SDR on IC HPA vs IBO for the proposed mappings.

a strongly non-linear channel,such as a Saleh HPA with an IBO equal to 0 dB.

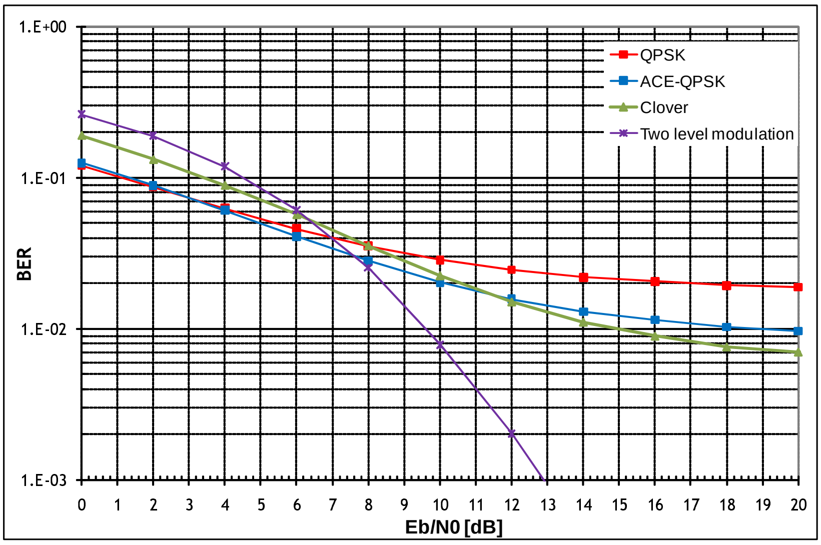

Figure 32: BER on Saleh HPA at IBO = 0 dB for the proposed mappings.

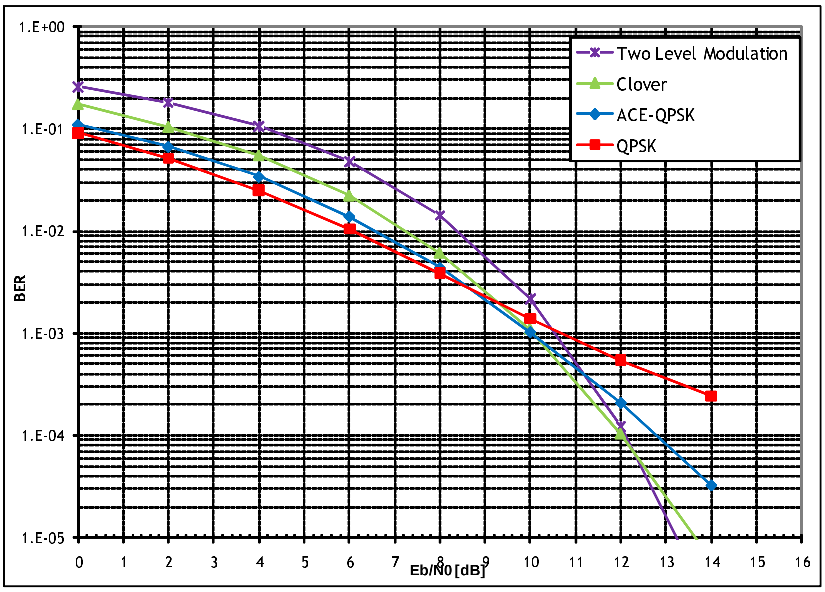

Figure 33: BER on IC HPA at IBO = 0 dB for the proposed mappings.

## 3.6 CONCLUSIONS

This chapter presented a novel concept for data mapping. Using rotationally invariant sub-carrier mapping we are able to reduce dramatically the PAPR, allowing thus to receive reliably over strongly non-linear channels. Our approach is based on a iterative optimization routine, which is an original broadening of the ACE method [52]. The innovation we proposed is in the active role of the symbol phases to effectively reduce the PAPR.

# 4

# FURTHER DEVELOPMENTS OF THE PRESENTED WORK

There are various possible developments for the work presented in this thesis. This final chapter recollects some of the future directions in which the research in the field of Physical Layer (PHY) optimization for Orthogonal Frequency Division Multiplexing (OFDM) systems will continue.

Multicarrier modulation, although already adopted in various transmission standards, has further room for improvements. First of all, the optimization of payload and pilots is an interesting area, now dominated by "rules of thumb" or "separate boxes" optimization of all receiving circuits. Secondly, the next years will see the adoption of multicarrier modulations in almost all possible scenarios. Therefore new methods are to be found to enhance the resilience of this waveform, or to increase the spectral efficiency. In this future scenario, the efforts on Single Frequency Satellite Networks and on Quasi-constant Envelope OFDM will be surely continued.

For the first case, i. e. Single Frequency Satellite Network (SFSN), the reuse of mobile satellite services bands is indeed a real problem, and the adoption of a SFSN would be of great utility. At any rate, the next possible study on SFSN should be an end-to-end simulation, including channel estimation and synchronization issues. We expect to see an obvious performance loss with respect to the ideal case, however we believe that the advantages of SFSN will be fully confirmed.

The resilience of OFDM to non-linearities is another topic that needs further investigations: the present approach to cope with this problem is to use more robust subcarrier mappings (i. e. Quaternary Phase Shift Keying (QPSK) rather than high order Quadrature Amplitude Modulation (QAM)) and to reduce the code rate. On the contrary, we believe that the OFDM waveform can be modified and improved, in order to achieve a more than satisfactory trade off between the reduction of the signal dynamics (and thus the increase of the signal robustness to non-linearities) and the Quality of Service (QoS) at the receiver.

Summarizing, the world is still going wireless, and the PHY research is not dead, notwithstanding all the catastrophic announcements on this regard which were given in the last decades. The extension of wideband signal to very harsh scenarios offers a lot of challenges, which will be accepted and solved by a mixture of creativity and technical knowledge.

# Part II

# INNOVATIONS IN SINGLE CARRIER SYSTEMS

# 5

# OPTIMIZATION OF CONSTELLATIONS OVER NON-LINEAR CHANNELS

## 5.1 INTRODUCTION

The non-linear satellite channel has been extensively studied in the literature, mainly through numerical evaluation, at least for those cases in which the High Power Amplifier (HPA) characteristics are only given empirically. However, analytical approaches to the optimization of signal constellations appear to be an interesting problem that needs to be addressed and can in fact be exploited in system design and air-interface definition.

In this chapter we will introduce an analytical approach for the optimization of signal constellations for the satellite channel, or more generally, for a noisy and non-linear channel, under the constraint of normalized constellation energy. Among all of the possible definitions of optimality, we consider the minimum average error probability criterion, that is, the optimal constellation leads to the minimum mean error probability under the assumption of using a maximum likelihood detector. As a consequence, the optimal constellation is the one which, for a given transmitted power, maximizes the mutual distance amongst constellation points.

Let

$$\{s_i\}, \quad i = 1 \dots M \tag{5.1}$$

be the constellation points, where $s_i \in \mathbb{C}$ and $M$ is the constellation cardinality, and let the constellation be normalized to unit average energy, i.e.

$$\frac{1}{M}\sum_{i=1}^{M} |s_i|^2 = 1 \tag{5.2}$$

The problem consists in finding optimal positions for the points. Foschini et al. in [35] proved that in a Additive White Gaussian Noise (AWGN) channel the optimal signal constellation, for increasing cardinality, tends to a triangular lattice, and showed that the optimum 16-point constellation gains 0.5dB in Signal-to-Noise Ratio (SNR) with respect to 16-Quadrature Amplitude Modulation (QAM). The problem of finding the optimal signal set was handled also by Kearson [39, 50], who released the assumption of Gaussian noise, finding the optimal signal constellation for various noise distributions. Due to the presence of non-linear distortion the above results cannot be readily applied to the satellite channel.

The effect of non-linear amplification on signal transmission are various: first of all, a rotation of the whole signal set is observed (AM-PM conversion). Constellation points are also more near each other, due to the saturation in the amplifier (warping). Lastly, clustering phenomenon appears, which consists of receiving a cluster of points instead of a single constellation point. This is due to non-linear processing of transmitted pulses and to the consequent violation of Nyquist condition for Inter-Symbol Interference (ISI) avoidance at the receiver.

There are various approach to model the satellite channel with distorting amplifier. A complete and analytic tool is given by Volterra series (see [9] or [10] for an example of application). The Saleh model [66] allows to determine analitically the constellation rotation and warping, while the evaluation of clustering must be performed through computer simulations. The approach used in [60] and [61], that is to consider the channel free from ISI, could be difficult to adapt in typical satellite transmission, considering the importance of filtering in order to reduce Adjacent Channel Interference (ACI). Our method follows a more realistic approach: the constellation rotation and warping is modeled according to Saleh [66], while the clustering is modeled as another additive white Gaussian noise. This simplified approach can be theoretically justified by Central Limit Theorem if the duration of transmitted pulse is significantly longer than symbol time, and has the advantage of requiring less simulation time and allowing to use formulas for error probability in AWGN, with the necessary corrections due to the warping.

The exact calculation of the error probability for complex signal constellations is still an open problem. It can be solved numerically, for example by the technique of decomposing decision region proposed in [24] or in [74], but a closed form solution, for a general constellation, is lacking. Various upper and lower bounds have been proposed in the last decades. The *Union Bound* is the simpler version of the Bonferroni inequality ([22, Chap. 2]) approach, and becames increasingly tighter for increasing SNR. High order Bonferroni inequalities are too computationally expensive, so other approaches have been preferred: Seguin [69], Kuai et al. [54] have proposed new forms of lower bounds, Poscetti [65], Hughes [44] and Swaszech [73] have proposed upper or lower bound based on a geometrical approach, but such a method is not suitable for analytic optimization. Thus the *Union Bound* is a good candidate for calculating error probability, because it is a good compromise between complexity and accuracy, for its analytical origin, and for the fact that an upper bound is a more conservative approach to our problem, and in general to communication systems design.

Summarizing, we aim at finding the constellations which yield the best performance over a noisy and nonlinear channel, and the method we propose is to optimize the constellation point positions by a gradient method, using as objective function the expression of symbol error probability given by the *Union Bound*

The rest of this chapter is structured as follows: Section 5.2 presents the system model and the probability of error for such a system. Section 5.3 describes the used algorithm and discusses its performance. Results are shown in Section 5.4 and the conclusion are presented in Section 5.5

## 5.2 SYSTEM MODEL

### 5.2.1 *Received Signal*

We consider a simplified two-dimensional M-ary synchronous data transmission, in which the message, mapped in a symbol from the constellation in Eq. (6.1), say the i-th, is processed by a pulse-shaping filter and a non-linear amplifier, is then transmitted through an AWGN channel, and, at the receiver, it undergoes matched filtering and sampling. Assuming ideal recovery of carrier phase and frequency, and of timing offset, the expression of the signal which is fed to the decision device at the k−th symbol time is

$$r_k = \sqrt{Es} \cdot c_{i,k} + \mu_k + \nu_k \tag{5.3}$$

where

$$\mu_k = \mu_{p,k} + j\mu_{q,k}, \quad \mu_{p,k}, \mu_{q,k} \sim \mathcal{N}(0, \frac{N_A}{2}) \tag{5.4}$$

is the noise due to nonlinear pulse processing, whose variance $N_A$ can be obtained experimentally, or via the method indicated in [9], and

$$\nu_k = \nu_{p,k} + j\nu_{q,k}, \quad \nu_{p,k}, \nu_{q,k} \sim \mathcal{N}(0, \frac{N_0}{2}) \tag{5.5}$$

is the AWGN term having variance $N_0/2$ per component. Both Gaussian processes are supposed to be white, and, for the interference contibution, we will omit its dependence from the constellation symbols, assuming thus a worst-case approach. Finally, $c_i$ is a point of the distorted constellation, whose value can be obtained from the original signal point $s_i$, characterizing the amplifier with the Saleh model [66]

$$c_i = \frac{1}{\sqrt{\sum_{j=1}^{M} |s_{j,d}|^2}} s_{i,d} e^{\jmath \phi_{i,d}} \tag{5.6}$$

where

$$s_{i,d} = \frac{2\sqrt{\beta}|s_i|}{1 + \beta|s_i|^2} \tag{5.7}$$

$$\phi_{i,d} = \frac{\pi}{3} \frac{\beta|s_i|^2}{1 + \beta|s_i|^2} \tag{5.8}$$

and $\beta$ is the Input Back Off (IBO), an indication about how far the amplifier is driven off saturation.

### 5.2.2 *Error Probability*

In this section we will determine the average symbol error probability, assuming equiprobable signalling, and using the *Union Bound*, for the ease of analytical tractability.

The average symbol error probability can be written as:

$$P_e = \frac{1}{M} \sum_{i=1}^{M} P_e(s_i) \tag{5.9}$$

where the last term is the conditional probability of error when symbol $s_i$ is transmitted, and can be upper bounded by:

$$P_e(s_i) \leqslant \sum_{\substack{j=1 \\ j \neq i}}^{M} \text{Prob}\left(\hat{s}_j | s_i\right) \tag{5.10}$$

The last term, $\text{Prob}\left(\hat{s}_j | s_i\right)$, the probability of deciding for $s_j$ when $s_i$ was transmitted, can be expressed as

$$\text{Prob}\left(\hat{s}_j | s_i\right) = \text{Prob}\left(\left\| r - \sqrt{E_s}\, c_j \right\| \leqslant \left\| r - \sqrt{E_s}\, c_i \right\|\right) \tag{5.11}$$

where we have assumed that the receiver knows the distorted constellation and the carrier phase was ideally recovered.

Recalling the properties of Gaussian variables, the expression for the error probability is

$$P_e \leqslant \frac{1}{M}\sum_{i=1}^{M}\sum_{\substack{j=1\\j\neq i}}^{M}\frac{1}{2}\mathrm{erfc}\left(\sqrt{\gamma}\frac{\left\|c_j-c_i\right\|}{2}\right) \tag{5.12}$$

where $\gamma = \frac{E_s}{N_A+N_0}$.

## 5.3 PROPOSED ALGORITHM

### 5.3.1 *Description*

The upper bound for the error probability written above, which depends on the signal constellation, can be used as the objective function in a constrained optimization problem. Solving the constrained optimization problem via an iterative gradient method yields the optimal constellation point displacement, constrained to have unit average energy

The algorithm used to optimize constellation is composed of the following steps:

1. Non-linear distortion application, obtaining $\{s_{i,d}e^{\jmath\Phi_{i,d}}\}, \quad i = 1\ldots M$
2. Normalization of constellation, obtaining $\{c_i\} \quad i = 1\ldots M$
3. Calculation of $\nabla P_e : [\nabla P_e]_k = \frac{\partial P_e}{\partial c_k}$
4. Constellation update: $s_k = s_k - \alpha\,[\nabla P_e]_k$
5. Constellation normalization $\{s_i\}, \quad i = 1\ldots M$
6. Apply stopping rule or iterate

The stopping rule could be the reaching of a maximum number of iterations, or the convergence of the solution (i.e. the constellations between two consecutive iteration differ for a given small value) The output of this procedure is the constellation that, on a noisy non-linear channel yields the lowest error probability. That is, the constellation that after the distortion preserves the distance between points.

The critical step which requires detailed mathematical consideration is the calculation of $\nabla P_e$ for the distorted constellation $\{c_i\}$. Considering the $i$–th component of the gradient, we have:

$$[\nabla P_e]_i = \frac{\partial P_e}{\partial c_i} \tag{5.13}$$

$$= \frac{1}{M}\sum_{\substack{j=1\\j\neq i}}^{M}\frac{\partial}{\partial c_i}\mathrm{erfc}\left(\sqrt{\gamma}\frac{\left\|c_j-c_i\right\|}{2}\right) = \tag{5.14}$$

$$= \frac{1}{M}\sum_{\substack{j=1\\j\neq i}}^{M}\frac{2}{\sqrt{\pi}}e^{-\frac{\gamma\left\|c_j-c_i\right\|^2}{4}}\frac{\sqrt{\gamma}}{2}\overline{1}\left[c_j-c_i\right] \tag{5.15}$$

where $\overline{1}(c_j - c_i)$ is a unit vector applied in $c_i$ and making an angle with the x-axis equal to arg $\left\{c_j - c_i\right\}$.

### 5.3.2 *Convergence*

The convergence of the algorithm can be assured using a result found in [12], if the function, say $F(x)$, to be minimized over the domain $\mathcal{D}$ satisfies the Lipschitz condition

$$\|\nabla F(x) - \nabla F(y)\|_2 \leqslant K \|x - y\|_2 \,, \quad \forall x, y \in \mathcal{D} \tag{5.16}$$

and the step $\alpha$ in the gradient method is chosen to satisfy $0 \leqslant \alpha \leqslant \frac{2}{K}$.

In this case, the fulfillment of the Lipschitz condition and the value of the parameter $K$ follow from the Mean Value Theorem for vector functions:

$$\nabla F(x) - \nabla F(y) = H(z)(x - y) \tag{5.17}$$

where $z \in \mathcal{D}$, and $H(\cdot)$ is the Hessian matrix, defined as $\left[h_{ij}\right] = \frac{\partial^2 F}{\partial x_i \partial x_j}$. Moreover,

$$\begin{aligned} \|\nabla F(x) - \nabla F(y)\|_2 &\leqslant \|H(z)\|_2 \, \|x - y\|_2 \\ &\leqslant \|H(z)\|_F \, \|x - y\|_2 \end{aligned} \tag{5.18}$$

where $\|H\|_F$ is the Frobenius (or Hilbert-Schmidt) norm, defined as

$$\|H\|_F = \sqrt{\sum_{i=1}^{N_r} \sum_{j=1}^{N_c} |h_{ij}|^2} \tag{5.19}$$

where $N_r$ and $N_c$ are, respectively, the number of rows and columns of $H$. Thus, setting $K$ as

$$K = \max_{z \in \mathcal{D}} \|H(z)\|_F \tag{5.20}$$

assures the satisfaction of the Lipschitz condition in Eq. (5.16)

In our case, the calculation of the Hessian matrix of the error probability function is easy due to the exponential nature of the function, and releasing the unit average energy constraint for signal points, a loose bound on the algorithm step can be obtained with some algebraic manipulations. After having assumed the negative exponentials equal to 1, we have

$$|h_{ij}|^2 \leqslant \frac{\gamma^3}{4\pi M^2} \|c_j - c_i\|^2 \tag{5.21}$$

the last factor, i. e. $\|c_j - c_i\|^2$ depends of course from the two points $c_i$ and $c_j$. At any rate, considering the placements of the point in one or more rings to cope with the non-linear distortion due to the HPA, it is very unlikely to see constellation points having an energy bigger than four times the average energy (see for example the constellation used in DVB-S2 [30]). Thus we can upper bound $|h_{ij}|^2$ as

$$|h_{ij}|^2_{max} \leqslant \frac{4\gamma^3}{\pi M^2} \tag{5.22}$$

and then

$$\|H\|_F \leqslant \sqrt{\sum_{i=1}^{M} \sum_{j=1}^{M} |h_{ij}|^2_{max}} = \sqrt{\frac{4\gamma^3}{\pi}} \tag{5.23}$$

Finally, we can fix the step $\alpha$ of the algorithm in a conservative way, due to this bound, having

$$\alpha \leqslant \sqrt{\frac{\pi}{\gamma^3}} \tag{5.24}$$

### 5.3.3 *Discussion*

The above algorithm has an intuitive explanation: since the error probability depends on the distance amongst signal points, the gradient of the error probability indicates (changing the sign) how to move points in order to reduce error probability. In other words, the constellation update tries to separe a point from its closest neighbor. However, the signal set must be subject, first of all, to the average energy constraint, in order to avoid trivial solution of this optimization problem. Secondly, the point must have good distance after the nonlinear distortion, but the points to be modified are the points belonging to signal set before distortion.

From the analysis of the objective function, which is non convex, it appears that the algorithm could stop also in a local minimum, or, more generally (see [12]), in a point $x^*$ where

$$(y - x^*)'\nabla F(x^*) \geqslant 0, \quad \forall y \in \mathcal{D} \tag{5.25}$$

At this point, it is worth to emphasize that the error probability gradient with respect to signal constellation points is obtained analytically and not numerically. Since minimization of the error probability corresponds to maximization of the constellation point distances, at each optimization step the constellation is normalized so as to have unitary average energy.

Interestingly, due to the circular symmetry of the amplifier distortion and Gaussian noise, results show that there is no a unique optimum, but rather a class of optimal constellations, differing one each other for a phase shift. Indeed, considering the behavior of the algorithm, there cannot be a unique optimum constellation: if $\{s_k^*\}$, $k = 1 \dots M$ is a constellation where the algorithm converges, also the signal set $\{s_k^* e^{\jmath\psi}\}$ satisfies the local optimality condition of Eq. (5.25), for all values of $\psi$.

At any rate, the final constellation can be somewhat varied, by changing the initial signal set of the algorithm, and if the algorithm terminates almost surely with a certain family of constellations (differing each other for a phase shift), there is a strong evidence of the global optimality of that constellation family.

## 5.4 RESULTS

As already noted in Section 5.3, the algorithm tries to maximize the minimum distance amongst distorted constellation points. Varying the IBO the relevance of the distortion varies, and so the output constellation should be different.

In the evaluation of results, both AWGN and HPA distortion should be taken into account: the effect of a noise-only scenario would result in a complicated constellation, with the points displaced on a triangular lattice (see the results in [35]). On the other hand, considering the HPA as the only impairment, the algorithm would return a constant envelope constellation, a Phase Shift Keying (PSK) (Phase Shift Keying).

A mixed scenario, as the one we have considered, would present more complex, although predictable, results. From the simulations, a sort of "threshold" back-off emerges, which is dependent from the thermal noise level. If the Input Back-Off is below this threshold, that is, if the amplifier is driven near saturation, the optimal constellations have PSK shape, in order to avoid the compression of signal points.

When the amplifier is stepped off saturation, multilevel constellations begin to appear. These constellations, however, maintain circular symmetry, in order to minimize the negative effects of such quasi-linear amplification. Driving the amplifier in the linear region, the number of levels increases, as a consequence of the reduced sensitivity of the constellation to amplitude compression, and of the need of displacing the points increasing the minimum distance.

Thus the optimization of signal sets seems to follow a Paretian approach, counteracting the main degradation source. If the HPA is driven much into saturation and compresses the multiple signal level, the only way to overcome this problem is a PSK signal set. If the amplifier shows a moderate non linearity, the thermal noise begins to became the main disturbance, and so multi-ring constellation are more suitable. Finally, if the system is linear, the signal set tends to the signal set described in [35].

Fig. 34 refers to the case when the amplifier is driven near saturation, or equivalently, below what we called threshold for Input Back-Off. The optimization procedure returns a PSK constellation, notwithstanding the noise level, which includes both AWGN and ISI interference due to non-linear distortion.

If the amplifier is driven in a quasi-linear region (i.e. not too far from saturation), the constellation, while mantaining its radial symmetry, begins to have more than one level, as shown in Fig. 35

On the contrary, if the amplifier is far from saturation, the output is strongly dependent from the signal-to-noise ratio, and the constellation generally has the shape of an Amplitude-Phase Shift Keying (APSK) (see Fig. 36 and Fig. 37).

While it is intuitive that constellations with various amplitude levels are disadvantaged in satellite transmission with respect to constant-envelope modulations, the proposed method analytically demonstrates it. However, in certain circumstances, the optimal constellations obtained by this method are different from the commonly used ones. For example, the DVB-S2 standard [30], which adopts also a 4-12 APSK and a 4-12-16 APSK constellation, is based on the assumption of transmitter predistortion, or at least the presence of an equalizer in the receiver, while the proposed method does not consider such features, taking into account only the HPA and AWGN.

## 5.5 CONCLUSIONS

In this chapter we have presented a method for the optimization of signal constellations over a nonlinear channel.

The results, obtained minimizing the average error probability for the distorted constellation, show the better performances given by PSK for a saturated amplifier, and for APSK for a quasi-linear amplifier.

This analysis, conducted by a simplified approach, confirmed from a theoretical point of view what was intuitive in constellation design, and gives a tool to the communication engineer to evaluate the performance of modulation schemes in transmitting environment different from the traditional AWGN case.

Further extensions of this work are possible, changing the statistical description of the ISI (the Gaussian distribution is somewhat a worst case approach) and considering other devices usually present in a transmission chain, such as predistorters.

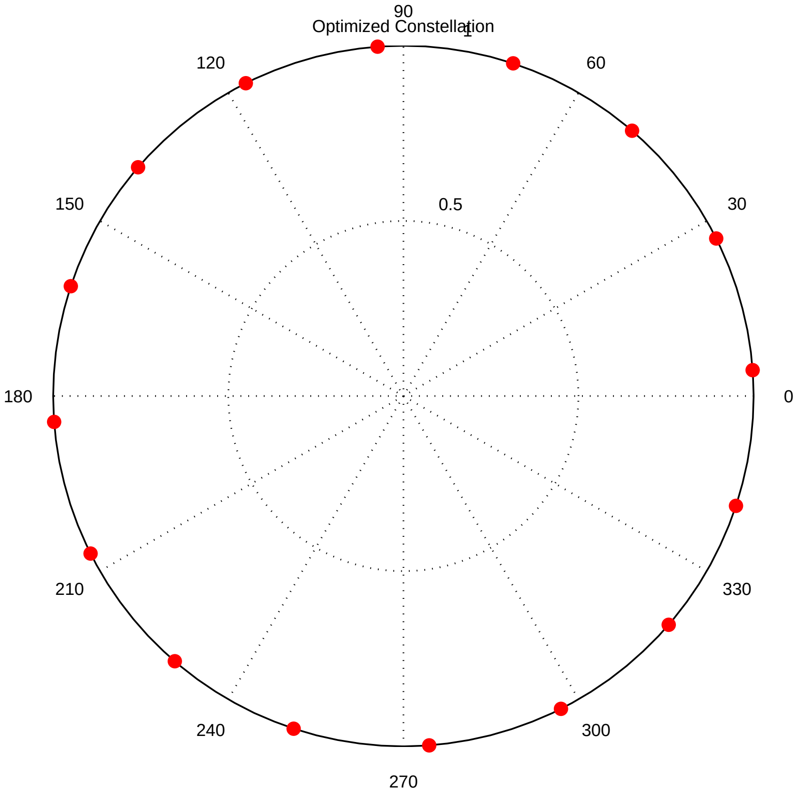

Figure 34: Optimal Signal Set for IBO $= 8$ dB, $\gamma = 10$ dB.

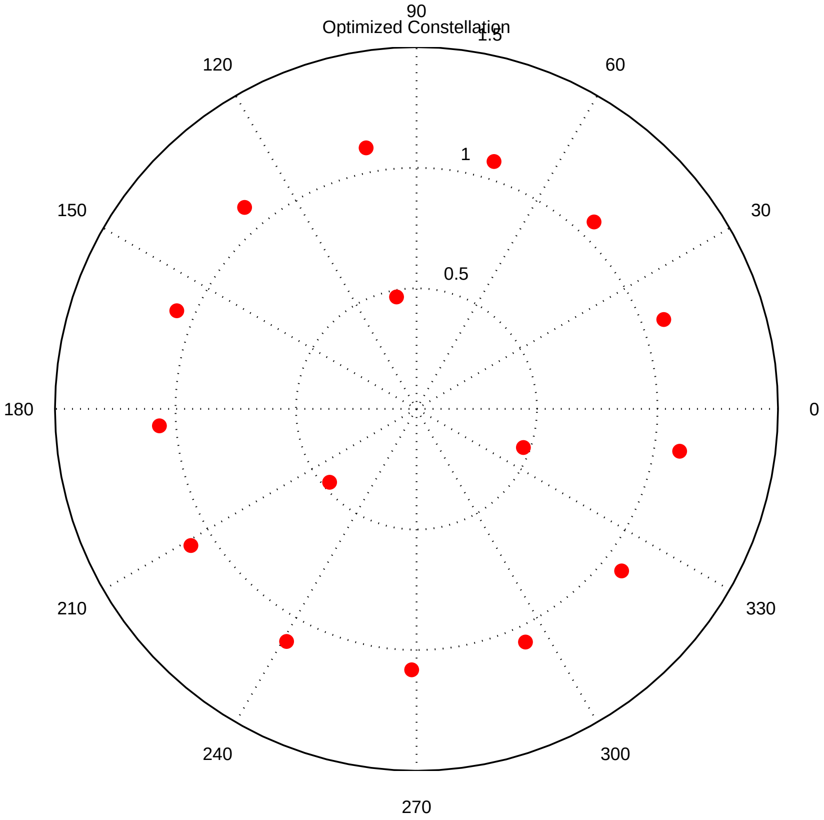

Figure 35: Optimal Signal Set for IBO $= 12$ dB, $\gamma = 10$ dB.

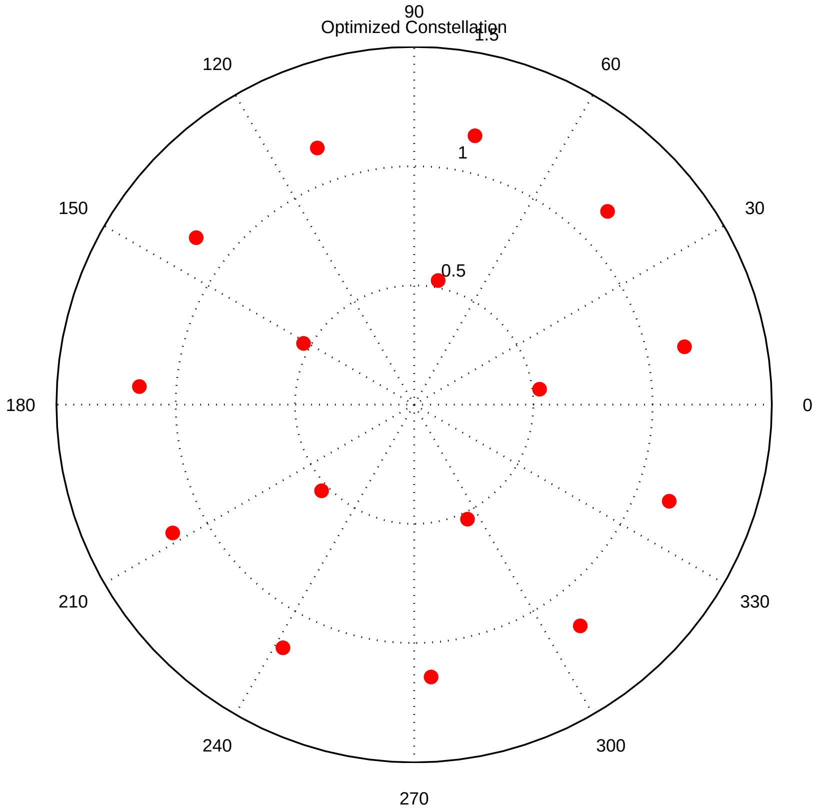

Figure 36: Optimal Signal Set for IBO = 16 dB, $\gamma = 10$ dB.

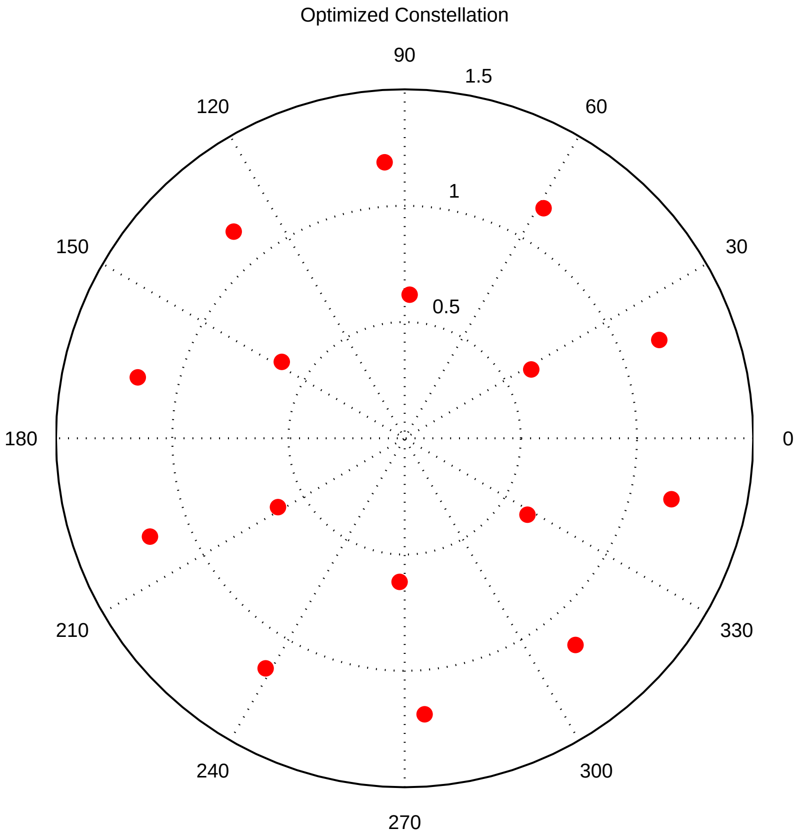

Figure 37: Optimal Signal Set for IBO = 16 dB, $\gamma = 14$ dB.

# 6

# A TIGHTER UPPER BOUND FOR ERROR PROBABILITY OF SIGNALS IN AWGN

## 6.1 INTRODUCTION

Various upper and lower bounds have been proposed in the last decades to approximate the error probability both in demodulation and decoding: although these problems can seem different, considering the number of hypotheses and the number of dimensions of the received signal, the mathematical approach is essentially the same. These upper or lower bounds are instrumental in solving an open problem, i.e. the exact calculation of the error probability for an arbitrary complex signal constellation of for a specific code. It can be solved numerically, for example by the technique of decomposing decision region proposed in [24**?** ], but a closed form solution, for a general signal set, is lacking, due to the complex form of the decision regions. The importance of this problem is increasing: nowadays the communication systems are adding more and more complex features, and analytical or semi-analytical techniques are very interesting, because these methods can save a dramatic amount of computer time with respect to Montecarlo simulations. This concept is shown in the collection of methods proposed in [46] to evaluate physical layer performance in WiMAX systems [45], or in the analysis of Space-Time Block Codes [81, 76].

The only way to avoid Montecarlo computation while achieving an exact result, is to resort to some method based on computational geometry, as in [24, 74]. However these methods suffer of loss of generality and require the evaluation of complex integrals.

The *Union Bound* is the simpler version of the Bonferroni inequality [22, Chap. 2] approach, and becomes increasingly tighter for increasing Signal-to-Noise Ratio (SNR). High order Bonferroni inequalities are too computationally expensive, so other approaches have been preferred: Seguin [69], Kuai et al. [54] have proposed new forms of lower bounds, Poscetti [65], Hughes [44], Swaszek [73], Berkelekamp [11] and Ozarow with the tangential-sphere bound [42] have proposed upper or lower bound based on a geometrical approach or on the numerical computation of non-trivial integrals (the interested reader can find a clear and exaustive analysis of the various approaches in [68]) At any rate, the Union Bound has been considered as a good candidate for calculating error probability, because it is a good compromise between complexity and accuracy, for its analytical origin, and for the fact that an upper bound is a more conservative approach to our problem, and in general to communication systems design. At least, it could be corrected for low SNR, as the authors of [76] did.

In this chapter we present a new bound which shares its origins with the Union Bound, but it also draws inspiration from the higher order Bonferroni inequalities, and it is more accurate, especially in the low SNR region. This increased accuracy, however, is achieved with almost the same complexity as the Union Bound: i.e. the same number of evaluations for `erfc` or Q functions is necessary.

Furthermore, the Union Bound over-estimates the error probability, being useless when returns a value greater than 1, while our proposed bound is effective even for very low SNR, being useful to characterize the performance of coded systems, which usually operate close to the Shannon limit.

The rest of this chapter is organized as follows: in Section 6.2 we will introduce the proposed bound to compute the Symbol Error Rate (SER) of a 2-dimensional signal set, highlighting its derivation and its similarity to the Union Bound. In Section 6.3 we will extend the proposed bound to the Codeword Error Rate (CER) evaluation for a binary linear code. Finally Section 6.4 will provide our conclusions.

## 6.2 SER COMPUTATION FOR 2-DIMENSIONAL SIGNAL CONSTELLATIONS

### 6.2.1 *Signal Model*

We consider a simplified two-dimensional $M$-ary synchronous data transmission, in which the message is mapped into a symbol from the constellation

$$\{s_i\}, \quad i = 1 \dots M \tag{6.1}$$

where $s_i \in \mathbb{C}$ and the costellation is normalized to unit average energy:

$$\frac{1}{M}\sum_{i=1}^{M} |s_i|^2 = 1 \tag{6.2}$$

The selected symbol, say the $i$—th, is processed by a pulse-shaping filter and a linear amplifier, and it is then transmitted through an Additive White Gaussian Noise (AWGN) channel. At the receiver, it undergoes matched filtering and sampling. Assuming ideal recovery of carrier phase, frequency, and timing offset, the expression of the signal which is fed to the decision device at the $k$—th symbol time is

$$r_k = \sqrt{E_s} \cdot s_i + \nu_k \tag{6.3}$$

where

$$\nu_k = \nu_{p,k} + j\nu_{q,k}, \quad \nu_{p,k}, \nu_{q,k} \sim \mathcal{N}(0, \frac{N_0}{2}) \tag{6.4}$$

represents the additive white Gaussian noise (AWGN) term and $E_s$ is the symbol energy.

For the sake of self-consistency of this chapter, we will briefly review the Union Bound for the average symbol and bit error probability, assuming equiprobable signalling. This result will be the benchmark for our proposed upper bound.

The average symbol error probability can be written as:

$$P_e = \frac{1}{M}\sum_{i=1}^{M} P_e(s_i) \tag{6.5}$$

where the last term is the conditional probability of error when symbol $s_i$ is transmitted. The exact value of $P_e(s_i)$ would be

$$P_e(s_i) = \sum_{\substack{j=1 \\ j \neq i}}^{M} \text{Prob}\left(r \in Z_j | s_i\right) \tag{6.6}$$

where $Z_j$ is the decision region associated to the $j-$th symbol, and thus the terms in the summation represent the probability that the received signal belongs to the decision region of $s_j$ while $s_i$ was transmitted. For the ease of the evaluation, the regions $Z_j$ are substituted by the regions $Z_{ji}$, where

$$Z_{ji} = \left\{ r \in \mathbb{C} | \left\| r - \sqrt{E_s}\, s_j \right\| \leqslant \left\| r - \sqrt{E_s}\, s_i \right\| \right\} \tag{6.7}$$

While the decision regions $Z_j$ do not have any overlap, the regions $Z_{ji}$ are overlapping, thus the error probability can be upper bounded by:

$$P_e(s_i) \leqslant \sum_{\substack{j=1 \\ j \neq i}}^{M} \text{Prob}\left(r \in Z_{ji} | s_i\right) \tag{6.8}$$

Recalling the properties of Gaussian variables, the expression for the error probability is

$$P_e \leqslant \frac{1}{2M} \sum_{i=1}^{M} \sum_{\substack{j=1 \\ j \neq i}}^{M} \mathit{erfc}\left( \frac{\left\| s_j - s_i \right\|}{2} \sqrt{\frac{E_s}{N_0}} \right) \tag{6.9}$$

While the computation of symbol error probability depends only on the constellation, the computation of bit error probability depends on both constellation and mapping from bits to symbols. Thus, in order to evaluate the bit error rate using the Union Bound in Eq. (6.9) must be modified, taking into account the bit tuples associated to both $s_i$ and $s_j$ and their Hamming distance $d_{ij}$. Based on these premises, the bit error probability can be approximated as

$$P_b \leqslant \frac{1}{2M \log_2 M} \sum_{i=1}^{M} \sum_{\substack{j=1 \\ j \neq i}}^{M} d_{ij} \frac{1}{2} \mathit{erfc}\left( \frac{\left\| s_j - s_i \right\|}{2} \sqrt{\frac{E_s}{N_0}} \right) \tag{6.10}$$

### 6.2.2 *Bonferroni inequalities*

The key step in the Union Bound is given by Eq. (6.8), in which the event of error in detection is upper bounded by the sum of the so-called *pairwise error probabilities*. More formally speaking, the probability of the union of non mutually exclusive events is upper bounded by the sum of the probabilities of the individual events

$$\text{Prob}\left( \bigcup_{i=1}^{M} A_i \right) \leqslant \sum_{i=1}^{M} \text{Prob}\left(A_i\right) \tag{6.11}$$

where $\{A_i\}$ is the set of non mutually exclusive events. This inequality, known as Boole's inequality, can be also considered as the first order Bonferroni inequalities. The first higher order inequalities are, for example:

$$\begin{aligned} \text{Prob}\left( \bigcup_{i=1}^{M} A_i \right) \geqslant & \sum_{i=1}^{M} \text{Prob}\left(A_i\right) + \\ & - \sum_{i<j}^{M} \text{Prob}\left(A_i \bigcap A_j\right) \end{aligned} \tag{6.12}$$

$$\begin{aligned}\text{Prob}\left(\bigcup_{i=1}^{M} A_i\right) \leqslant & \sum_{i=1}^{M} \text{Prob}\left(A_i\right) + \\ & -\sum_{i<j}^{M} \text{Prob}\left(A_i \bigcap A_j\right) + \\ & + \sum_{i<j<k}^{M} \text{Prob}\left(A_i \bigcap A_j \bigcap A_k\right)\end{aligned} \tag{6.13}$$

In general, defining

$$S_1 = \sum_{i=1}^{M} \text{Prob}\left(A_i\right) \tag{6.14}$$

$$S_2 = \sum_{i_1<i_2}^{M} \text{Prob}\left(A_{i_1} \bigcap A_{i_2}\right) \tag{6.15}$$

$$S_k = \sum_{i_1<i_2<\ldots<i_k}^{M} \text{Prob}\left(A_{i_1} \bigcap A_{i_2} \bigcap \ldots \bigcap A_{i_k}\right) \tag{6.16}$$

we have

$$\Pr\left(\bigcup_{i=1}^{M} A_i\right) \leqslant \sum_{j=1}^{k} (-1)^{j-1} S_j \quad \text{for odd } k \tag{6.17}$$

$$\Pr\left(\bigcup_{i=1}^{M} A_i\right) \geqslant \sum_{j=1}^{k} (-1)^{j-1} S_j \quad \text{for even } k \tag{6.18}$$

when $k = M$, then equality holds and the resulting identity is the inclusion-exclusion principle

The main difficulty which prevents the use of high order inequalities, such as Eq. (6.13) is the high number of computations involved. Furthermore, while the simple $\text{Prob}(A_i)$ can be evaluated, in our case, by a single integral, the probability of intersection of events must be evaluated as double integrals of a Gaussian probability density function (pdf) over a particular region, which can be polygonal or semi-infinite, thus resorting to numerical integration techniques.

### 6.2.3 *Proposed Upper Bound*

Our approach starts by writing the $(M-1)$-th order Bonferroni inequality to compute the error probability for the $i$-th symbol: since $M$ is a power of 2 in communication systems, $M-1$ will be odd, thus the $(M-1)$-th order Bonferroni inequality will be an upper bound. This upper bound on error probability will be computed as in Eq. (6.17), and in this case

$$A_j = \text{Prob}\left(r \in Z_{ji} | s_i\right) \tag{6.19}$$

Generally speaking,the events $r \in Z_{ji}$ and $r \in Z_{ki}$ are not independent for $j \neq k$. These events are independent if and only if the boundaries of the decision regions $Z_{ji}$ and $Z_{ki}$ are orthogonal. At any rate, since the computation of

$$\text{Prob}\left(r \in Z_{ji} \bigcap r \in Z_{ki} | s_i\right) \tag{6.20}$$

would require the numerical computation of the integral of a Gaussian pdf over a polygonal domain, we propose a simple approximation, that is

$$\mathrm{Prob}\left(r \in Z_{ji} \bigcap r \in Z_{ki}|si\right) = \mathrm{Prob}\left(r \in Z_{ji}|si\right) \cdot \mathrm{Prob}\left(r \in Z_{ki}|si\right) \tag{6.21}$$

due to this simplification, which is exact in certain cases, the computation of a two dimensional integral is converted into the product of two one-dimensional integrals, for which the solution is known (the *erfc* function).

After this initial simplification, there remains the problem of organizing the computation in order to avoid all the multiple summations as in Eq. (6.17). This can be done observing the probabilities of correct decision: let $P_c(s_i)$ be the probability of correctly deciding for $s_i$, this expression can be approximated as

$$P_c(s_i) \geqslant \prod_{\substack{j=1 \\ j\neq i}}^{M} \left(1 - \mathrm{Prob}\left(r \in Z_{ji}|s_i\right)\right) \tag{6.22}$$

Evaluating the right hand side of Eq. (6.22) we will have

$$\begin{aligned} P_c(s_i) \quad = \quad & 1 - \sum_{\substack{j=1 \\ j\neq i}}^{M} \mathrm{Prob}\left(r \in Z_{ji}|s_i\right) \qquad (6.23) \\ & + \sum_{\substack{j=1 \\ j\neq i}}^{M} \sum_{\substack{k>j \\ k\neq i}}^{M} \mathrm{Prob}\left(r \in Z_{ji}|s_i\right) \cdot \mathrm{Prob}\left(r \in Z_{ki}|s_i\right) + \\ & - \sum_{\substack{j=1 \\ j\neq i}}^{M} \sum_{\substack{k>j \\ k\neq i}}^{M} \sum_{\substack{l>k \\ l\neq i}}^{M} \mathrm{Prob}\left(r \in Z_{ji}|s_i\right) \cdot \mathrm{Prob}\left(r \in Z_{ki}|s_i\right) \\ & \cdot \mathrm{Prob}\left(r \in Z_{li}|s_i\right) + \ldots \end{aligned}$$

which is exactly the subtraction from 1 of the $(M-1)$-th Bonferroni inequality where the probability of intersections are computed by the simplification proposed in Eq. (6.21).

Then averaging on all the symbols, the symbol error probability can be upper-bounded as

$$P_e \leqslant 1 - \frac{1}{M} \sum_{i=1}^{M} \prod_{\substack{j=1 \\ j\neq i}}^{M} \left(1 - \mathrm{Prob}\left(\hat{s}_j|s_i\right)\right) \tag{6.24}$$

It is easy to verify that Eq. (6.24) requires the same number of pairwise error probabilities evaluations as the Union Bound (which computationally means the same number of $\mathrm{erfc}$ or $Q$ computations).

Summarizing, our proposed bound employs the same number of $\mathrm{erfc}$ evaluations of the traditional Union Bound, but these values are rearranged in order to approximate a higher order Bonferroni inequality rather than the first order inequality given by the Union Bound.

Finally, our bound can be calculated as

$$P_e \leqslant 1 - \frac{1}{M} \sum_{i=1}^{M} \prod_{\substack{j=1 \\ j\neq i}}^{M} \left[1 - \frac{1}{2} \mathit{erfc}\left(\frac{\|s_j - s_i\|}{2} \sqrt{\frac{E_s}{N_0}}\right)\right] \tag{6.25}$$

and similarly to Eq. (6.10), the bit error probability can be approximated as

$$P_b \leqslant 1 - \frac{1}{M}\sum_{i=1}^{M}\prod_{\substack{j=1\\ j\neq i}}^{M}\left[1 - \frac{d_{ij}}{\log_2 M}\frac{1}{2}\mathit{erfc}\left(\frac{\|s_j - s_i\|}{2}\sqrt{\frac{E_s}{N_0}}\right)\right] \tag{6.26}$$

### 6.2.4 *Numerical Results*

In this section we will apply the bound in Eq. (6.25) and Eq. (6.26) to Amplitude-Phase Shift Keying (APSK) constellations. This family of constellation has been chosen in DVB-S2 standard [30] and then in the newer DVB-RCS+M [32], due to its good compromise between minimum distance and resilience to non-linear distortion. A closed form expression for the symbol or bit error probability of APSK constellation does not exist, due to the shape of symbol decision regions. So the Union Bound was commonly used to derive an analytical performance curve, eventually adding some heuristic considerations to have a tighter bound [18].

APSK constellations are composed of two or more rings in which the points are equally spaced. The radius of those rings, as well as the number of points per ring and the angular offset are important design parameters: indeed the ratios between the rings radius can vary, and the allowed values depend on the code rate.

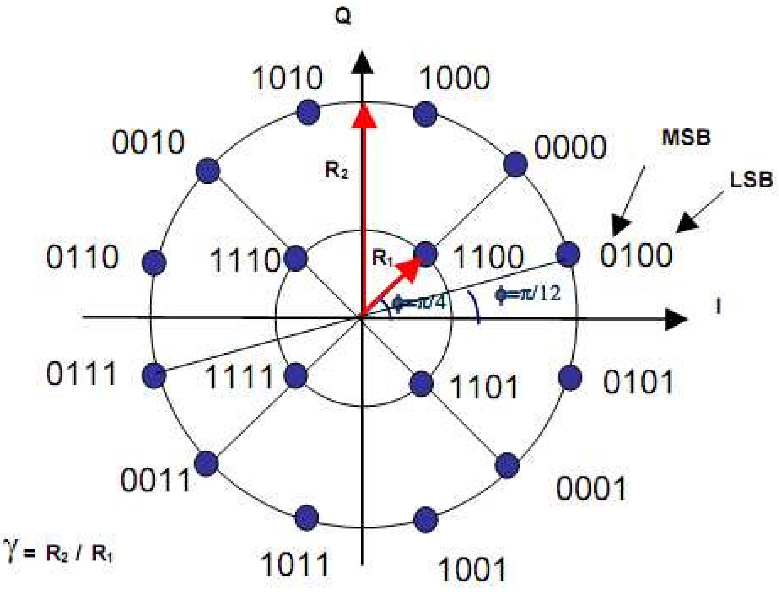

Figure 38: Constellation and bit mapping for 16-APSK, as prescribed in [30].

Fig. 38 shows the constellation and the bit mapping for 16-APSK, according to [30]. To evaluate the bounds and simulate the results, we have chosen the value $\gamma = R_2/R_1 = 2.7$, which is one of the standard values. A significant improvement over the Union Bound is depicted in Fig. 39, where the symbol error probability is considered.

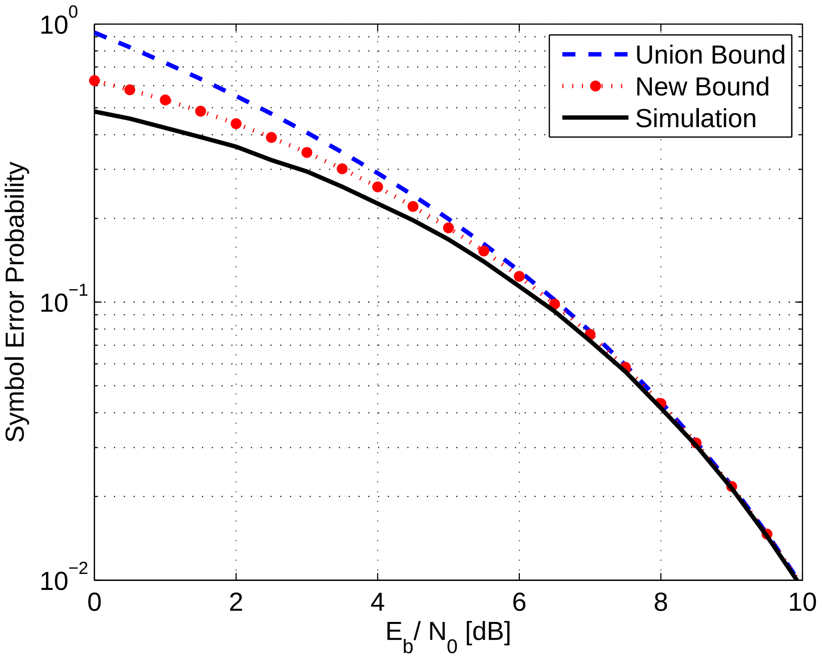

Figure 39: Symbol error Probability for 16-APSK.

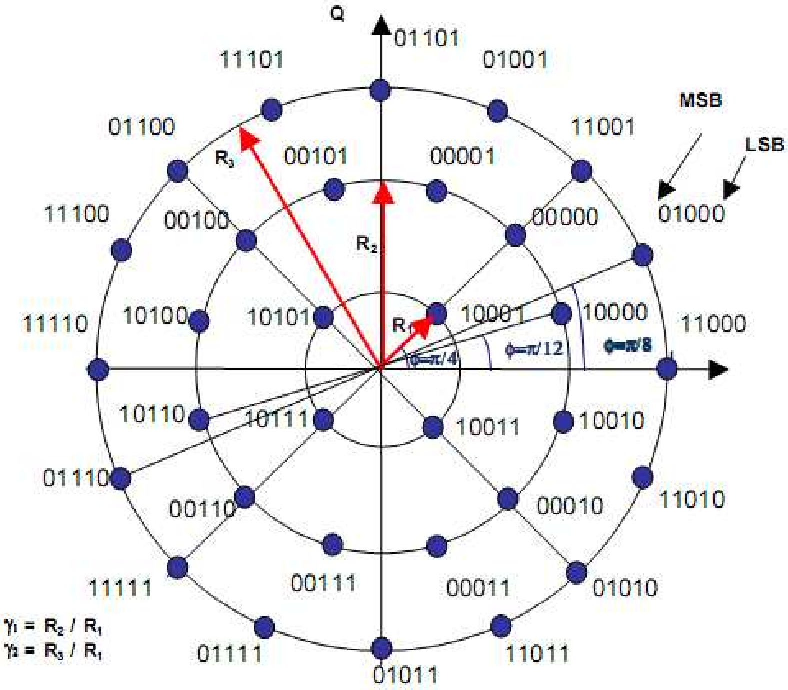
Q
01101
11101
01001
MSB
11001
LSB
01100
$R_3$
00101
00001
11100
00100
$R_2$
00000
01000
11110
10100
10101
$R_1$
10001
10000
11000
$\phi=\pi/4$
$\phi=\pi/12$
$\phi=\pi/8$
10110
10111
10011
10010
01110
00110
00010
11010
11111
00111
00011
01010
$\gamma_1 = R_2 / R_1$
$\gamma_2 = R_3 / R_1$
01111
11011
01011

Figure 40: Constellation and bit mapping for 32-APSK, as prescribed in [30].

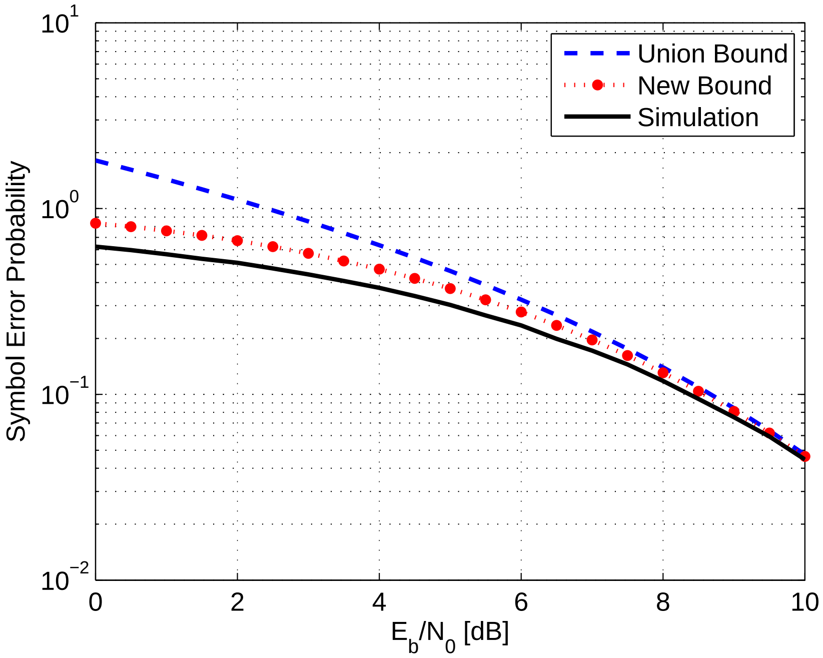

Figure 41: Symbol error Probability for 32-APSK.

Similarly, Fig. 40 presents the 32-APSK constellation and bit mapping, and the adopted numerical parameters are

$$\begin{aligned}\gamma_1 &= R_2/R_1 = 2.64\\ \gamma_2 &= R_3/R_1 = 4.64\end{aligned}$$

Fig. 41 show the results for symbol error probability, respectively. As it can be seen, the gap between our proposed bound and the Union Bound is wider than for the 16-APSK case. Furthermore, the Union Bound is above $P_e = 1$ for $E_b/N_0$ less than 2.5 dB, and is therefore useless in that range. On the other hand, the new bound maintains full significance also in that range. This is very important in view of the fact that modern systems are coded and work with $E_b/N_0$ close to the Shannon limit.

Regarding the bit error probability, in this case the Union Bound is very unreliable, converging for very high SNR. Nevertheless, our proposed bound provides a better accuracy than the Union Bound.

## 6.3 CODEWORD ERROR RATE COMPUTATION FOR BINARY BLOCK CODES

### 6.3.1 *Signal Model*

We consider the transmission of codewords of a binary linear $(n, k)$ code, Binary Phase Shift Keying (BPSK) modulated, through an AWGN channel. The receiver, after ideal recovery of all auxiliary parameters, performs maximum likelihood soft decision decoding. The received signal can thus be written as

$$r_k = \sqrt{E_s} \cdot c_{i,k} + \nu_k \tag{6.27}$$

where $E_s$ represents the energy per coded bit ($E_s = \frac{k}{n} E_b$), $c_{i,k} = \pm 1$ is a BPSK-modulated symbol being the k-th component of the codeword $c_i$, and $\nu_k \sim \mathcal{N}(0, \frac{N_0}{2})$ represents the AWGN term. In this case the Euclidean norm of each codeword is $\sqrt{nE_s}$ and the Euclidean distance between two codewords having Hamming distance $w$ is $2\sqrt{wE_s}$

For the sake of self-consistency in this different scenario, we will briefly review the Union Bound and the Sphere Bound. These results will be the benchmark for our proposed upper bound.

Due to the linearity of the code, we can use the all-zero codeword as transmitted codeword, and then compute the error probability, which is

$$P_e = \sum_{i=1}^{2^k} \mathrm{Prob}\left[\hat{c}_i | c_0\right] \tag{6.28}$$

where the summation is over the probability that the i-th codeword is decoded when the 0-th is transmitted. This expression is not acceptable for two main reasons: the excessive length of the summation, and the difficulty in computing $\mathrm{Prob}\left[\hat{c}_i | c_0\right]$. Thus the *Union Bound* approximates the error probability as

$$P_e \leqslant \sum_{i=1}^{2^k} \mathrm{Prob}\left[\|r - c_i\| < \|r - c_0\|\right] \tag{6.29}$$

solving the second problem, because the probabilities in the summation can be easily computed as

$$\mathrm{Prob}\left[\|r - c_i\| < \|r - c_0\|\right] = \frac{1}{2} \mathit{erfc}\left(\sqrt{\frac{w_i E_s}{N_0}}\right) \tag{6.30}$$

where $w_i$ is the Hamming weight of the codeword $c_i$. To reduce the computation time, the concept of the *Spectrum* of the code is used, i.e. the number of codeword at a given Hamming weight, such spectrum of a code is easy to calculate for the "average" code (see for example [6, 38]).

So the Union Bound reduces to

$$P_e \leqslant \sum_{i=1}^{n} S_i \frac{1}{2} \mathit{erfc}\left(\sqrt{\frac{w_i E_s}{N_0}}\right) \tag{6.31}$$

where $S_i$ is the number of codewords having weight $w_i$. Summarizing, the Union Bound replaces the probability that the received signals fall into a given decision region with the so-called pairwise error probability, i.e. the probability that the received signal is closer to another codeword rather than the transmitted one.

The cone bound [? ] is based on a different approach: the decision region for a given codeword can be decomposed into truncated polyhedral cones, and an upper bound to the error probability can be obtained by deforming these polyhedral cones into circular cones having the same angle. The error probability can thus be bounded as

$$P_e \leqslant \sum_{i=1}^{2^k} A_n\left(\frac{2\sqrt{w_i E_s}}{\alpha_0}, \sqrt{\frac{E_s}{N_0}}\right) \tag{6.32}$$

where $\alpha_0$ is the unique solution of

$$\sum_{i=1}^{2^k} A_n\left(\frac{2\sqrt{w_i E_s}}{\alpha_0}, 0\right) = 1 \tag{6.33}$$

and

$$\begin{aligned} A_n(x,y) &= \frac{\Gamma\left(\frac{2^k}{2}\right)}{\sqrt{\pi}\Gamma\left(\frac{2^k-1}{2}\right)} \\ &\int_0^{\arccos(x)} (\sin\phi)^{(2^k-2)}\,\bar{\Gamma}\left(\frac{2^k}{2},\frac{y^2\sec^2\phi}{2}\right)d\phi \end{aligned} \tag{6.34}$$

where $\bar{\Gamma}$ is the incomplete Gamma function.

### 6.3.2 *Proposed Bound*

Using an approach similar to Section 6.2.3, and recalling the Union Bound in Section 6.3.1 in this case we can use the linearity of the code to compute the error probability for the all-zero codeword, and then extend this result to all the codewords. We have

$$P_e \leqslant 1-\prod_{i=1}^{n}\left(1-\text{Prob}\left(r\in Z_{i0}|c_0\right)\right)^{S_i} \tag{6.35}$$

where $Z_{i0}$ is the decision region associated to a codeword having $i$ ones and $(n-i)$ zeros. Recalling Eq. (6.31) we have, finally

$$P_e \leqslant 1-\prod_{i=1}^{n}\left(1-\frac{1}{2}erfc\left(\sqrt{w_i\frac{E_s}{N_0}}\right)\right)^{S_i} \tag{6.36}$$

It is simple to verify that the proposed bound requires the same number of *erfc* evaluation of the Union Bound in Eq. (6.31), and next section will show that this re-arrangement of the computations provides an additional accuracy.

### 6.3.3 *Numerical Results*

In this section we will evaluate the error probability, as given by Union Bound, Sphere Bound and this proposed bound for a family of BCH codes. We will consider four primitive BCH codes with parameters $(63,24)$, $(63,30)$, $(63,36)$, $(63,39)$, because the spectra of these codes is close to the spectrum of the "average" code. This family of codes has been chosen for two reasons: the ease of computation of the codes' parameters and performance, and the excellent reference in [64], where several different bounds are compared for this family of codes. Table 3 recollects the first terms of the codes spectra, computed as in [6]

Fig. 42,43,44,45 show a comparison of Union Bound, proposed bound and Sphere Bound for BCH codes $(63,24)$, $(63,30)$, $(63,36)$, $(63,39)$ respectively. All the figures agree in the fact that our proposed bound is tighter than the Union Bound, although some more complex bounds can be tighter.

## 6.4 CONCLUSIONS

The bound presented in this chapter has some interesting properties. First of all, it requires the same number of operations of the simplest known bound, i. e. the Union Bound. Secondly, and more importantly, it is tighter, and finally, it never exceeds the value $P_e = 1$.

| (63, 24) | | (63, 30) | | (63, 36) | | (63, 39) | |
|---|---|---|---|---|---|---|---|
| w | $S_w$ | w | $S_w$ | w | $S_w$ | w | $S_w$ |
| 15 | 651 | 13 | 1764 | 11 | 5670 | 9 | 2170 |
| 16 | 1953 | 14 | 6300 | 12 | 24750 | 10 | 11718 |
| 17 | 3024 | 15 | 7707 | 13 | 77616 | 11 | 32382 |
| 18 | 7728 | 16 | 23121 | 14 | 277200 | 12 | 140322 |
| 19 | 0 | 17 | 177660 | 15 | 895755 | 13 | 628866 |
| 20 | 0 | 18 | 454020 | 16 | 2687265 | 14 | 2245950 |
| 21 | 74449 | 19 | 352800 | 17 | 7623504 | 15 | 7302603 |
| 22 | 142128 | 20 | 776160 | 18 | 19482288 | 16 | 21907809 |

Table 3: Spectra of the BCH codes used in simulations.

This bound has shown to be more effective for symbol error probability computation in 2-dimensional modulation rather than for codeword error probability computation. This can be justified considering the substantial difference in the ratio between number of hypotheses and dimensions of the signal in the two cases.

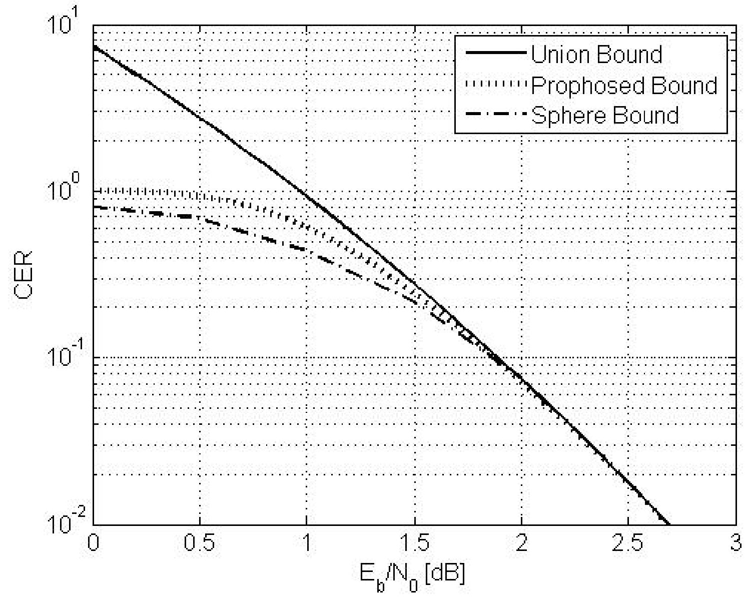

Figure 42: Codeword Error Probability for the BCH (63,24) code.

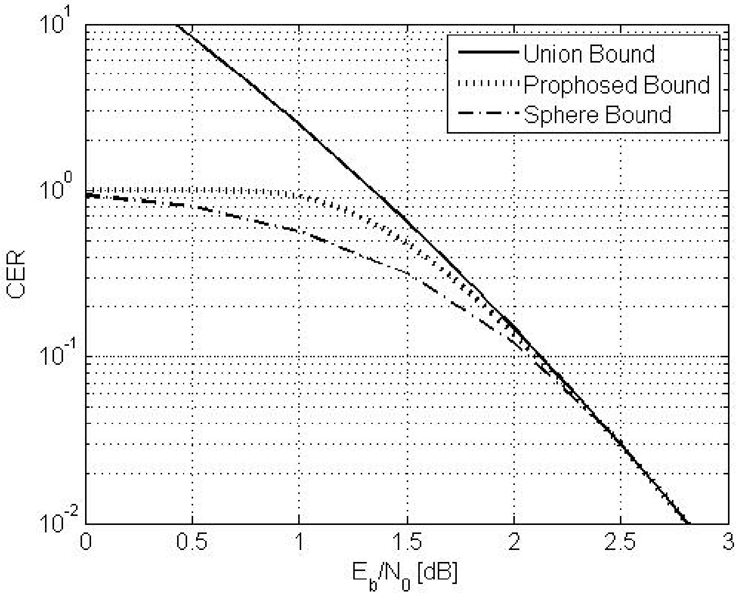

Figure 43: Codeword Error Probability for the BCH (63,30) code.

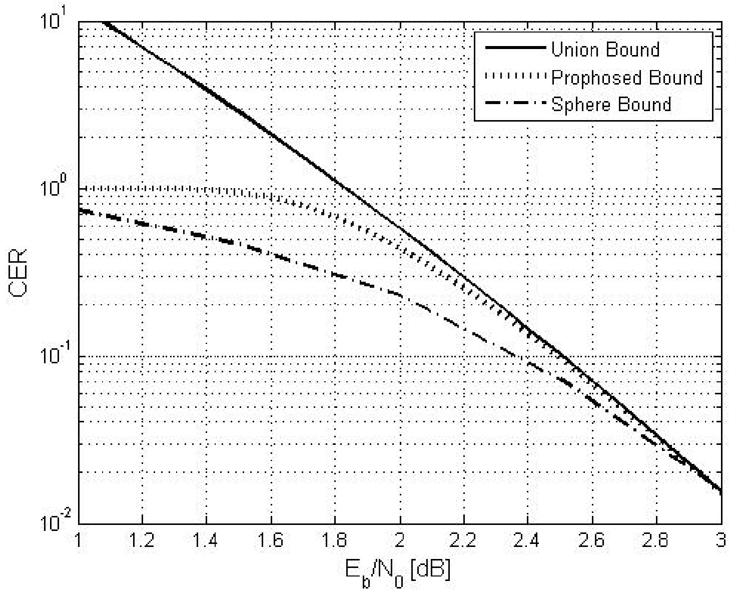

Figure 44: Codeword Error Probability for the BCH (63,36) code.

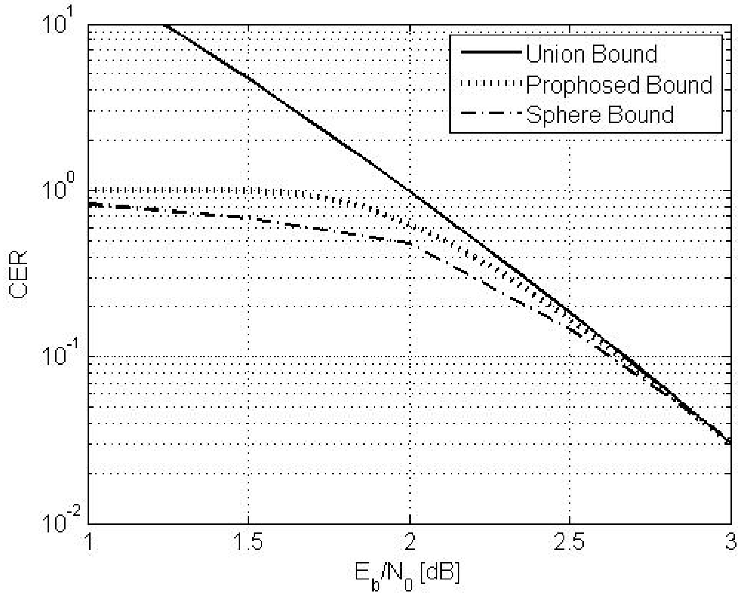

Figure 45: Codeword Error Probability for the BCH (63,39) code.

# 7

# A REDUCED COMPLEXITY SIGNAL TO NOISE RATIO ESTIMATOR

## 7.1 INTRODUCTION

Signal-to-Noise Ratio (SNR) estimation is a fundamental task in modern communication systems, being a pre-requisite for diversity combining, demodulation and soft decoding, adaptive coding and modulation strategies, upper layer resource management, et cetera.

Several SNR estimators have been presented (see [63] for a comprehensive overview), both data-aided and non data-aided. The former type has better performance and higher complexity, while the latter may return inaccurate estimates at low SNR.

In this chapter we introduce a novel data-aided SNR estimator which strikes a new balance between performance and complexity. Since the estimator requires phase coherence, we also analyze the performance in the presence of phase errors, comparing its performance with respect to the well known Maximum Likelihood (ML) SNR estimator [20, 36, 51]. We also show that a small phase fluctuation, such as the residual angle error after phase/frequency estimation, significantly reduces the bias of the estimate. While such positive results happen for a phase variance lower than $0.01 \text{ rad}^2$, the bias increases in magnitude if the phase estimation is absolutely unreliable. However, the positive effect is shown for all realistic conditions of use of this estimator. So the proposed circuit is quite appealing for its robustness and reduced complexity. Furthermore, this complexity reduction is achieved at arguably no expense in terms of end-to-end performance: it has been shown that both diversity combining and turbo decoding are robust to a slight mismatch on the SNR estimated value, as stated in [34, 49, 72].

Such an estimator can be applied in different scenarios such as low-cost satellite receivers and wireless sensor networks. In the first case the channel has a very slow dynamics and several frames, interleaved by pilots, are available for the estimation process. Having in this case a longer estimation window, this circuit saves in complexity but keeps the performance very close to the ML estimator results. In the second case, a wireless sensor networks, every possible saving in complexity is significant, increasing the lifetime of the sensor and thus of the network.

In this chapter we present an analytical model of the circuit and its performance: under both ideal (Section 7.3) and non-ideal (Section 7.4) phase estimation, the estimated SNR is shown to be described by a F-distribution [1], and our analytical results are validated by numerical simulations (Section 7.5). Finally, we will provide some concluding remarks in Section 7.6.

## 7.2 SIGNAL-TO-NOISE RATIO ESTIMATORS

To the authors' knowledge, the non data-aided maximum likelihood estimator for SNR has first been presented in [36, 51]. The extension to a data-aided estimation is straightforward, and its analysis can be found, for example, in [20]. Following ideal frequency, phase and timing recovery (the assumption on ideal frequency/phase recovery will be released in Section 7.4), matched filter and sampling (at a sampling rate of 1 sample per symbol), this circuit is fed by $N_p$ samples of the form

$$r_k = \sqrt{E_s} d_k + n_k \qquad k = 1, \dots, N_p \tag{7.1}$$

where $E_s$ is the energy per symbol, $d_k$ is a known complex pilot symbol, with energy normalized to 1 and $n_k$ is a sample of complex Gaussian noise, whose real and imaginary parts are i.i.d. with zero mean and variance equal to $N_0/2$. The ML circuit performing SNR estimation is depicted in Fig. 46, where $\hat{P}_s$, $\hat{P}_r$ and $\hat{P}_n$ represent, respectively, the estimated signal power, total power, and noise power and they are obtained as

$$\hat{P}_s = \left[ \frac{1}{N_p} \sum_{k=1}^{N_p} \mathbb{R}\mathrm{e}\left[ r_k d_k^* \right] \right]^2 \tag{7.2}$$

$$\hat{P}_r = \frac{1}{N_p} \sum_{k=1}^{N_p} |r_k|^2 \tag{7.3}$$

$$\hat{P}_n = \hat{P}_r - \hat{P}_s \tag{7.4}$$

and $\hat{\gamma}$ is the estimated SNR, computed as $\hat{P}_s/\hat{P}_n$

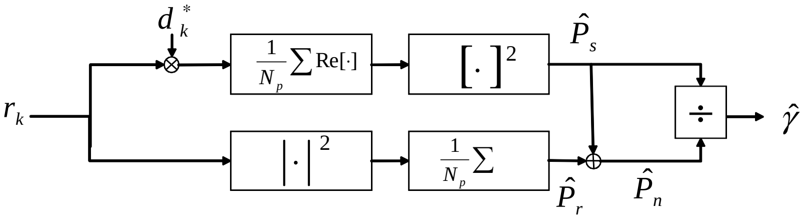

Figure 46: ML SNR Estimator.

Our reduced complexity circuit is based on the same signal model and can be interpreted as derived from the ML estimator through a fundamental simplification. Since the SNR estimator operates in data-aided mode, after multiplying the received signal by the conjugate of the known data, the useful signal will lie on the real axis, while the noise will be present on both real and imaginary components. Thus the imaginary component itself can be used to estimate the noise variance by square and accumulate. In this way both branches of the circuit operate with real values, rather than complex, and this allows a significant saving in complexity. This circuit is shown in Fig. 47, where $\hat{P}_s$, $\hat{P}_n$ and $\hat{\gamma}$ have the same meaning as in the ML circuits, but $\hat{P}_n$ is computed as

$$\hat{P}_n = \frac{2}{N_p} \sum_{k=1}^{N_p} |\mathbb{I}\mathrm{m}\left[ r_k d_k^* \right]|^2 \tag{7.5}$$

These circuits have different complexity, summarized in Table 4, and it can clearly be seen that the reduction of complexity attainable with our proposed estimator is roughly a factor of 2 for multiplications, and 3/2 for additions.

The aim of the next sections is to show that the complexity reduction is obtained without significantly affecting the performance.

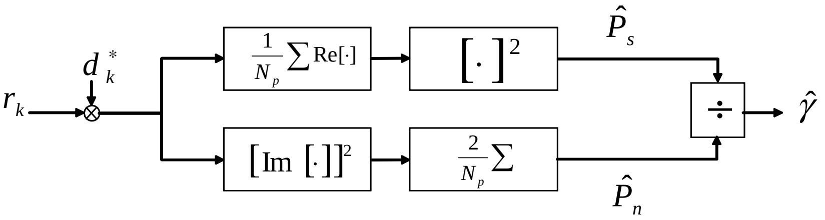

Figure 47: Reduced Complexity SNR Estimator.

| | ML Estimator | Reduced Complexity Estimator |
|---|---|---|
| Additions | $3N_p + 1$ | $2N_p + 1$ |
| Multiplications | $2N_p + 1$ | $N_p + 1$ |

Table 4: Complexity comparison of two Data-Aided SNR circuits.

## 7.3 ANALYTICAL MODEL OF THE REDUCED COMPLEXITY ESTIMATOR

Observing the received signal in Eq. (7.1) we have

$$\mathbb{R}\mathrm{e}\,[r_k] \sim \mathcal{N}\left(\sqrt{E_s}, \frac{N_0}{2}\right) \tag{7.6}$$

$$\mathbb{I}\mathrm{m}\,[r_k] \sim \mathcal{N}\left(0, \frac{N_0}{2}\right) \tag{7.7}$$

where the symbol $\sim$ indicates that a random variable on the l.h.s. is distributed according to the probability distribution on the r.h.s., and $\mathcal{N}(a, b)$ is a shorthand notation for a Gaussian distribution with mean $a$ and variance $b$. Processing the signal along the two branches in Fig. 46, it holds

$$\hat{P}_s \sim \frac{N_0}{2N_p}\chi_1^2\left(\frac{2E_sN_p}{N_0}, 1\right) \tag{7.8}$$

$$\hat{P}_n \sim \frac{N_0}{N_p}\chi_{N_p}^2\,(0, 1) \tag{7.9}$$

The estimated signal to noise ratio, $\hat{\gamma}$, can then be modeled as the quotient of a noncentral chi-square distribution having 1 degree of freedom and a statistically independent central chi-square distribution having $N_p$ degrees of freedom. After having scaled the two random variable for the degrees of freedom of their respective distribution, their ratio can be represented as a noncentral F distribution [1]:

$$\hat{\gamma} \sim \frac{1}{2N_p}\Phi\left(1, N_p, \frac{2E_sN_p}{N_0}\right) \tag{7.10}$$

where $\Phi(n_1, n_2, \lambda)$ is a noncentral F distribution having $n_1$ and $n_2$ degrees of freedom and noncentrality parameter $\lambda$. So the mean and variance of the estimated SNR can be calculated as

$$\mathbb{E}\,[\hat{\gamma}] = \frac{1 + 2N_p\gamma}{2\,(N_p - 2)} \tag{7.11}$$

$$\mathrm{Var}\,[\hat{\gamma}] = \frac{(1 + 2N_p\gamma)^2 + (1 + 4N_p\gamma)\,(N_p - 2)}{2\,(N_p - 2)^2\,(N_p - 4)} \tag{7.12}$$

where $\gamma$ is the true SNR, $E_s/N_0$. As it can be seen, the mean value converges to the true value, and the variance converges to zero when the number of pilots tends to infinity. However, for a finite number of pilots, a bias can be observed, and the variance (normalized by the square of the true signal-to-noise ratio), converges to a finite value. More exactly, Paoluzzi and Beaulieu [63] show that the Cramer-Rao Bound (CRB) for the SNR estimation is

$$\mathrm{Var}\left[\hat{\gamma}\right] \geqslant \frac{2\gamma + \gamma^2}{N_p} \tag{7.13}$$

which, normalized by $\gamma^2$ tends, for an infinite SNR, to the inverse of the pilot number, thus being finite for a finite number of pilots.

The results shown in Eq. (7.11) and Eq. (7.12) will be compared, in Section 7.5 with the performance of the ML SNR estimator, for which we have

$$\mathbb{E}\left[\hat{\gamma}_{ML}\right] = \frac{2N_p}{2N_p - 3}\left(\frac{1}{2N_p} + \gamma\right) \tag{7.14}$$

$$\mathrm{Var}\left[\hat{\gamma}_{ML}\right] = \frac{N_p^2\left(8\gamma^2 + 16\gamma\right) + N_p\left(4 - 16\gamma\right) - 4}{8N_p^3 - 44N_p^2 + 78N_p - 45} \tag{7.15}$$

## 7.4 NON-IDEAL PHASE REFERENCE

To include the phase error, we augment the system model in Eq. (7.1) obtaining

$$r_k d_k^* = \sqrt{E_s}\, e^{j\phi_k} + n_k \qquad k = 1, \dots, N_p \tag{7.16}$$

where $\phi_k \sim \mathcal{N}(0, \sigma_\phi^2)$. Then, denoting the real and the imaginary component of the noise as $n_{p,k}$ and $n_{q,k}$, and using a truncated Taylor series expansion, we have

$$\mathbb{R}\mathrm{e}[r_k] = \sqrt{E_s}\,\cos\left(\phi_k\right) + n_{p,k} \approx \sqrt{E_s}\left(1 - \frac{\phi_k}{2}\right) + n_{p,k} \tag{7.17}$$

$$\mathbb{I}\mathrm{m}[r_k] = \sqrt{E_s}\,\sin\left(\phi_k\right) + n_{q,k} \approx \sqrt{E_s}\phi_k + n_{q,k} \tag{7.18}$$

Based on these assumptions, it is straightforward to see that

$$\mathbb{I}\mathrm{m}[r_k] \sim \mathcal{N}\left(0, E_s\sigma_\phi^2 + \frac{N_0}{2}\right) \tag{7.19}$$

while the distribution of the real part of the signal is more involved, being the sum of a chi-square and a Gaussian random variables. By adopting a simple Gaussian approximation, we can write

$$\mathbb{R}\mathrm{e}[r_k] \sim \mathcal{N}\left(\sqrt{E_s}\left(1 - \frac{\sigma_\phi^2}{2}\right), \frac{N_0 + \sigma_\phi^4}{2}\right) \tag{7.20}$$

.

Due to this approximation, which we will show to be increasingly tight for increasing SNR, we are allowed to model $\hat{\gamma}$ again as a noncentral F distribution , we have

$$\widehat{P}_s \sim \frac{N_0 + \sigma_\phi^4}{2N_p}\chi_1^2\left(\frac{2N_pE_s}{N_0 + \sigma_\phi^4}\left(1 - \frac{\sigma_\phi^2}{2}\right), 1\right) \tag{7.21}$$

$$\widehat{P}_n \sim \frac{N_0 + 2E_s\sigma_\phi^2}{N_p}\chi_{N_p}^2\left(0, 1\right) \tag{7.22}$$

then

$$\widehat{\gamma} \sim \frac{N_0 + \sigma_\Phi^4}{2N_p\left(N_0 + 2E_s\sigma_\Phi^2\right)}\Phi\left(1, N_p, \frac{2N_pE_s}{N_0+\sigma_\Phi^4}\left(1-\frac{\sigma_\Phi^2}{2}\right)\right) \tag{7.23}$$

The mean and variance are given by

$$\mathbb{E}[\widehat{\gamma}] = \frac{\xi + 2N_p\gamma\zeta}{2\left(N_p-2\right)\left(1+2\gamma\sigma_\Phi^2\right)} \tag{7.24}$$

$$\mathrm{Var}[\widehat{\gamma}] = \frac{\xi^2\left[\left(1+\frac{2N_p\zeta}{\xi}\gamma\right)^2 + \left(N_p-2\right)\left(1+\frac{4N_p\zeta}{\xi}\gamma\right)\right]}{2\left(N_p-2\right)^2\left(N_p-4\right)\left(1+2\gamma\sigma_\Phi^2\right)} \tag{7.25}$$

where $\xi = 1 + \frac{\sigma_\Phi^4}{N_0}$ and $\zeta = 1 - \frac{\sigma_\Phi^2}{2}$.

Assuming that the phase error magnitude tends to zero increasing the number of pilots, we have again

$$\lim_{N_p\to\infty} \mathbb{E}\left[\widehat{\gamma}\right] = \gamma \tag{7.26}$$

$$\lim_{N_p\to\infty} \mathrm{Var}\left[\widehat{\gamma}\right] = 0 \tag{7.27}$$

## 7.5 NUMERICAL RESULTS

This section analyzes the reduced complexity estimator and its sensitivity to phase errors from a numerical point of view. We assume that the number of pilots for SNR estimation is 64, and that a similar number of pilots was employed in phase estimation, thus leading to

$$\sigma_\Phi^2 = \frac{1}{2N_p\gamma} \tag{7.28}$$

Fig. 48 shows the normalized Mean Square Error (MSE) of the estimators in Additive White Gaussian Noise (AWGN) only. The solid line represents the theoretical lower bound given by the Cramer-Rao Bound, while the dash-dotted line shows the performance of the ML estimator. The dashed line and the marked dotted line present simulation results and the analytical model for the reduced complexity estimator, respectively. Fig. 49 depicts the behavior of the normalized MSE of the estimators in presence of a phase error. The positive effect of phase estimation can be noticed: the MSE is slightly reduced, due to a significant reduction in the mean and a slight reduction of the variance. In this case the analytical model becomes accurate increasing the SNR, and this behavior is a consequence of the Gaussian assumption for the mean of the real component of the signal in Eq. (7.20), which has proven to be a better approximation for higher signal-to-noise ratios. Fig. 50 and Fig. 51 show the estimators' performance when using $N_p = 1024$. As we can see, the curves are significantly closer, and there is no mismatch between the theoretical model described in Section 7.4. This fact can be interpreted observing that SNR increase and observation window enlargement are somehow interchangeable in leading to an improved accuracy, as usually happens in Estimation Theory.

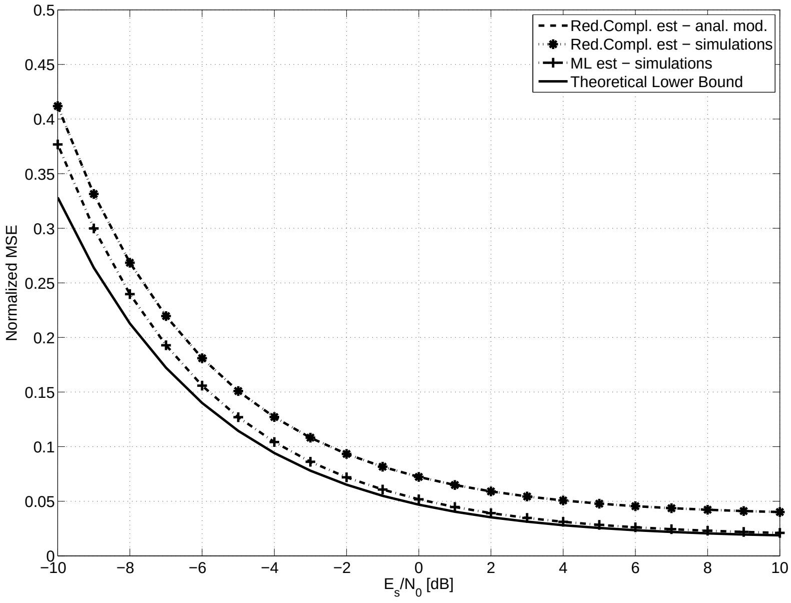

Figure 48: Normalized MSE in AWGN only, $N_p = 64$.

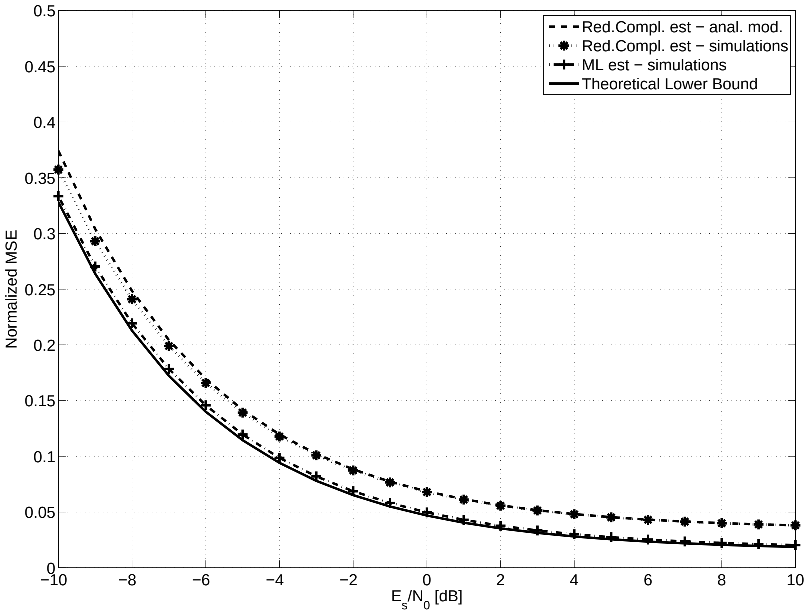

Figure 49: Normalized MSE in presence of phase error, $N_p = 64$.

## 7.6 CONCLUSIONS

In this chapter we have introduced an SNR estimator with reduced complexity, and we discussed its resilience to phase errors, comparing its performance to the ML SNR estimator.

Analytical and numerical results both show the positive effect of a non-ideal phase recovery over a data-aided SNR estimator: there is a significant reduction of the bias and a slight decrease of the variance. Furthermore, even the theoretical lower bound for SNR estimation presents a floor, and our proposed circuit shows a very limited loss from this theoretical value.

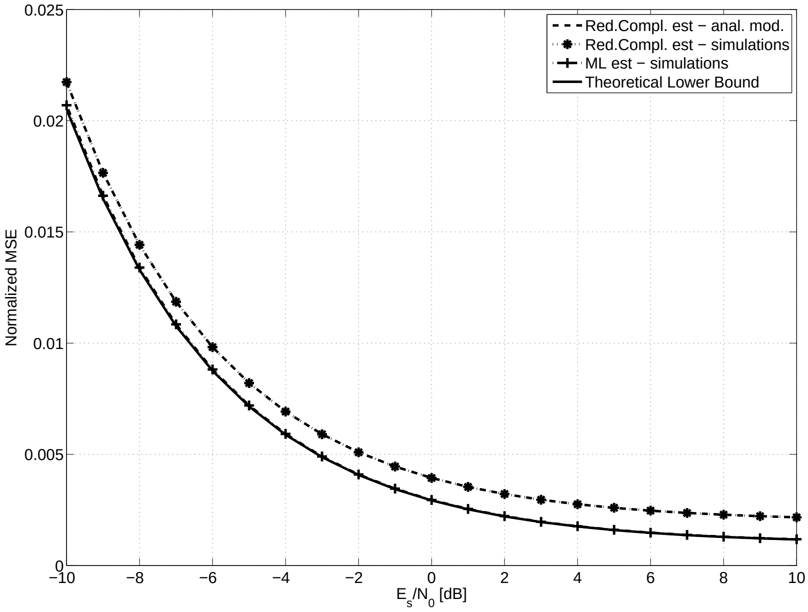

Figure 50: Normalized MSE in AWGN only, $N_p = 1024$.

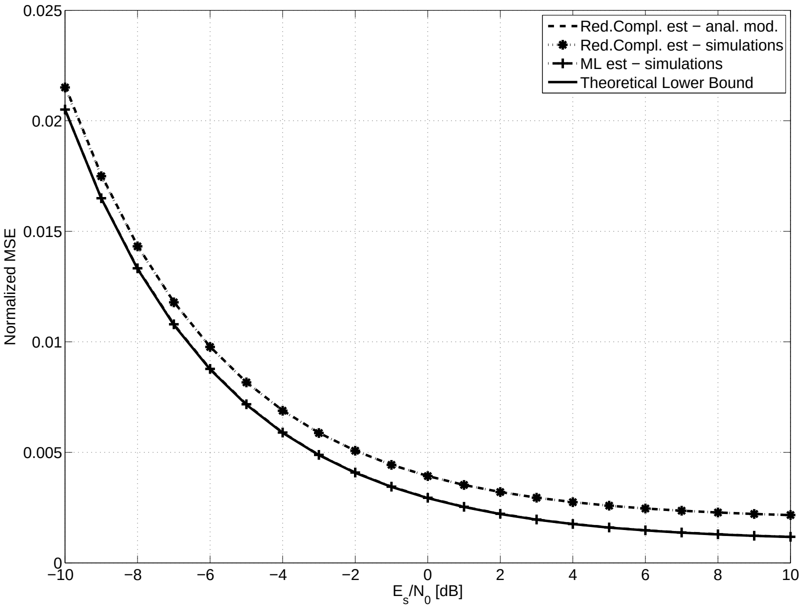

Figure 51: Normalized MSE in presence of phase error, $N_p = 1024$.

In this scenario the choice of the estimator to be implemented is harder, and it may depend on other parameters, such as the complexity or the available chip area, or the importance of an accurate SNR estimate for the other signal processing units, although various significant applications have proven to be resilient to a slight mismatch between estimated and actual SNR. On the other hand, if the channel presents very slow fluctuations and several pilot fields are available, the differences between the estimators become negligible.

Concluding, we have presented a novel data-aided signal-to-noise-ratio estimator, and shown that a significant saving in complexity can be achieved while remaining close to the ML estimator.

# 8

# FURTHER DEVELOPMENTS OF THE PRESENTED WORK

Single Carrier systems are and will be a sound benchmark for all the modulation and coding techniques. They allow for simple analytical expressions or even closed forms in a majority of cases of practical interest. Research on these systems will continue to appear, and fruitful contribution will be presented first assuming a single carrier scenario, and then moving to more complex communication architectures.

Moreover, single carrier system will continue to operate in very particular scenarios, where the bandwidth is very scarce or the environment is very harsh. Furthermore, since the circuits for single carrier transmission are already established, and widely deployed, this transmission method will be used where the circuitry cost is at a prime.

Based on these premises, the work presented in the previous chapters can be augmented either with the conversion from single-carrier to multi-carrier, or with the adoption of the presented techniques in the scenarios that still adopt single carrier transmission. For this case, computational techniques are useful to obtain an approximate assessment of the system performance within a reasonable computation time, while on the other hand, there is still room for optimization for both circuitry and waveform.

For the case of constellation optimization, it would be interesting to take into account several possible models for the amplifier, trying to highlight the common patterns of the optimal constellations over these different kinds of non-linearity. The modified Union Bound will surely be extended to fading channels and Space-Time Block Codes (STBC), to have a more powerful tool to be applied in different scenarios. The reduced complexity Signal-to-Noise Ratio (SNR) estimator should easily be applied to satellite communication, to be employed in iterative decoding and diversity combining.

Concluding, there are still challenges related to single carrier transmission, and further developments for the presented work.

# Part III

# APPENDIX

# A

# ON THE EFFICIENCY OF PAPR REDUCTION METHODS IN SATELLITE OFDM

## A.1 INTRODUCTION

The DVB-SH [31] standard is the outcome of a standardization process that went through a number of iterations and discussions amongst the contributors. A large number of lab and field trials are currently ongoing, and progresses towards implementation are being made at a quick pace. Many important features were included in the standard, such as the use of very strong channel coding, support for long time interleaving at the physical layer, and support of terrestrial and hybrid Single Frequency Network (SFN). Other features, that may enhance the system performance or enable the support for different situations, were left out. Furthermore, the drafting of version 2 of the implementation guidelines is currently ongoing, and the optimization of system and Physical Layer (PHY) parameters according to the different deployment scenarios is one of its objectives. Taking this framework into account, this section reports the outcomes of one the activities carried out on the optimization of the Orthogonal Frequency Division Multiplexing (OFDM) PHY for the Land Mobile Satellite Scenario. A large effort has been devoted to these activities, resulting in a significant number of solutions laying the foundations of a possible Satellite-OFDM PHY. Starting from the current DVB-SH [31] standard, and taking into account the benchmark performance available from the literature, from industrial research projects, and from ongoing trials, a number of relevant focus areas have been identified, related to spectral efficiency increase, mobility support, zapping time and power saving, syncronization, Quality of Service (QoS) Flexibility and Peak-to-Average-Power Ratio (PAPR) reduction. In the following section we will focus on the latter aspect, which aims at improving waveform resilience to non-linear distortion.

## A.2 PAPR REDUCTION TECHNIQUES

The tails in PAPR distribution for OFDM signals are very significative, and this implies an important source of distortion in a satellite scenario, where the amplifier is driven near saturation. To have an idea of the cumulative distribution of PAPR, a Gaussian approximation can be used. With this approach, if OFDM symbols in time domain are assumed to be Gaussian distributed, their envelope can be modeled with a Rayleigh distribution. Thus, the probability that the PAPR does not exceed a given value $\gamma$ is:

$$\mathbb{P}\left[\mathrm{PAPR} \leqslant \gamma\right] = \left(1 - e^{-\gamma}\right)^{N_{\mathrm{FFT}}} \tag{A.1}$$

A more meaningful measure is given by the Complementary Cumulative Density Function (CCDF), which gives the probability that PAPR exceeds a given value $\gamma$, and can be written as:

$$\mathbb{P}\left[\mathrm{PAPR} \geqslant \gamma\right] = 1 - \left(1 - e^{-\gamma}\right)^{N_{\mathrm{FFT}}} \tag{A.2}$$

Using this simple approximation, which becomes increasingly tight increasing the Fast Fourier Transform (FFT) size, it is easy to check that a PAPR of 9 dB is exceeded with a probability of 0.5 assuming $N_{FFT} = 2048$, while a PAPR of 12 dB is exceeded with a probability of $2.7 \cdot 10^{-4}$.

This argument motivates the use of a PAPR reduction technique, in order to lower the PAPR and increase the power efficiency in the amplifiers. This is interesting for both satellite communication, where a lower Input Back Off (IBO) of the High Power Amplifier (HPA) directly translates into an increase of the coverage area, and mobile systems, where power efficiency is at a prime, and as such amplifiers should be driven into saturation. PAPR reduction problem has raised the interest of both research and industrial community leading to a variety of methods, three of whose will be described in the following subsections.

### A.2.1 *Active Constellation Extension*

The Active Constellation Extension (ACE) approach is based on dynamically extending frequency domain constellation points in order to reduce the peaks of the time domain signal (due to a coherent sum of a subset of the frequency domain data) without increasing Error Rate: the points are distanced from the borders of their Voronoi regions. The extension is performed iteratively, according to the following procedure:

1. Start with the frequency domain representation of a OFDM symbol;
2. Convert into the time-domain signal, and clip all samples exceeding a given magnitude $V_{clip}$. If no sample is clipped, then exit;
3. Re-convert into the frequency domain representation and restore all constellation points which have been moved towards the borders of their Voronoi regions;
4. Go back to 2 until a fixed number of iteration is reached;

This algorithm ( whose detailed description can be found in [52] ) is applied to data carriers only, excluding thus pilots, preamble/signalling and guard bands. In the performance evaluation of the algorithm, the amplitude clipping value will be expressed in term of the corresponding PAPR, which will be called *PAPR Target*.

### A.2.2 *Tone Reservation*

Tone Reservation (TR) technique operates in the time domain, trying to cancel the highest peak with a proper signal, which is a Minimum Mean Square Error (MMSE) approximation of Dirac delta and its spectral content is present only in a certain number of given carriers (a small fraction of the total number). The MMSE approach to construct a pulse close to the discrete Dirac delta is to have a flat spectrum only on the allowed carriers and zero otherwise. Once obtained this pulse, often referred to as a “kernel”, it must be time-shifted, in order to be centered on the peak of the time-domain signal, and its amplitude and phase must be calculated in order to reduce the value of the peak to a chosen target value (which will be calculated in order to achieve a given *PAPR target*).

This procedure is performed in an iterative fashion, whose algorithm is sketched below (the interested reader can find a more detailed explanation in [75] and [53])

1. Start with the time domain representation of a OFDM symbol;
2. If there is a peak in the signal exceeding the given value $V_{\mathtt{clip}}$, the kernel must be time shifted (to align its peak to the signal peak) and scaled. After these operations, the sum of signal and kernel should have reduced the peak under consideration below the given value $V_{\mathtt{clip}}$ ;
3. If there is another peak having amplitude greater than $V_{\mathtt{clip}}$ than go back to 2 else transmit the sum of signal and kernel;

### A.2.3 *Selected Mapping*

Selected Mapping (SLM) technique represents a probabilistic approach to PAPR reduction: a certain number of equivalent data symbol vectors are generated, and the one with the lowest PAPR is chosen. The generation of these “candidates” is done by the multiplication of the original data symbol vector for different vectors composed of phase shifts. In order to simplify the signal processing, the phase shift considered will be multiples of $\pi/2$. This means that the signal will be multiplied for vector composed with the symbols $1, \jmath, -1, -\jmath$. Then the Inverse Fast Fourier Transform (IFFT) of all these equivalent representation is computed, and the sequence with the lowest PAPR is transmitted, joint with the number of the sequence used (in the scenario we have considered, 8 sequences have proved to reduce enough the PAPR). Although this approach, described in [8] requires only a few bits of overhead, in [14] the Authors propose the use of scrambling instead of multiplication for a pseudo-random sequence. The advantage of this method is that no side information is required, because a receiver with adequate processing capability could perform all the possible scramblings and recognise the correct one due to certain characteristics of the signal (the presence of pilots, preambles, etc.)

## A.3 PERFORMANCE RESULTS

A first parameter optimization was performed in order to determine the optimal values for the PAPR Target in ACE or TR and the number of sequences in SLM. This optimization has been done evaluating the CCDF of the PAPR of the processed signal.

After this initial stage, the merit figure we consider is the *Total Degradation*, which is the sum of Signal-to-Noise-Ratio penalty with respect to linear case, at a given Bit Error Rate, and the measured Output Back Off (OBO). The simulation were performed considering a FFT size of 2048, with 1705 active carrier, 1512 of which bearing data. Three configuration of modulation and coding will be considered, namely Quaternary Phase Shift Keying (QPSK) code rate 1/5, QPSK code rate 1/2, 16-Quadrature Amplitude Modulation (QAM) code rate 2/3. The effectiveness of ACE, TR and SLM has been compared, in terms of Total Degradation, to the benchmark case in which no PAPR reduction techiniques are employed

The simulations highlighted two interesting considerations. The first is related to the usefulness of PAPR reduction if the amplifier as a pre-distorter or is driven far from saturation. In this case, a strong modulation and coding scheme, such as QPSK code rate 1/5 offers itself an high resiliency to distortion, vanishing the necessity of a PAPR reduction technique, whose gain can be estimated around 0.3 dB. The second result of the simulations concerns the use of Tone Reservation in a satellite scenario. This technique was developed to counteract cable distortion in wired OFDM systems, having no power constraints and different kind of distortion (i.e. the intermodulation effect is different). In the satellite case, the reserved carriers, for their large power, create a considerable nuisance to the other tones, which is not balanced by the beneficial effects of PAPR reduction. Furthermore, the allocation of reserved carriers is obtained by a further puncturing of the code, causing losses in the order of 0.4 dB.

Finally, Fig. 52,53,54 show the results for QPSK code rate 1/5, QPSK code rate 1/2, and 16-QAM code rate 2/3 respectively, plotting the Total Degradation vs. the Output Back-Off (OBO). The gain offered by these techniques is significantly dependent on the robustness of the modulation and the code themselves. It is almost negligible for QPSK 1/5, while it can be estimated to be around 0.5 dB for 16-QAM 2/3. The better performances of ACE with respect to SLM can in part be justified considering the steepness of PAPR statistics after ACE processing, and in part due to the constellation extension, which offers an increased margin against noise.

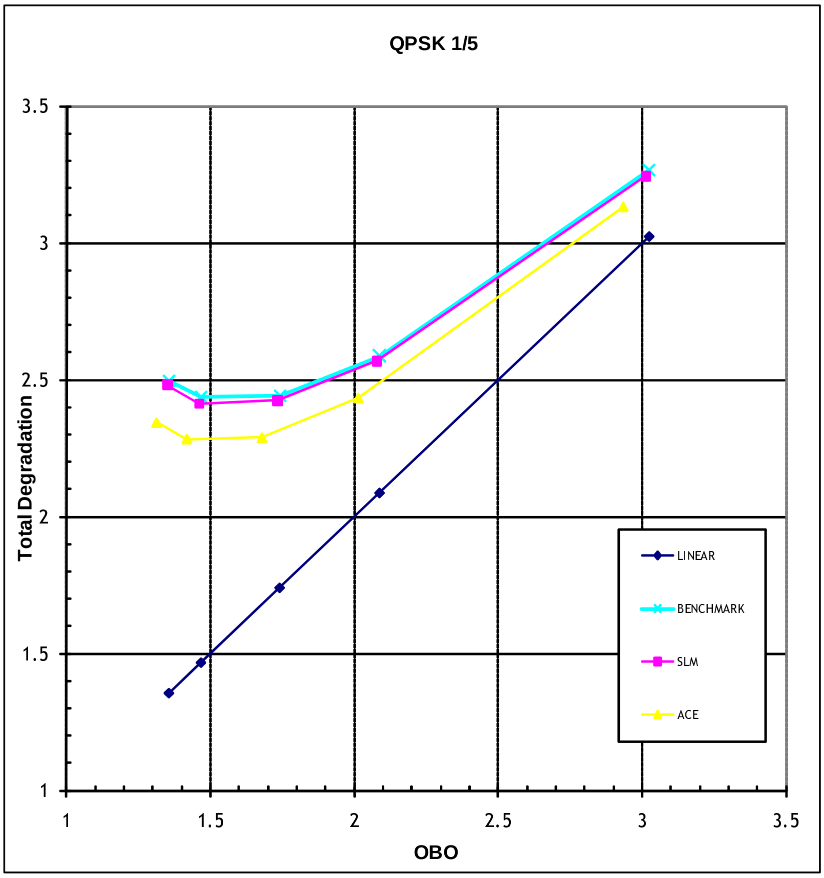

Figure 52: Total Degradation for QPSK code-rate 1/5 and various PAPR reduction techniques-

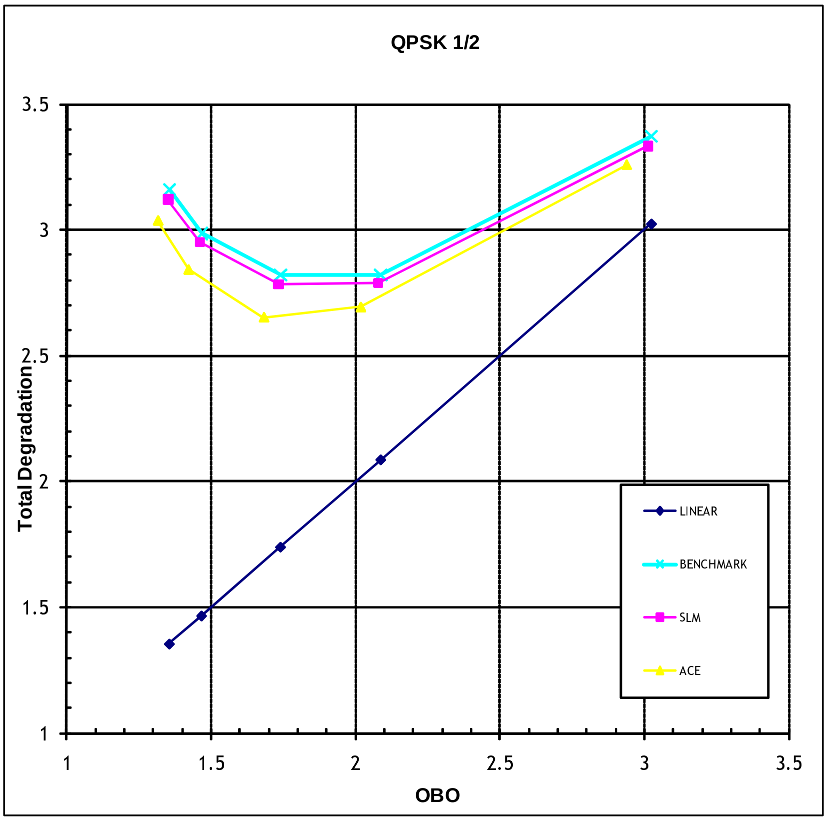

Figure 53: Total Degradation for QPSK code-rate 1/2 and various PAPR reduction techniques-

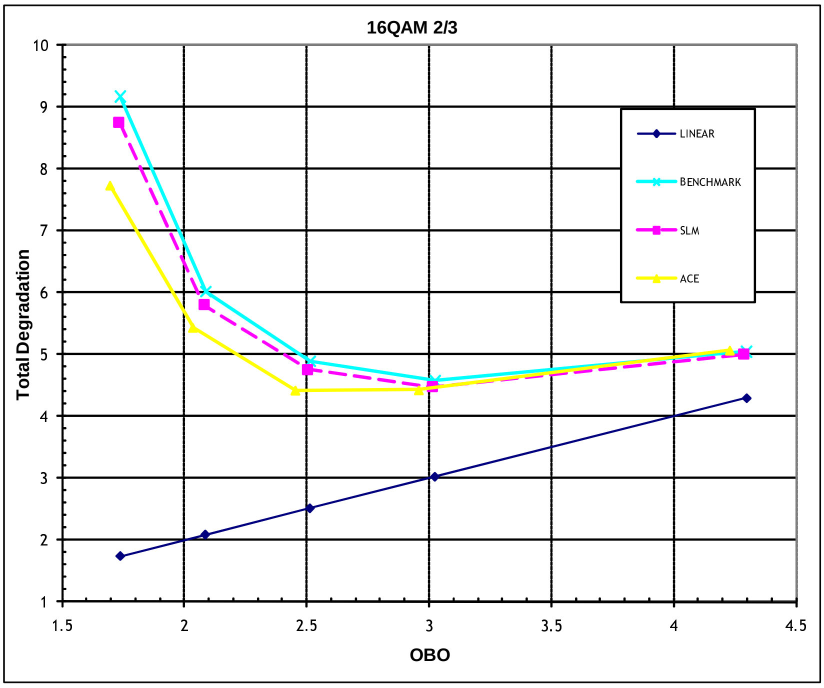

Figure 54: Total Degradation for 16-QAM code-rate 2/3 and various PAPR reduction techniques-

# BIBLIOGRAPHY

[1] M. Abramowitz and I. A. Stegun. *Handbook of Mathematical Functions with Formulas, Graphs, and Mathematical Tables*. Dover, New York, NY, USA, 9-th edition, 1964.

[2] M. A. Arcones. Limit theorems for nonlinear functionals of a stationary gaussian sequence of vectors. *The Annals of Probability*, 22(4):2242–2274, Oct. 1994.

[3] J. Baltersee, G. Fock, and H. Meyr. An information theoretic foundation of synchronized detection. *IEEE Trans. Commun.*, 49 (12):2115–2123, December 2001.

[4] P. Banelli. Theoretical analysis and performance of OFDM signals in nonlinear fading channels. *IEEE Trans. Wireless Commun.*, 2(2): 284–293, March 2003.

[5] P. Banelli and S. Cacopardi. Theoretical analysis and performance of OFDM signals in nonlinear AWGN channels. *IEEE Trans. Commun.*, 48(23):430–441, March 2000.

[6] A.M. Barg and I.I. Dumer. On computing the weight spectrum of cyclic codes. *IEEE Trans. Inf. Theory*, 38(4):1382–1386, July 1992.

[7] G. Bauch. Capacity optimization of cyclic delay diversity. In *Proceedings of the 60th IEEE Vehicular Technology Conference, (VTC2004 - Fall)*, volume 3, pages 1820–1824, Los Angeles, USA, September 2004.

[8] R. Bäuml, R. Fischer, and J. Huber. Reducing the peak-to-average power ratio of multicarrier modulation by selected mapping. *Electr. Lett.*, 32(22):2056–2057, October 1996.

[9] S. Benedetto, E. Biglieri, and R. Daffara. Performance of multilevel baseband digital systems in a nonlinear environment. *IEEE Trans. Commun.*, COM-24(10):1166–1175, October 1976.

[10] S. Benedetto, E. Biglieri, and R. Daffara. Modelling and performance of nonlinear satellite links- a volterra series approach. *IEEE Trans. Aerosp. Electron. Syst.*, AES-15(4):494–507, July 1979.

[11] E.R. Berlekamp. The technology of error correction codes. *Proc. IEEE*, 68(5):564–593, May 1980.

[12] D.P. Bertsekas and J.P. Tsitsiklis. *Parallel and Distributed Computation: Numerical Methods*. Prentice-Hall, Upper Saddle River, NJ, USA, 1989.

[13] M. Blum. On the central limit theorem for correlated random variables. In *Proc. IEEE*, volume 52, pages 308–309, March 1964.

[14] M. Breiling, S.H. M uller-Weinfurtner, and J.B Huber. Sml peak-power reduction without explicit side information. *IEEE Commun. Lett.*, 5(6):239–241, June 2001.

[15] J.J. Bussgang. Cross correlation function of amplitude-distorted gaussian signals. Technical Report Tech. Rep. 216, Sect. 3, Res. Lab. Electron. MIT, Cambridge, MA, USA, March 1952.

[16] C. Caini, G.E. Corazza, G. Falciasecca, M. Ruggieri, and F. Vatalaro. A spectrum- and power-efficient ehf mobile satellite system to be integrated with terrestrial cellular system. *IEEE J. Sel. Areas Commun.*, 10(8):1315–1325, October 1992.

[17] J.W. Choi and Y.H Lee. A comparison of pilot-aided channel estimation methods for OFDM systems. *IEEE Trans. Wireless Commun.*, 4(5):2083–2088, September 2005.

[18] Y.C. Chow, A.R. Nix, and J.P. McGeehan. Analysis of 16-APSK modulation in AWGN and rayleigh fading channel. *Electr. Lett.*, 28 (17):1608–1610, August 1992.

[19] L. J. Cimini Jr. Analysis and simulation of a digital mobile channel using orthogonal frequency division multiplexing. *IEEE Trans. Commun.*, COM-33(7):665–675, July 1985.

[20] S. Cioni, G. E. Corazza, and M. Bousquet. An analytical characterization of maximum likelihood signal-to-noise ratio estimation. In *Proc. 2nd International Symposium on Wireless Communication Systems, 2005. (ISWCS'05)*, pages 290–294, Siena, Italy, September 2005.

[21] A. Clark, P. J. Smith, and D. P Taylor. Instantaneous capacity of OFDM on rayleigh fading channels. *IEEE Trans. Inf. Theory*, 53(12): 355–361, January 2007.

[22] G. E. Corazza, editor. *Digital Satellite Communications*. Information Technology: Transmission, Processing and Storage. Springer, New York, NY, USA, 2007.

[23] D. J. Costello Jr., J. Hagenauer, H. Imai, and S. B. Wicker. Applications of error-control coding. *IEEE Trans. Inf. Theory*, 44(6): 2531–2560, October 1998.

[24] J. W. Craig. A new, simple and exact result for calculating the probability of error for two-dimensional signal constellations. In *Proceeding of IEEE Military Communications Conference MILCOM'91*, pages 571–575, McLean, VA, USA, November 1991.

[25] A. Dammann, S. Plass, and S. Sand. Cyclic delay diversity- a simple, flexible and effective multi-antenna technology for OFDM. In *Proceedings of the 10th IEEE International Symposium on Spread Spectrum Techniques and Applications, (ISSSTA 2008)*, Bologna, IT, August 2008.

[26] S. Dammann and S. Kaiser. Transmit/receive antenna diversity techniques for OFDM systems. *Eur. Trans. on Telecomm.*, 13(5): 531–538, September 2002.

[27] D. Dardari, V. Tralli, and A. Vaccari. A theoretical characterization of nonlinear distortion effects in OFDM systems. *IEEE Trans. Commun.*, 48(10):1755–1764, October 2000.

[28] A. C. Davidson and D. R. Cox. Some simple properties of sums of random variables having long-range dependence. *Proceedings of the Royal Society of London, Series A*, 424(1867):255–262, August 1989.

[29] M. V. S. de Naranjo. A central limit theorem for nonlinear functionals of stationary gaussian vector processes. *Statistics and Probability Letters*, 22:223–230, 1995.

[30] Digital Video Broadcasting (DVB). Second generation framing structure, channel coding and modulation systems for broadcasting, interactive services, news gathering and other broadband satellite applications. Technical Report EN 302 307 v1.1.1, ETSI, January 2004.

[31] Digital Video Broadcasting (DVB). Framing structure, channel coding and modulation for satellite services to handheld devices (SH) below 3 ghz. Technical Report EN 302 583, ETSI, 2008.

[32] Digital Video Broadcasting (DVB). Interaction channel for satellite distribution systems. Technical Report EN 301 790 v 1.5.1, ETSI, May 2009.

[33] Digital Video Broadcasting (DVB). Frame structure channel coding and modulation for a second generation digital terrestrial television broadcasting system (DVB-T2). Technical Report EN 302 755 V1.1.1, ETSI, September 2009.

[34] J. P. Fonseca, Y. Yin, and I. Korn. Sensitivity to fading estimates in maximal ratio combining. *IEE Proc. Commun.*, 150(4):269–274, August 2003.

[35] G. J. Foschini, R. D. Gitlin, and S. B. Weinstein. Optimization of two-dimensional signal constellations in the presence of gaussian noise. *IEEE Trans. Commun.*, COM-22(1):28–38, January 1974.

[36] R. M. Gagliardi and C. M. Thomas. PCM data reliability monitoring through estimation of signal to noise ratio. *IEEE Trans. Commun.*, COM-16(3):479–486, June 1968.

[37] R. G. Gallager. *Information Theory and Reliable Communications*. Wiley, New York, NY, USA, 1968.

[38] R.G. Gallager. *Low Density Parity Check Codes*. MIT Press, Boston, MA, USA, 1963.

[39] M. S. Gockenbach and A. J. Kearsley. Optimal signal sets for non-gaussian detectors. *SIAM Journal on Optimization*, 9(2):316–326, 1999.

[40] S.H Han and J.H. Lee. An overview of peak-to-average-power-ratio reduction techniques for multicarrier transmission. *IEEE Wireless Commun. Mag.*, 12(2):56–65, April 2005.

[41] B. Hassibi and B.M. Hochwald. How much training is needed im multiple-antenna wireless links? *IEEE Trans. Inf. Theory*, 49(9): 951–963, April 2003.

[42] H. Herzberg and G. Polytrev. The error probability of m-ary PSK block coded modulation schemes. *IEEE Trans. Commun.*, 44: 427–433, April 1996.

[43] P. Hoerer, S. Kaiser, and P. Robertson. Two-dimensional pilot-symbol-aided channel estimation by wiener filtering. In *Proceedings of the IEEE International Conference on Acoustics, Speech, and Signal Processing, 1997. ICASSP-97.*, volume 3, pages 1845 – 1848, Munich, Germany, April 1997.

[44] B. Hughes. On the error probability of signals in additive white gaussian noise. *IEEE Trans. Inf. Theory*, 37(1):151–155, January 1991.

[45] IEEE. IEEE standard for local and metropolitan area networks part 16: Air interface for fixed and mobile broadband wireless access systems. Technical Report Amendement 2 and Corrigendum 1, IEEE, February 2006.

[46] IEEE. IEEE 802.16m evaluation methodology. Technical Report IEEE 802.16m-08/004, IEEE 802.16 Broadband Wireless Access Working Group, March 2008.

[47] W. C. Jakes. *Microwave Mobile Communications*. IEEE Press, Piscataway, NJ, USA, 1994.

[48] T. Jang and Y. Wu. An overview of peak-to-average-power ratio reduction techniques for OFDM signals. *IEEE Trans. Broadcast.*, 54 (2):257–268, June 2008.

[49] M. A. Jordan and R. A. Nichols. The effects of channel characteristics on turbo code performance. In *Proc. 2nd IEEE Military Communications Conference, 1996. (MILCOM'96)*, volume 1, pages 17–21, October 1996.

[50] A. J. Kearsley. Global and local optimization algorithms for optimal signal set design. *NIST Journal of Research*, 106(2):441–454, 2001.

[51] R. B. Kerr. On signal and noise level estimation in a coherent PCM channel. *IEEE Trans. Aerosp. Electron. Syst.*, AES-2(4):450–454, July 1966.

[52] B.S. Krongrold and D.L. Jones. PAR reduction in OFDM via active constellation extension. *IEEE Trans. Broadcast.*, 49(3):258–268, September 2003.

[53] B.S. Krongrold and D.L. Jones. An active set approach for OFDM PAR reduction via tone reservation. *IEEE Trans. Signal Process.*, 52 (2):495–509, February 2004.

[54] H. Kuai, F. Alajaji, and G. Takahara. Tight error bounds for nonuniform signalling over AWGN channels. *IEEE Trans. Inf. Theory*, 46 (7):2712–2718, November 2000.

[55] R. K. Mallick. On multivariate rayleigh and exponential distributions. *IEEE Trans. Inf. Theory*, 49(6):1499–1515, June 2003.

[56] M. Medard. The effect upon channel capacity in wireless communications of perfect and imperfect knowledge of the channel. *IEEE Trans. Inf. Theory*, 46(3):933–946, May 2000.

[57] J. Minkoff. The role of AM-to-PM conversion in memoryless nonlinear systems. *IEEE Trans. Commun.*, COM-33(2):139–144, February 1985.

[58] M. Morelli and U. Mengali. A Comparison of Pilot-Aided Channel Estimation Methods for OFDM Systems. *IEEE Trans. Signal Process.*, 49(6):3065–3073, dec. 2001.

[59] R. Negi and J.M. Cioffi. Pilot tone selection for channel estimation in a mobile OFDM system. *IEEE Trans. Consum. Electron.*, 44(3): 1122–1128, August 1998.

[60] N. G. Ngo and S. S. Barbulescu, S. A. Pietrobon. Performance of nonuniform m-ary QAM constellation on nonlinear channels. In *Proc. 6th Australian Communication Theory Workshop*, pages 79–83, February 2005.

[61] N. G. Ngo and S. S. Barbulescu, S. A. Pietrobon. Optimization of 16-APSK constellation with a new iterative decoder on the nonlinear channel. In *Proc. 7th Australian Communication Theory Workshop*, pages 71–75, February 2006.

[62] H. Ochiai and H. Imai. Performance of the deliberate clipping with adaptive symbol selection for strictly band-limited OFDM systems. *IEEE J. Sel. Areas Commun.*, 18(11):2270–2277, November 2000.

[63] D. R. Paoluzzi and N. C. Beaulieu. A comparison of SNR estimation techniques for the AWGN channel. *IEEE Trans. Commun.*, 48 (10):1681–1691, October 2000.

[64] G. Polytrev. Bounds of the decoding error probability of binary linear codes via their spectra. *IEEE Trans. Inf. Theory*, 40(4):1284–1292, July 1994.

[65] G. M. Poscetti. An upper bound for probability of error related to a given decision region in $N$-dimensional signal set. *IEEE Trans. Inf. Theory*, 17(2):203–206, March 1971.

[66] A.A.M. Saleh. Frequency-independent and frequency-dependent nonlinear models of TWT amplifiers. *IEEE Trans. Commun.*, COM-29(11):1715–1720, November 1981.

[67] P. Salmi, M. Neri, and G.E. Corazza. Design and performance of predistortion techniques in ka-band satellite networks. In *Proceedings of 22nd AIAA ICSSC2004*, Monterey, CA, USA, May 2004.

[68] I. Sason and S. Shamai. *Performance Analysis of Linear Codes under Maximum-Likelihood Decoding: a Tutorial*. Foundations and Trends in Communications and Information Theory. Now, Boston-Delft, 2006.

[69] G.E. Seguin. A lower bound on the error probability for signals in white gaussian noise. *IEEE Trans. Inf. Theory*, 44(7):3168–3175, November 1998.

[70] T.B. Sorensen, P.E. Mogensen, and F. Frederiksen. Extension of the itu channel models for wideband OFDM systems. In *Proceedings of the IEEE 62nd Vehicular Technology Conference, 2005. VTC-2005-Fall.*, volume 4, pages 392 – 396, Chicago, IL,USA, September 2005.

[71] P. Soulier. Moment bounds and central limit theorem for functions of gaussian vectors. *Statistics and Probability Letters*, 54:193–203, 2001.

[72] T. A. Summers and S. G. Wilson. SNR mismatch and online estimation in turbo decoding. *IEEE Trans. Commun.*, 46(4):421 – 423, April 1998.

[73] P. Swaszek. A lower bound on the error probability for signals in white gaussian noise. *IEEE Trans. Inf. Theory*, 41(3):837–841, May 1995.

[74] L. Szczecinski, S. Aïssa, C. Gonzalez, and M. Bacic. Exact evaluation of bit- and symbol-error rates for arbitrary 2-d modulation and nonuniform signaling in AWGN channel. *IEEE Trans. Commun.*, 54(6):1049–1056, June 2006.

[75] J. Tellado. *Peak to average power reduction for multicarrier modulation*. PhD thesis, Stanford University, Stanford, CA, USA, 2000.

[76] M. Vajapeyam, G. Geng, and U. Mitra. Tools for performance analysis and design of space-time block codes. *IEEE Trans. Commun.*, 55(2):367–379, February 2007.

[77] J.J. van de Beek, O. Edfors, M. Sandell, S.K. Wilson, and P.O. Börjesson. On channel estimation in OFDM systems. In *Proceedings of the IEEE Vehicular Technology Conference, 1995. VTC'95.*, volume 2, pages 815–819, Chicago, IL, USA, September 1995.

[78] F. Vatalaro, G.E. Corazza, and C. Caini. Analysis of leo, meo, and geo global mobile satellite systems in the presence of interference and fading. *IEEE J. Sel. Areas Commun.*, 13(2):291–300, February 1995.

[79] S.B. Weinstein and P.M. Ebert. Data transmission by frequency division multiplexing using the discrete fourier transform. *IEEE Trans. Commun.*, COM-19(5):628–634, October 1971.

[80] P. Zillmann and G.R. Fettweis. On the capacity of multicarrier transmission over nonlinear channels. In *Proceedings of IEEE 61st Vehicular Technology Conference, VTC 2005-Spring4*, pages 1148 – 1152, Stockolm, Sweden, May 2005.

[81] S.A. Zummo and W.E. Stark. Error probability of coded STBC systems in block fading environments. *IEEE Trans. Wireless Commun.*, 5(5):972–977, May 2006.